LODZ UNIVERSITY OF TECHNOLOGY

Faculty of Mechanical Engineering

Division of Dynamics

Anna Karmazyn

Synchronization of coupled mechanical oscillators in the presence of noise and parameter mismatch

Supervision: **prof. dr hab. inż. Andrzej Stefański**

Assistant supervisor: **dr hab. inż. Przemysław Perlikowski**

Lodz 2014

Preface

This doctoral thesis is a part of "Project TEAM of Foundation for Polish Science" realising the investigation and analysis of the project "Synchronization of Mechanical Systems Coupled through Elastic Structure". It is supported by "Innovative Economy: National Cohesion Strategy". The programme is financed by "Foundation for Polish Science" from the European funds as the plan of "European Regional Development Fund". The project is mainly focused on the following issues:

- *Identification of possible synchronous responses of coupled oscillators and existence of synchronous clusters as well;*
- *Dynamical analysis of identical coupled systems suspended on elastic structure in context of the energy transfer between systems;*
- *Investigation of phase or frequency synchronization effects in groups of coupled non-identical systems;*
- *Developing methods of motion stability control of considered systems;*
- *Investigation of time delay effects in analysed systems;*
- *Developing the idea of energy extraction from ocean waves using a series of rotating pendulums.*

INNOVATIVE ECONOMY
NATIONAL COHESION STRATEGY
FNP
Foundation for Polish Science
EUROPEAN UNION
EUROPEAN REGIONAL
DEVELOPMENT FUND

Contents

Introduction

Synchronization is a powerful basic concept in nature regulating a large variety of complex processes. Synchronous behaviour has attracted a large volume of interest in physics, engineering, biology, ecology, sociology, communication and other fields of science and technology [1, 2, 3]. It is known that synchrony is rooted in human life from the metabolic processes in our cells to the highest cognitive tasks we perform as a groups of individuals. Therefore, synchronization phenomena have been extensively studied and models robustly capturing the dynamical synchronization process have been proposed.

Historically, the analysis of synchronization in the evolution of dynamical systems has been a subject of investigation since the earlier days of physics [4]. It started when the Dutch researcher, Christian Huygens discovered that two very weakly coupled pendulum clocks (hanging at the same beam) can be synchronized in phase [5, 6, 7, 8, 9, 10]. In the last two decades it has been demonstrated that any set of chaotic systems can synchronize by linking them with mutual coupling or with a common signal or signals [11, 12, 13, 14]. Synchronization has been to employ control theory as a control problem. Particularly this approach can be applied in robotics when two or more robot manipulators have to operate synchronously in a dangerous environment [15, 16]. Pogromsky et al. [17] designed a controller for a synchronization problem comprising two pendulums suspended on an elastically supported rigid beam.

Recently the search for synchronization has been moved to chaotic systems. Dynamical system is called chaotic whenever its evolution sensitively depends on the initial conditions. It means that two trajectories taking off from two different closely initial conditions separate exponentially in the course of the time. As a result, chaotic systems intrinsically defy synchronization, because even two

autonomous chaotic systems starting from slightly different initial conditions would evolve in time in an desynchronized manner (the differences in the states of systems would grow exponentially).

The field of chaotic synchronization has grown considerably since early 80's [20, 21, 22]. Synchronization of chaos is a process wherein two (or many) chaotic systems (either equivalent or non-equivalent) adjust a given property of their motion to a common behaviour, due to coupling or forcing. This ranges from complete agreement of trajectories to locking of phases. Many different synchronization states of coupled chaotic systems have been observed in the past 20 years, namely complete or identical synchronization (CS) [11, 14, 18, 26], imperfect complete or practical synchronization (ICS) [26, 27, 28] , phase (PS) [14, 18, 19, 23] and lag (LS) synchronization [14, 24], generalized synchronization (GS) [14, 29, 30, 31, 32, 33, 35], intermittent lag synchronization (ILS) [24, 36] and imperfect phase synchronization (IPS) [37], almost synchronization (AS) [29], cluster synchronization [38, 39, 40, 41, 47, 49, 48, 50].

Generally, the proposed doctoral dissertation is composed of two parts, where

- theoretical background and historical outline about synchronization of dynamic systems are described,

- numerical and experimental analysis of several dynamical systems are presented and compared.

In first Chapter major ideas involved in the field of synchronization of chaotic systems are reviewed, and several types of synchronization features are presented in detail. In the following Chapter classification and properties of the coupling between dynamical systems are presented. Next Chapter presents the theoretical background necessary for the analysis of dynamics of the nonlinear oscillators. Stability of synchronization states, the algorithm of the Lyapunov exponents and transversal Lyapunov exponents was discussed and idea of the MSF allowing synchronization stability test was presented. At the beginning of next Chapter a method of studied systems modelling is shown. The content of Chapter 4 is a numerical analysis of the oscillators network with physical pendulums attached

to these oscillators. Two particular but representative cases of one ($n = 1$) and three ($n = 3$) oscillators have been considered. A review of numerical results to determine the synchronization, and its types, for nominally identical dynamical systems and its equivalent with parameter's mismatch is demonstrated. In the penultimate Chapter the results of experiment for one and three oscillator nodes are presented. Finally, numerical results for one and three oscillator nodes for slight differences of parameters and results obtained from experimental rig for one and three oscillator nodes are compared and conclusions are summarised.

Subject of the dissertation

In doctoral dissertation the dynamics of number of physical pendulums located on (coupled through) an elastic structure, as shown in Fig. 1, is considered. The adopted model takes the form of a series of n identical masses concentrated in the point connected to the light elastic beam. To each of the masses attached two identical physical pendulums (on each side of the beam). The excitation in the position of mass M_{bn} is expressed by the formula $x_{ex\,n} = x_{z1} + \frac{l_{b\,n}}{l_b}(x_{z2} - x_{z1})$, where l_b is a total length of the elastic beam. In the present case, the excitation on both sides of the elastic beam are the same $x_{z1} = x_{z2} = x_z = z\,\sin\Omega t$, therefore we have $x_{ex\,i} = x_{ex\,n-(i-1)}$ for $i = 1,\ 2, \ldots,\ n$. We assumed that the oscillators were located symmetrically on the beam.

The next assumption is that the beam is simply supported at both ends. Hence, we have the following boundary conditions: $z(0,\ t) = 0$, $z(l_b,\ t) = 0$, $\frac{d^2\,z(0,\,t)}{d\,x^2} = 0$ and $\frac{d^2\,z(l_b,\,t)}{d\,x^2} = 0$.

It should be pointed out that this work is concentrated on the analysis of a quite general model of the coupling trough the elastic structure (beam). This coupling is common in mechanical systems and can be treated as a model of a number of machines operate in the same hall or a crowd of people walks on a bridge. The continuous beam of the mass M_b was replaced by the massless beam on which $\hat{n}$ discrete identical bodies of mass M_{bn} are located, i.e., $\hat{n}\,M_{bn} = M_b$. Mass M_{bn} are constrained to move only in vertical direction and thus are described by the coordinate x_n. The number of discrete masses has been selected in such

a way as to obtain the first two eigenfrequencies of the continuous and discrete beam approximately equal. In our numerical simulations we assumed for the sake of simplicity that $\hat{n}$ is equal to the number of oscillators, i.e, $n = \hat{n}$ which are attached to the beam. The considered discrete model is shown in Fig. 1.

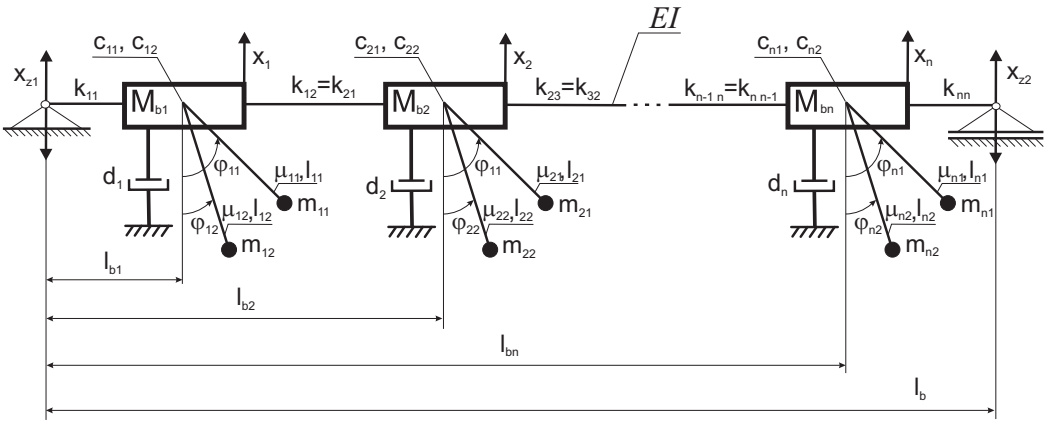

Figure 1: System of n masses and $2n$ pendulums located on (coupled through) a light elastic structure.

The equations of motion of system presenting in Fig. 1 can be derived using Lagrange equations of the second type. The kinetic energy T, potential energy V and Rayleigh dissipation D are given respectively by

$$T = \sum_{i=1}^{n} \left(\frac{1}{2} M_i \dot{x}_i^2 + \sum_{j=1}^{2} \left(\frac{1}{2} B_{ij} \dot{\varphi}_{ij}^2 + (m_{ij} + \mu_{ij})\, b_{ij}\, \dot{x}_i\, \dot{\varphi}_{ij}\, \sin\varphi_{ij} \right) \right), \tag{1a}$$

$$V = \sum_{i=1}^{n} \sum_{j=1}^{2} (m_{ij} + \mu_{ij})\, g\, b_{ij}\, (1 - \cos\varphi_{ij}), \tag{1b}$$

$$D = \sum_{i=1}^{n} \left(\frac{1}{2} d_i \dot{x}_i^2 + \sum_{j=1}^{2} \left(\frac{1}{2} c_{ij} \dot{\varphi}_{ij}^2 \right) \right). \tag{1c}$$

where

$$B_{i1,\,i2} = B_{i\,S1,i\,S2} + (m_{i1,\,i2} + \mu_{i1,\,i2})\, {b_{i1,\,i2}}^2,$$

$$M_i = M_{bi} + m_{i1} + \mu_{i1} + m_{i2} + \mu_{i2},$$

where M_{bi} – mass of the oscillator $[kg]$, $m_{i1,i2}$ – mass concentrated at the point in the and of rod $[kg]$, $\mu_{i1,i2}$ – mass of the rod $[kg]$, $l_{i1,i2}$ – length of the rod $[m]$, $B_{i\,S1,i\,S2}$ is the inertia moment of the mass $[kg\,m^2]$ given by $B_{i\,S1,i\,S2} = m_{i1,i2}(l_{i1,i2} - b_{i1,i2})^2 + \frac{1}{12}\mu_{i1,i2} l_{i1,i2}^2 + \mu_{i1,i2}(b_{i1,i2} - \frac{1}{2} l_{i1,i2})^2$ and $b_{i1,i2} = \frac{(m_{i1,i2} + \frac{1}{2}\mu_{i1,i2})l}{(m_{i1,i2} + \mu_{i1,i2})}$ is distance

from the center of mass to the center of rotation of the rod and ball $m_{i1,i2}$, $c_{i1,i2}$ – damping factor at the node $[Nms]$, d_i – viscous damping $[Ns/m]$, g – acceleration due to the gravity $[m/s^2]$. Parameters of the beam: mass M_b $[kg]$, length l_b $[m]$, modulus of elasticity E $[N/m^2]$ and the inertial momentum of cross-section I $[m^4]$.

The discertisation is based on flexibility coefficients method [51]. The stiffness of the beam fulfils the relation $[k_{ji}] = [a_{ji}]^{-1}$, where $[a_{ji}]$ is the $n \times n$ dimensional matrix of flexibility coefficients and it is dependent on the quantity $E\,J\,l_b$ and the location of masses M_{bi}. Hence, from the result of such a discretisation we obtain the following equation describing the dynamics of the i-th 3DoF segment (masses M_{bi}, m_{i1} and m_{i2}, $i = 1,\ 2, \ldots,\ n$) of the system

$$B_{i1}\ \ddot{\varphi}_{i1} + A_{i1}\ \ddot{x}_i\ \sin\varphi_{i1} + A_{i1}\ g\ \sin\varphi_{i1} + c_{i1}\ \dot{\varphi}_{i1} = 0 \tag{2a}$$

$$B_{i2}\ \ddot{\varphi}_{i2} + A_{i2}\ \ddot{x}_i\ \sin\varphi_{i2} + A_{i2}\ g\ \sin\varphi_{i2} + c_{i2}\ \dot{\varphi}_{i2} = 0 \tag{2b}$$

$$M_i\ \ddot{x}_i + A_{i1}\ (\ddot{\varphi}_{i1}\ \sin\varphi_{i1} + \dot{\varphi}_{i1}^2\ \cos\varphi_{i1}) + A_{i2}\ (\ddot{\varphi}_{i2}\ \sin\varphi_{i2} + \dot{\varphi}_{i2}^2\ \cos\varphi_{i2}) + d_i\ \dot{x}_i + \sum_{j=1}^{n} k_{ji}\ (x_i - x_{ex\,i}) = 0 \tag{2c}$$

where

$A_{i1,\,i2} = (m_{i1,\,i2} + \mu_{i1,\,i2})\ b_{i1,\,i2}$,

k_{ji} – spring stiffness coefficients $[N/m]$, $\Delta c_i = c_{i1} - c_{i2}$ is damping factor mismatch at the node and $i,\ j\ =\ 1,\ 2, \ldots,\ n$.

Introducing $\omega = \sqrt{\frac{k_{11}}{M_1}}$ (the natural frequency), $x_S = \frac{M_1\,g}{k_{11}}$ and dividing Eqs. (2a), (2b) by $l_1\ k_{11}\ x_S$ and Eqs. (2c) by $k_{11}\ x_S$ we obtain the dimensionless equations:

$$\alpha_{i1}\ \ddot{\varphi}_{i1} + \beta_{i1}\ \ddot{x}_i\ \sin\varphi_{i1} + \gamma_{i1}\ \sin\varphi_{i1} + \zeta_{i1}\ \dot{\varphi}_{i1} = 0 \tag{3a}$$

$$\alpha_{i2}\ \ddot{\varphi}_{i2} + \beta_{i2}\ \ddot{x}_i\ \sin\varphi_{i2} + \gamma_{i2}\ \sin\varphi_{i2} + \zeta_{i2}\ \dot{\varphi}_{i2} = 0 \tag{3b}$$

$$\varepsilon_i\ \ddot{x}_i + \rho_{i1}\ (\sin\varphi_{i1}\ \ddot{\varphi}_{i1} + \cos\varphi_{i1}\ \dot{\varphi}_{i1}^2) + \rho_{i2}\ (\sin\varphi_{i2}\ \ddot{\varphi}_{i2} + \cos\varphi_{i2}\ \dot{\varphi}_{i2}^2) + \delta_i\ \dot{x}_i + \sum_{j=1}^{n} \kappa_{ji}(x_i - X_{ex\,i}) = 0 \tag{3c}$$

where

$$\alpha_{i1,\,i2} = \frac{B_{i1,\,i2}}{M_1\ b_{11}\ x_S},\quad \beta_{i1,\,i2} = \frac{A_{i1,\,i2}}{M_1\ b_{11}\ x_S},\quad \gamma_{i1,\,i2} = \frac{A_{i1,\,i2}}{M_1\ b_{11}},\quad \zeta_{i1,\,i2} = \frac{c_{i1,\,i2}}{\omega\ M_1\ b_{11}\ x_S},$$

$$\varepsilon_i = \frac{M_i}{M_1},\qquad \rho_{i1,\,i2} = \frac{A_{i1,\,i2}}{M_1\ x_S},\qquad \delta_i = \frac{d_i}{\omega\ M_1},\qquad \kappa_{ji} = \frac{k_{ji}}{k_{11}},$$

$$X_{ex\,i} = \frac{x_{ex\,i}}{x_S},\qquad Z = \frac{z}{x_S},\qquad \eta = \frac{\Omega}{\omega}$$

are dimensionless parameters and

$$x_i = \frac{1}{x_S}\frac{dx_i}{d\tau}, \quad \varphi_{i1,\,i2} = \frac{d\varphi_{i1,\,i2}}{d\tau}, \quad \tau = \omega\, t$$

are dimensionless variables. The derivatives in Eqs. (3) are calculated with respect to nondimensional time τ.

Coupling through an elastic structure allows one to investigate how the dynamics of the particular pendulum is influenced by the dynamics of other subsystems and this is the main purpose of the research. Synchronization in coupled dynamical systems is associated with the emergence of collective coherent behaviour between identical or similar subsystems. In this doctoral dissertation attention is focused on the possibility of the occurrence of complete and phase synchronization of pendulums, the creation of clusters (groups of pendulums with synchronous behaviour) and the influence of parameter's mismatch on the synchronization and behaviour of pendulums.

Aim and thesis of the doctoral dissertation

The main aim of the doctoral dissertation is to identify the essence of the transition mechanism from synchronous regime to a state of desynchronization, as a result of growing the external disturbances (noise) and slight differences between parameters of nominally identical coupled mechanical oscillators.

The specific objectives of the thesis:

- Numerical modelling and bifurcation analysis of a single oscillator node with two degrees of freedom - the kinematically forced system consisting of a elastically supported mass with physical pendulum.

- Numerical modelling and bifurcation analysis of a single oscillator node with three degrees of freedom - the kinematically forced system consisting of a elastically supported mass with two physical pendulums.

- Numerical modelling and bifurcation analysis of three oscillator nodes with three degrees of freedom - the kinematically forced system consisting of a elastically supported two masses with two physical pendulums.

- Numerical stability analysis of a series synchronization states in the presence of noise and parameter mismatch.

- Numerical identification of ranges of parameters, in which dominates stable rotational motion of pendulums.

- Design and construction of the experimental rig optimized on the basis of numerical simulations.

- Experimental investigations.

- Comparison of experimental results and numerical simulation.

- Detailed analysis of the impact of noise and parameter mismatch on the existence and stability of the synchronous motion of groups (clusters) of respondents oscillators.

- Identification of synchronization or desynchronization mechanisms.

- Analysis of the results and conclusions.

In the context of the main results contained in the PhD dissertation, thesis of this can be expressed as follows:

The common forcing a series of coupled mechanical oscillators induces a reduction in the impact of the real effects of external noise and parameter mismatch on the destruction process of synchronization (desynchronization) a series of coupled, nominally identical mechanical oscillators.

Chapter 1

Synchronization

The phenomenon of synchronization in dynamical and, in particular, mechanical systems has been known for a long time. Synchronization is desire subsystems of more complex dynamical system to perform "similar" dynamics of such manifested by periodic motions of subsystems with the same periods, consequently causing the synchronization, that mean the periodic motion of the same period the entire system [52].

It was initially thought that the phenomenon of synchronization relates to the systems with periodic or quasi-periodic behaviour, while chaos, due to sensitivity to initial conditions, excludes the appearance of synchronization. Two identical chaotic systems started at nearly the same initial points in the phase space have trajectories which quickly become uncorrelated in the course of the time, even though both evolve to the same attractor in the phase space.

However, the idea of synchronization has been adopted for chaotic systems [1] – [24]. It has been demonstrated that two or more chaotic systems can synchronize by linking them with mutual coupling or with a common signal or signals.

This Chapter provides an overview of the literature concerning the synchronization, i.e. the most commonly encountered types of synchronization phenomena are listed and described.

1.1. Complete synchronization

Complete synchronization (CS) was discovered as the first and it is the simplest form of synchronization in chaotic systems. In the early 1980s, Fujisaka and Yamada [21, 22] showed how two identical chaotic oscillators under variation of the coupling strength can attain a state of complete synchronization in which the motion of the coupled system takes place on an invariant subspace in the phase space, the synchronization manifold. This type of synchronization has subsequently been studied by a significant number of investigators, and a variety of applications for chaos suppression, for monitoring and control of dynamical systems, and for different communication purposes have been suggested [2, 5]. It is also described in the literature as the identical or full synchronization [11, 24]. Pecora and Carroll [11] have defined the complete synchronization as a state when two arbitrarily chosen trajectories $\mathbf{x}(t)$ and $\mathbf{y}(t)$ converge to the same values and continue in such a relation further in time. This kind of synchronization can appear only in the case of identical coupled systems defined by the same set of ODEs with the same values of the system parameters, say $\dot{\mathbf{x}} = \mathbf{f}(\mathbf{x})$ and $\dot{\mathbf{y}} = \mathbf{f}(\mathbf{y})$.

Definition 1.1 (Complete synchronization)
The complete synchronization of two dynamical systems represented with their phase plane trajectories $\mathbf{x}(t)$ *and* $\mathbf{y}(t)$*, respectively, takes place when for all* $t > 0$*, the following relation is fulfilled:*

$$\lim_{t->\infty} ||\mathbf{x}(t) - \mathbf{y}(t)|| = 0. \tag{1.1}$$

Thus the complete synchronization takes place when all trajectories converge to the same value and remain in step with each other during further evolution. In such a situation all subsystems of the augmented system evolve on the same manifold on which one of these subsystems evolves (the phase space is reduced to the synchronization manifold).

1.2. Imperfect complete synchronization

Synchronization of real systems can not be defined by the same relationship as in the case of identical oscillators. It is impossible to obtain two identical springs, dampers, resistors, etc., each of these elements have tolerances and differences in the structure of the material. Taking into account this fact in experimental settings must be applied other criteria for detection of CS. Introduced, so the concept of imperfect complete synchronization (ICS) (Definition 1.2).

Definition 1.2 (Imperfect complete synchronization)
The imperfect complete synchronization of two dynamical systems represented with their phase plane trajectories $\mathbf{x}(t)$ *and* $\mathbf{y}(t)$*, respectively, occurs when for all* $t > 0$*, the following inequality is fulfilled:*

$$\lim_{t->\infty} ||\mathbf{x}(t) - \mathbf{y}(t)|| < \varepsilon, \tag{1.2}$$

where ε is a small parameter, such that $\varepsilon \ll \sup ||\mathbf{x}(t) - \mathbf{y}(t)||$, generally not more than 1%, 2% of the maximum synchronization error. Among the many works on this subject it is worth mentioning an article which presents the experimental results. Blakely et. al [53] presented in the theoretical part of the work a full review of criteria for the occurrence of ICS, while presenting the results of the experimental part of the modelled electrical oscillators. None of the criteria are not allowed for precise determination of the behaviour of coupled oscillators (ICS threshold).

1.3. Generalized synchronization

One of the most interesting ideas concerning the chaos synchronization, which have emerged in the last years, is a concept called the generalized synchronization (GS) [25, 29, 30]. GS is a generalization of ICS for unidirectionally coupled non-identical oscillators. When there is a clear difference in the dimension or differential equations between the oscillators, their evolution may not be described on the basis of synchronization research. However, it was found that there is

then strict relationship between the drive and response system. In the literature one can find many definitions of GS, but the differences between them are small and have little impact on the detection of this phenomenon. This term has been proposed by Rulkov et al. [29] as a generalization of the synchronization idea for unidirectionally coupled systems:

$$\dot{\mathbf{x}} = \mathbf{F}(\mathbf{x}), \tag{1.3a}$$

$$\dot{\mathbf{y}} = \mathbf{G}(\mathbf{y}, \mathbf{h}(\mathbf{x})), \tag{1.3b}$$

where $\mathbf{x} \in \Re^k$, $\mathbf{y} \in \Re^k$, $\mathbf{F} : \Re^m \to \Re^m$, $\mathbf{G} : \Re^k \to \Re^k$. The coupling between the drive (1.3a) and the response (1.3b) system is defined by a vector field $\mathbf{h}(\mathbf{x}) : \Re^m \to \Re^k$, where the parameter μ determines the strength of the coupling. Such kind of interaction of dynamical systems is also called the master-slave coupling. For $\mathbf{h}(\mathbf{x}) = 0$ evolution enforced oscillator is independent. For $\mathbf{h}(\mathbf{x}) \neq 0$ trajectories of the two oscillators are synchronized if there is asymptotically stable transformation $\boldsymbol{\psi} : \mathbf{x} \to \mathbf{y}$ given by the following relationship

$$\mathbf{y}(t) = \boldsymbol{\psi}[\mathbf{x}(t)]. \tag{1.4}$$

Generally, the GS problems have been researched both in the context of identical (when separated) systems Eq.(1.3a) and Eq.(1.3b), and also in cases when the response system (the same set of ODEs with different values of system parameters) is slightly or strictly different (another set of ODEs) than the driving oscillator [14, 30, 39, 55]. The GS phenomena can be also observed in discrete time systems [33, 34]. However, in any of these cases the CS can be applied as a tool for recognizing the GS. In order to detect the presence of the GS, a numerical method called the mutual false nearest neighbours [29] and the related auxiliary system approach [35] have been proposed. According to these methods, the criterion for the GS existence is an appearance of the CS between the response subsystem Eq.(1.3b) and its identical replica, i.e.,

$$\lim_{t->\infty} ||\mathbf{y}(t, \mathbf{x}_0, \mathbf{y}_{01}) - \mathbf{y}(t, \mathbf{x}_0, \mathbf{y}_{02})|| = 0, \tag{1.5}$$

where $\mathbf{y}(t, \mathbf{x}_0, \mathbf{y}_{01})$ and $\mathbf{y}(t, \mathbf{x}_0, \mathbf{y}_{02})$ are two generic initial conditions of systems Eq.(1.3a) and Eq.(1.3b). An occurrence of such CS Eq.(1.5) indicates that slave

systems forget their initial states, so their functional control defined by Eq.(1.4) takes place.

The properties of the synchronization manifold allow us to divide the GS into two types [35]:

1. The weak GS, which takes place for the continuous but non-smooth map $\boldsymbol{\psi}$ when the global dimension of the strange attractor d^G, located in the whole phase space $\mathbf{X} \oplus \mathbf{Y}$, is larger than the attractor dimension of the driving system d^D, i.e.,
$$d^G > d^D. \tag{1.6}$$

2. The strong GS, when the functional $\boldsymbol{\psi}$ is smooth and we have:
$$d^G = d^D. \tag{1.7}$$
i.e., the response oscillator does not influence the global attractor.

The attractor dimensions d^G and d^D can be approximated by the Lyapunov dimension d^L calculated from the spectrum of Lyapunov exponents, written in order $\lambda_1 > \lambda_2 > \cdots > \lambda_k$, according to the Kaplan and Yorke conjecture [56] defined by the formula
$$D_L = j + \frac{\sum_{i=1}^{j} \lambda_i}{|\lambda_{j+1}|}, \tag{1.8}$$
where j is the largest integer number for which the following inequality is fulfilled:
$$\sum_{i=1}^{j} \lambda_i \geq 0. \tag{1.9}$$

1.4. Phase and imperfect phase synchronization

Huygens first has observed the phenomenon of phase synchronization (PS) and described the anti-phase synchronization of periodic self-excited pendulums [57]. This effect, also called the out of phase, found many practical applications [1], it was observed i.e. in the excited periodically Van der Pol oscillator [58]. PS can be defined based on the definition of the classical linear theory of vibrations.

Considering two coupled oscillators phases ϕ_1 and ϕ_2 was found that PS occurs when inequality is satisfied inequality $|n\phi_1 - m\phi_2| < const$ for any integer values of n and m. This relationship does not impose any conditions attaching amplitude of these oscillators, they remain arbitrary and completely uncorrelated with each other. This phenomenon is related to the weak interactions (weak interaction) between the systems. With the increase of the feedback value (strong interaction), in the case of identical oscillators, synchronized amplitude occurs, namely CS or, when systems are almost identical, ICS.

From an engineering point of view precise and easy determine the phase of the oscillator is vary important. We can not always define exactly phase, especially in the non-coherent phase systems still looking for a PS detection methods. However, for oscillators, the phase portrait (x, y) is phase coherent (it looks like a rotation around a fixed point, which is characteristic of all linear systems and certain chaotic), phase ϕ can be represented by

$$\phi = \arctan\left(\frac{y}{x}\right), \tag{1.10}$$

where x and y are the coordinates making up the phase plane, for many oscillators x corresponds to displacement and y corresponds to derivative of displacement - velocity. In [19] with the definition of the phase based on a Hilbert transform, however, this method is cumbersome in practical use, because it requires the use of fast Fourier transform (FFT) and its inverse (IFFT). Another worth noting detection method is based on the number of passes through the plane Poincaré, the average value of the frequency takes the value

$$\omega = \lim_{t->\infty} 2\pi\frac{N_t}{t} = 0 \tag{1.11}$$

where N_t is the number to go by plane Poincaré at the time of observation t. Its main advantage is the simplicity and averaged.

The occurrence of the PS in the autonomous systems is connected with the spectrum of Lyapunov exponents. Such cases have been studied in paper [19, 24].

Analogously, IPS is a situation where phase slips occur within a PS regime [37].

1.5. Lag and imperfect lag synchronization

LS is a step between PS and CS. It implies the asymptotic boundedness of the difference between the output of one system at time t and the output of the other shifted in time of a lag time τ_{lag} [24]. This implies that the two outputs lock their phases and amplitudes, but with the presence of a time lag [24].

ILS implies that the two systems are most of the time verifying LS, but intermittent bursts of local non-synchronous behaviour may occur [24, 36] in correspondence with the passage of the system trajectory in particular attractor regions wherein the local Lyapunov exponent along a globally contracting direction is positive [24, 36].

1.6. Cluster synchronization

In networks composed of more than two elements can observe the appearance of the cluster synchronization (partial) [47, 49, 50]. In the case of CS entire network, time evolution of all its nodes is identical (after a transitional period), regardless of the initial conditions. In contrast, when the emerging group of mutually synchronized oscillators phenomenon of cluster synchronization is observed in spite of absence of CS of entire network. This behaviour was discovered in networks of coupled map [42] and coupled chaotic oscillator [43, 44, 45, 46]. The problem of existence of clusters is related to the existence and stability of the synchronization.

Chapter 2

Types of couplings

Very important in the study of a networks are also types of couplings between oscillators. In the literature dealing with networks of coupled oscillators or multi-degree-of-freedom systems, a huge number of definitions and terms describing various kinds of couplings between the dynamical systems can be found (Pikovsky et. al. in [2], Pecora and Carroll in [11, 59], Boccaletti et. al. in [14] and many others [26, 60, 61, 62, 63, 64]). Consequently, in these works various criterions of the coupling classification are given [34]. The classification of couplings presented here can be treated as a part of the theoretical background for the investigation of the complete synchronization phenomenon. Therefore, this survey is mainly focused on cases making an occurrence of such synchronization possible.

The dynamics of any set of N interacting oscillators can be described in the following block form

$$\dot{\mathbf{x}} = \mathbf{F}(\mathbf{x}) + \sum_{j=1}^{M} \sigma[\mathbf{G}_j \otimes \mathbf{H}_j(\mathbf{x})]. \tag{2.1}$$

Here $\mathbf{x} = (\mathbf{x}_1, \mathbf{x}_2, \ldots, \mathbf{x}_N) \in \Re^m$, $\mathbf{F}(\mathbf{x}) = (\mathbf{f}_1(\mathbf{x}_1), \ldots, \mathbf{f}_N(\mathbf{x}_N))$, $\mathbf{H}_j : \Re^m \rightarrow \Re^m$ are linking (output) functions of each oscillator variables that are used in the coupling, $\mathbf{G}_j$ is the connectivity matrix, i.e., the Laplacian matrix representing the M-number of possible topologies of connections between the network nodes corresponding to a given linking function $\mathbf{H}_j$, σ is an overall coupling coefficient and $\otimes$ is a direct (Kronecker) product of two matrices [65]. Such a product of two

matrices $\mathbf{G}$ and $\mathbf{H}$ is given in the block form by

$$\mathbf{G} \otimes \mathbf{H} = \begin{pmatrix} G_{11} & G_{12} & \dots & G_{1N} \\ G_{21} & G_{22} & \dots & G_{2N} \\ \vdots & \vdots & \ddots & \vdots \\ G_{N1} & G_{N2} & \dots & G_{NN} \end{pmatrix}$$

The Eq. (2.1) describe a general case of the oscillatory connections, where there are different (i.e., they can be non-identical) m-dimensional node systems $\mathbf{f}_i(\mathbf{x}_i)$ with an arbitrary topology of connections and different linking functions $\mathbf{H}_j$.

Here are some examples of couplings and connections between dynamical systems which can be seen in the context of the systems analysed in this dissertation (Fig. 1).

2.1. Negative feedback

Negative feedback is a process commonly met in nature and human environment naturally within living organisms [66], and can be seen in many other fields from chemistry and economics to social behaviour and the climate research. It occurs when the result of a process influences the operation of the process itself in such a way as to reduce changes. Feedback can produce stability and reduce the effect of fluctuations. Negative feedback loops in which just the right amount of correction is applied in the most timely manner can be very stable, accurate, and responsive. It is also widely used in mechanical and electronic engineering. General negative feedback of systems are studied in control systems engineering. A more qualitative application of feedback is found in educational and management assessment, which is related by Roos and Hamilton [67] to the early work on cybernetics by Norbert Wiener [68, 69].

Negative feedback causes that a part of the system output, inverted, is supplied into the system input; generally, as a result, fluctuations are damped (their amplitude decreases). Many real-world physical, biological, chemical and engineering systems have one or several points around which the system oscillates. In response to a perturbation, a negative feedback system with such

point(s) will tend to re-establish the equilibrium. In engineering, mathematics and physical and biological sciences, common terms for the points around which the system gravitates include: attractors, stable states, equilibrium points. The term negative refers to the sign of the multiplier in mathematical models for the feedback.

It may be noted that the signals in the system change form point to point. So, for example, a disturbance in heat input to a house (maybe a change in weather) is interpreted by a thermometer as a change in temperature, converted by the thermostat into an electrical error signal to the controller that commands gas control valves and an igniter, ultimately changing the heat provided by a furnace to counteract the initial disturbance in heat input to the house.

In contrast, positive feedback is a feedback in which the system responds in the same direction as the perturbation, resulting in amplification of the original signal instead of stabilizing it. This kind of feedback tends to cause system instability. Positive feedback in mechanical design causes tipping-point, or 'over-centre', mechanisms to snap into position, for example in switches and locking pliers. Out of control, it can cause bridges to collapse.

Negative feedback as a control and self-regulation technique may be seen in the dynamical systems. It is also the most common method that leads the synchronization of coupled oscillators. In general, an i-th subsystem connected to other $N-1$ subsystems of the entire system can be represented by

$$\dot{\mathbf{x}}_i = \mathbf{f}(\mathbf{x}_i) + \sum_{j=1}^{N-1} \sigma G_{ij} \mathbf{D}\mathbf{g}(\mathbf{x}_i, \mathbf{x}_j), \tag{2.2}$$

where $\mathbf{g}(\mathbf{x}_i, \mathbf{x}_j) \in \Re^k$ is a coupling vector and $\mathbf{D}$ is an $m \times m$ linking matrix of constant components. $\mathbf{D}$ and $\mathbf{g}$ are the same for each pair of coupled oscillators. According to Eq. (2.1) the output function is $\mathbf{H}(\mathbf{x}) = \mathbf{D}\mathbf{g}(\mathbf{x}_i, \mathbf{x}_j)$. Various schemes and kinds of the negative feedback coupling can be classified with different forms of the coupling vector $\mathbf{g}$, the connectivity matrix $\mathbf{G}$ and the output function $\mathbf{H}$.

2.1.1 Linear and nonlinear coupling

The coupling between dynamical systems is called linear coupling if all components of the coupling vector **g** (Eq. (2.1)) are linear terms, in example

$$\mathbf{g}(\mathbf{x}_i, \mathbf{x}_j) = [x_{j1} - x_{i1},\, x_{j2} - x_{i2},\, \ldots,\, x_{jm} - x_{im}]^T. \tag{2.3}$$

On the other hand, if components of the coupling vector are not defined linearly, then the coupling is nonlinear, e.g.,

$$\mathbf{g}(\mathbf{x}_i, \mathbf{x}_j) = [(x_{j1} - x_{i1})^3,\, (x_{j2} - x_{i2})^3,\, \ldots,\, (x_{jm} - x_{im})^3]^T. \tag{2.4}$$

2.1.2 Mutual and unidirectional coupling

Let consider the simplest, double-oscillators case for $N = 2$ of the system Eq. (2.1) with the negative feedback coupling described by

$$\begin{Bmatrix} \dot{\mathbf{x}}_1 \\ \dot{\mathbf{x}}_2 \end{Bmatrix} = \begin{Bmatrix} \mathbf{f}_1(\mathbf{x}_1) \\ \mathbf{f}_2(\mathbf{x}_2) \end{Bmatrix} + \sigma \begin{pmatrix} -\mathbf{D}_1 & \mathbf{D}_1 \\ \mathbf{D}_2 & -\mathbf{D}_2 \end{pmatrix} \begin{Bmatrix} \mathbf{x}_1 \\ \mathbf{x}_2 \end{Bmatrix}, \tag{2.5}$$

which is schematically depicted in Fig. 2.1. The corresponding connectivity matrix is:

$$\mathbf{G} = \begin{pmatrix} -1 & 1 \\ 1 & -1 \end{pmatrix}. \tag{2.6}$$

The connection of subsystems in system (2.5) is called the mutual coupling due

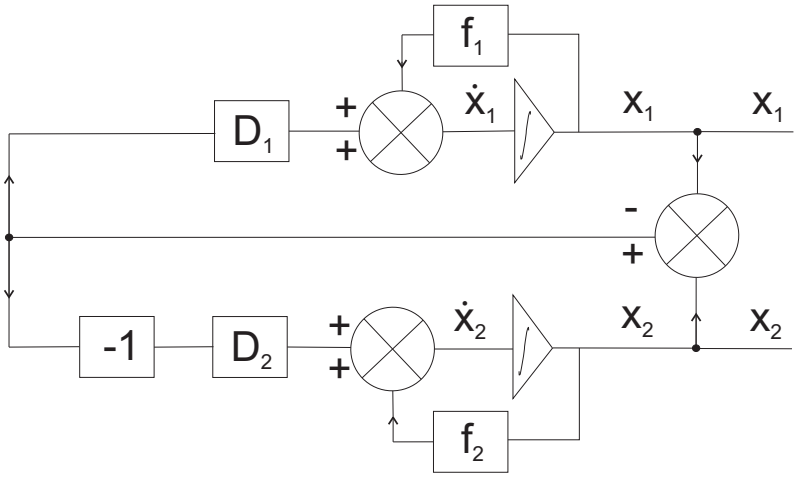

Figure 2.1: A scheme the negative feedback coupling of two systems.

to a bidirectional interaction between both subsystems, which causes reciprocal control of each other behaviour. For $\mathbf{D}_1 = \mathbf{D}_2$, a symmetrical mutual coupling takes place.

When one of the linking matrices in Eq. (2.5) possesses all zero elements (say $\mathbf{D}_1 = 0$), the coupling is unidirectional. Then, the dynamics of one of the coupled systems (i.e., $\dot{\mathbf{x}}_1 = \mathbf{f}_1(\mathbf{x}_1)$) is independent of the coupling because the related connectivity matrix has a form:

$$\mathbf{G} = \begin{pmatrix} 0 & 0 \\ 1 & -1 \end{pmatrix}. \tag{2.7}$$

Thus, in this scheme of the coupling, the dominant (reference) system controls the behaviour of its disturbed neighbour. Therefore, such a configuration is called a drive-response or master-slave coupling.

2.1.3 Diffusive and global coupling

The previous 2.1.2 has shown that the coupling can be classified by a form of the matrix G. The structure of the connectivity is a good property for categorizing the type of coupling in larger populations (networks) of oscillators. One of well-understood coupling mechanisms in such networks is the global coupling (also called the all-to-all coupling) through which each oscillator interacts with equal strength with all of the other oscillators in the system (Fig. 2.2a). Hence, the matrix G has a regular symmetrical structure:

$$\mathbf{G} = \begin{bmatrix} 1-N & 1 & \dots & 1 \\ 1 & \ddots & \ddots & \vdots \\ \vdots & \ddots & \ddots & 1 \\ 1 & \dots & 1 & 1-N \end{bmatrix}, \tag{2.8}$$

and the dynamics of a single node of such a network with the linear coupling is described by:

$$\dot{\mathbf{x}}_i = \mathbf{f}(\mathbf{x}_i) + \sum_{j=1}^{N} G_{ij}\mathbf{D}(\mathbf{x}_j - \mathbf{x}_i). \tag{2.9}$$

On the other hand, the diffusive coupling is a qualitatively different scheme of interactions in the network due to its local character. Such a connection is equally

referred to as the nearest-neighbour coupling (Fig. 2.2b). For an arbitrary i-th oscillator, we have:

$$\dot{\mathbf{x}}_i = \mathbf{f}(\mathbf{x}_i) + \mathbf{D}\mathbf{g}(\mathbf{x}_{j-1} + \mathbf{x}_{j+1} - 2\mathbf{x}_i), \tag{2.10}$$

and the corresponding connectivity matrix is also symmetrical:

$$\mathbf{G} = \begin{bmatrix} -2 & 1 & 0 & \dots & 0 & 1 \\ 1 & -2 & 1 & \ddots & \dots & 0 \\ 0 & 1 & \ddots & \ddots & \ddots & \vdots \\ \vdots & \ddots & \ddots & \ddots & 1 & 0 \\ 0 & \dots & \ddots & 1 & -2 & 1 \\ 1 & 0 & \dots & 0 & 1 & -2 \end{bmatrix}, \tag{2.11}$$

The diffusive coupling has been initially introduced on the basis of a diffusion-like process [70]. Unlike the global coupling, which generates a mean field in the ensemble of oscillators, the diffusive coupling produces a local interaction only between each component of the network and its nearest neighbours [71].

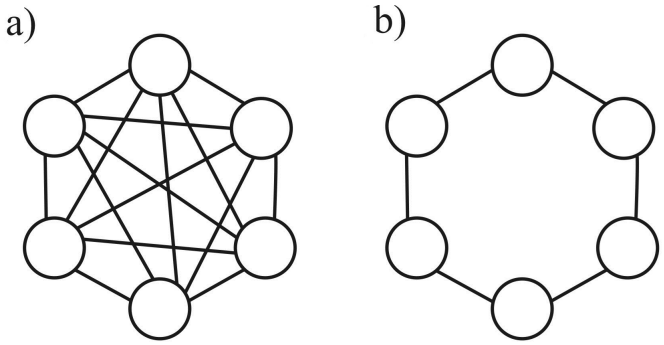

Figure 2.2: Types of network connections: a) global (all-to-all) coupling, b) diffusive (nearest-neighbour) coupling.

In general, the system under consideration (Fig. 1) can be classified as a case of diffusive coupling due to nearest-neighbour structure of connections.

2.1.4 Real and imaginary coupling

The structure of the connectivity matrix is not a sole factor that can be used for the coupling classification. They can be classified also on the basis of eigenvalues

γ_j ($j = 0,\ 1,\ 2,\ \ldots,\ N-1$) of the matrix G. According to the Master Stability Function (MSF) concept [72, 73], described in the next Sec., the synchronizability of a network of oscillators can be quantified by the eigenvalue spectrum of the connectivity matrix. For an arbitrary configuration of connections between network nodes, all or a part of these eigenvalues can be complex numbers, i.e.,

$$\gamma_j = \alpha_j - i\beta_j, \tag{2.12}$$

where α_j and β_j are real and imaginary components of the eigenvalue, respectively. Let us consider two extremely opposite variants, i.e., only real (i) or only imaginary (ii) eigenvalues of the matrix G.

If the coupling between the oscillators is mutual and symmetrical, then it results in the symmetric connectivity matrix G. Such a situation takes place in coupled mechanical systems, where an interaction is mutual. Then matrix G possesses only real eigenvalues, so $\alpha_j \neq 0$ and $\beta_j = 0$. Hence, this symmetric coupling is called the real coupling and can be interpreted as a kind of damping [73]. The instances of the real coupling are global and diffusive couplings represented by symmetric matrices in Eq.(2.8) and Eq.(2.11), respectively. All the real eigenvalues of them can be calculated according to following analytical formulas:

$$\gamma_j = -N, \tag{2.13}$$

for the global, and

$$\gamma_j = -4\sin^2\frac{j\pi}{N}, \tag{2.14}$$

for diffusive coupling.

Thus the coupling in the system under consideration (Fig. 1) can be interpreted as a real case.

2.1.5 Dissipative, conservative and inertial coupling

Such possibilities of diffusive couplings are in fact counterparts of the diagonal and non-diagonal coupling cases described above and these terms can be used interchangeably. In order to demonstrate this equivalence of the terms, let us consider simple examples of the coupled mechanical systems depicted

in Figs. 2.3. The motion of each mass in the double-oscillatory system from Fig. 2.3a is described by the following pair of ODEs:

$$\dot{x}_i = y_i, \tag{2.15a}$$

$$\dot{y}_i = -x_i - hy_i + \sigma_c(x_j - x_i) + \sigma_d(y_j - y_i), \tag{2.15b}$$

where i, j = 1,2. The corresponding linking matrix is:

$$\mathbf{H} = \begin{pmatrix} 0 & 0 \\ \sigma_c & \sigma_d \end{pmatrix}, \tag{2.16}$$

For $\sigma_c = 0$ and $\sigma_d > 0$, the coupling has a dissipative character because

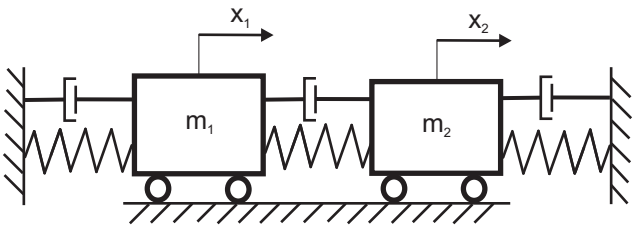

Figure 2.3: 2-DoF coupled mechanical systems: a) Masses-springs-dampers connection, b) double pendulum.

it is realized by the damping component (viscous damper) with dissipation proportional to the velocity y. Therefore, it is also called the velocity coupling [74]. In the opposite case ($\sigma_c > 0$ and $\sigma_d = 0$) we can observe a position coupling, which uses the displacement x [74]. Its character is conservative because it does not contribute in any way to dissipation, so the divergence of the system does not change in the presence of the coupling. If both coupling coefficients are nonzero, then we have a combined conservative-dissipative coupling.

In Fig. 2.3b an inertial coupling of two mathematical pendulums is shown. Here, a cause of linking are inertial components of differential equations. The linear version of the double pendulum from Fig. 2.3b is given in the form:

$$\ddot{\varphi}_1 + 0.5\ddot{\varphi}_2 + \omega^2\varphi_1 = 0, \tag{2.17a}$$

$$\ddot{\varphi}_1 + \ddot{\varphi}_2 + \omega^2\varphi_1 = 0, \tag{2.17b}$$

where $\omega^2 = g/l$. It is clearly visible (Eqs. (2.17b) that both pendulums are coupled with inertial variables, so we can refer to it as the acceleration coupling.

In the considered case of mechanical structure (Fig. 1) combination of dissipative, conservative and inertial coupling can be observed.

2.2. Drive with a common signal

Another kind of coupling which can lead to the synchronous behaviour of dynamical systems is a drive with a common signal. In order to demonstrate such a case, let us consider an array of N identical oscillators driven by the common external excitation $e(t)$ for flows or en for maps. There is not any kind of direct linking between them (a negative feedback, a diffusive or inertial coupling, etc.). Thus, this case can be reflected as a star-type connection between oscillators, where a unidirectional coupling from the central node (exciter) to the remaining oscillators is realized, as shown schematically in Fig. 2.4. The dynamics of the entire system can be described in the block form:

$$\dot{\mathbf{X}} = \mathbf{F}(\mathbf{X}) + q(\mathbf{1}_N \otimes \mathbf{h}(\mathbf{e})), \tag{2.18}$$

for flows, and

$$\mathbf{X}_{n+1} = \mathbf{F}(\mathbf{X}_n) + q(\mathbf{1}_N \otimes \mathbf{h}(\mathbf{e}_n)) \tag{2.19}$$

for maps. Here $X = [x_1,\, x_2,\, \ldots,\, x_N]^T$, $x_i \in \Re$, $F(X) = [f(x_1),\, \ldots,\, f(x_N)]^T$, $1N$ is the $N \times N$ identity matrix, q is the overall driving strength, is a direct (Kronecker) product of two matrices, and h : is an output function of the external excitation variables $e = [e_1,\, e_2,\, \ldots,\, e_k]^T$ that are used in the drive.

In order to recognize the synchronizability of response oscillators (Eqs. (2.18) and (2.19)), the properties of the GS have been employed.

The system from Fig. 1 is driven by common signal - external kinematic excitation, which is independent on the system response.

2.3. Autonomous driver decomposition

An idea of autonomous driver decomposition was introduced by [11] as a one of the first coupling configurations making the chaos synchronization possible.

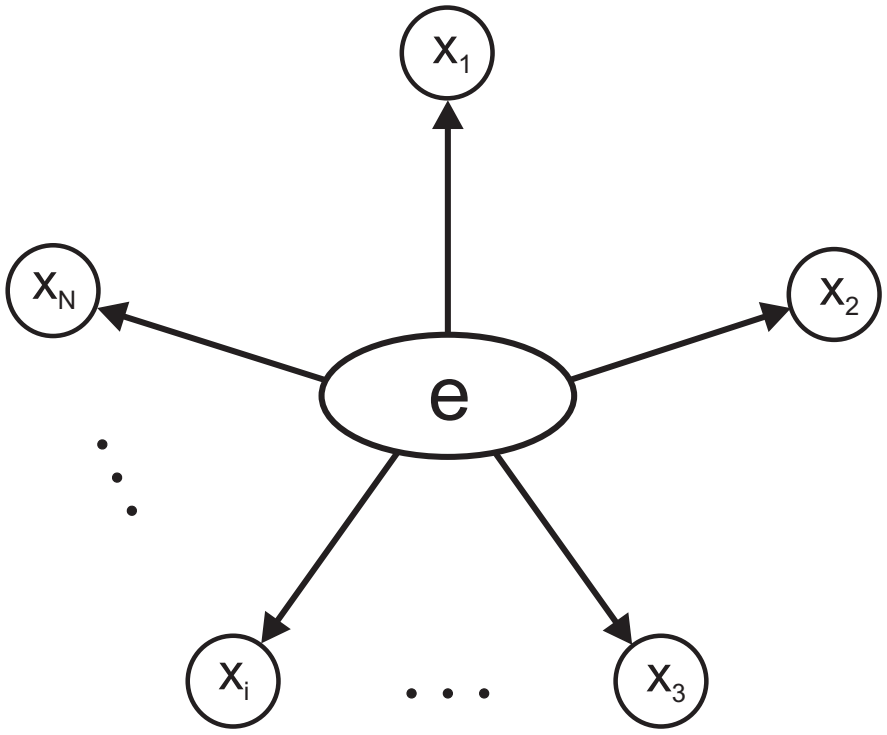

Figure 2.4: Common drive - a star configuration with a unidirectional coupling.

In order to explain this issue, let us consider an autonomous k-dimensional ($z \in \Re^k$) dynamical system:

$$\dot{\mathbf{z}} = \mathbf{f}(\mathbf{z}), \tag{2.20}$$

The system (2.20) can be arbitrarily divided into two subsystems. One of them is m-dimensional, thus the second one is $(k-m)$-dimensional, i.e.,

$$\dot{\mathbf{z}} = \mathbf{g}(\mathbf{y},\ \mathbf{w}), \tag{2.21a}$$

$$\dot{\mathbf{w}} = \mathbf{h}(\mathbf{y},\ \mathbf{w}). \tag{2.21b}$$

where $y = [z_1, z_2, \ldots, z_m]^T$, $g = [f_1(z), f_2(z), \ldots, f_m(z)]^T$, $w = [z_{m+1}, z_{m+2}, \ldots, z_k]^T$ and $h = [f_{m+1}(z), f_{m+2}(z), \ldots, f_k(z)]^T$. Create now a new subsystem $\dot{w}$ identical to the w subsystem:

$$\dot{\mathbf{w}}' = \mathbf{h}(\mathbf{y},\ \mathbf{w}'). \tag{2.22}$$

As a result, we obtained an augmented $(2k-m)$-dimensional system. Here, Eqs. (2.21a) and (2.21b) define the driving system, whereas the system of Eq. (2.20) represents the response subsystem. Its evolution is controlled by a driving signal y from subsystem.

The concept of autonomous driver decomposition can be illustrated more clearly by substituting, e.g., a classical Rössler system into general Eqs. (2.21a-b) and (2.22):
drive :

$$\dot{\mathbf{y}} = \mathbf{g}(\mathbf{y},\ \mathbf{w}) \quad \rightarrow \quad \dot{x} = -y - z \tag{2.23a}$$

$$\dot{\mathbf{w}} = \mathbf{h}(\mathbf{y},\ \mathbf{w}) \quad \rightarrow \quad \begin{aligned} \dot{y} &= x - ay \\ \dot{z} &= b + z(x - c), \end{aligned} \tag{2.23b}$$

response :

$$\dot{\mathbf{w}}' = \mathbf{h}(\mathbf{y},\ \mathbf{w}') \quad \rightarrow \quad \begin{aligned} \dot{y}' &= x - ay' \\ \dot{z}' &= b + z'(x - c). \end{aligned} \tag{2.24a}$$

In Eqs. (2.23) and (2.24), the x-driving is realized because the same driving signal x is applied to both subsystems w and $\dot{w}$. The CS of signals w and $\dot{w}$ is possible if the so-called conditional Lyapunov exponents (CLEs) are negative.

2.4. Active-passive decomposition

A scheme of active-passive decomposition, proposed by [75], can be treated as even a more general drive-response configuration than the autonomous driver decomposition described in the previous section. The idea of active-passive decomposition consists in rewriting the original autonomous system (2.20) as a non-autonomous one:

$$\dot{\mathbf{z}} = \mathbf{f}(\mathbf{z}, \mathbf{s}(t)), \tag{2.25}$$

where $s(t)$ is a driving signal. However, this signal is not an independent external drive, like in Eqs. (2.18) and (2.19), but it is a function of autonomous system variables, i.e., $s(t) = h(x)$ or $ds/dt = h(x)$. Here, the CS state is also understood as an identical behaviour of the non-autonomous system (2.25) and its copy (or copies) representing the response system:

$$\dot{\mathbf{z}}' = \mathbf{f}(\mathbf{z}', \mathbf{s}(t)), \tag{2.26}$$

In order to exemplify the considered type of the system decomposition, let us substitute the Lorenz system into Eqs. (2.25) and (2.26):

drive :

$$\dot{x} = -\sigma x + s(t) \tag{2.27a}$$

$$\dot{y} = x(r-z) - y \tag{2.27b}$$

$$\dot{z} = xy - bz, \tag{2.27c}$$

response :

$$\dot{x}' = -\sigma x' + s(t) \tag{2.28a}$$

$$\dot{y}' = x'(r-z') - y' \tag{2.28b}$$

$$\dot{z}' = x'y' - bz', \tag{2.28c}$$

where the driving signal is $s(t) = y$. The results presented in Ref. [75] show that for the classical Lorenz oscillator, the CS of the drive with the response system occurs for regular and also for chaotic behaviour of the driving signal $s(t)$.

Last two cases presenting in Sec. 2.3 and Sec. 2.4 do not occur in the coupled system under consideration (Fig. 1). However their properties can be helpful in explanation of possible synchronous behaviour of pendulums.

Chapter 3

Stability of synchronous state

This chapter presents the theoretical background necessary for the analysis of dynamics of coupled nonlinear oscillators, especially in context of synchronization. Stability of synchronization states, the idea and application of Lyapunov exponents and concept of transversal and conditional Lyapunov exponents are discussed. Also the idea of master stability function (MSF) allowing synchronization stability test is presented.

3.1. Lyapunov stability

The notion of stability is as old as the world is and has a very clear intuitive meaning. Take, for example, an ordinary pendulum – placed in the lowest position, is stable, but put in the utmost upper position, is unstable. Stable and unstable situations can be met everywhere - in mechanical motion, in technical devices, in medical treatment (stable or unstable state of the patient), in currency exchange and so on. The rigorous mathematical theory of stability had appeared in the course of studying mechanical motions with some early definitions of stability given by Joseph L. Lagrange (for example, a stable position for a pendulum is when its potential energy attains a minimum). Another definitions were introduced later by others, including by S. Poisson [76, 77].

Perhaps the most widely known theory of stability of motion well applicable to engineering and many other applied problems is due to Alexander M. Lyapunov - a distinguished Russian mathematician famous for his work on stability theory

and problems in probability [78]. Lyapunov's concepts and methods are widely used in the mathematical and engineering communities. The notions of Lyapunov stability and asymptotic stability are followed by those of exponential stability, conditional stability, stability over a part of the variables, stability under persistent disturbances and other. In terms of such notions many natural phenomena were explained (as in astronomy, for example).

Tool to assess the quality of motion of dynamic system is the criterion of stability introduced by Lyapunov.

Definition 3.1 (Stability according to Lyapunov)
The trajectory $\mathbf{x}(t)$ *is stable in the Lyapunov sense, if for any, arbitrary small* $\varepsilon > 0$*, there exists such* $\delta > 0$ *that for any initial point of trajectory taken from the neighbourhood* $\mathbf{x}(0)$*,* $\| \mathbf{x}(0) - \mathbf{y}(0) \| < \delta$*, for every* $t > 0$*, the inequality*

$$\| \mathbf{x}(t) - \mathbf{y}(t) \| < \varepsilon \tag{3.1}$$

is fulfilled.

The interpretation of this definition leads to the conclusion that the system is stable according to Lyapunov criterion in the case when the two phase system trajectories initialized with slightly different initial conditions are close to each other during the subsequent time evolution of the system. A stronger version of this theorem defines asymptotic stability [80].

Definition 3.2 (Asymptotic stability according to Lyapunov)
The trajectory $\mathbf{x}(t)$ *is asymptotically stable in the Lyapunov sense, when for any, arbitrary small* $\varepsilon > 0$*, there exists such* $\delta > 0$ *that under the condition* $\| \mathbf{x}(0) - \mathbf{y}(0) \| < \delta$ *(for any initial point of* $\mathbf{x}(0)$*), for all* $t > 0$*, the following relation takes place*

$$\lim_{t \to \infty} \| \mathbf{x}(t) - \mathbf{y}(t) \| = 0. \tag{3.2}$$

These definitions can also be used in the context of determining the stability synchronization status. Indicate analogies between the stability criteria by Lyapunov (3.1) and its asymptotic version (3.2) according to practical synchronization conditions (3.2) and complete (3.1).

3.2. Lyapunov exponents

Over the past few decades greatly increased interest in the theory of nonlinear dynamical systems. Undoubtedly, this growth has contributed to rapid advances in computational capabilities of computers, which enabled the numerical analysis of these dynamical systems, which resulted in the penetration of nonlinear dynamics to other research areas in which it had not yet apply, such as physics, biology, economics, chemistry, mechanics and even quantum mechanics. The natural result of interest in nonlinear dynamical systems is to develop techniques for presentation and evaluation of the motion quality of these systems. A simple method of presenting the dynamics of the system, such as time series, phase portraits, Poincaré maps, bifurcation diagrams, are not always accurately assess the nature of its motion. A more precise tools to assess the quality of motion is a frequency spectrum basing on fast Fourier transform (FFT), and in particular the criteria expressed in numerical form, such as Lyapunov exponents, fractal dimension, the autocorrelation function, the Kolmogorov entropy and the winding number.

Lyapunov exponents are one of the most reliable criteria for identifying the nature of motion of nonlinear dynamical systems [78, 79]. These numbers illustrate the exponential divergence or convergence of close trajectories on the attractor. To make a satisfactory assessment of the motion quality the knowledge of only the highest value of this exponent is enough. If this value does not exceed zero the motion of the system is regular (periodic or quasi-periodic). Otherwise (the largest positive Lyapunov exponent), the solution tends to the chaotic attractor. However, in practice, experimental motion manifests with the phenomenon of regular synchronization. On the other hand, the lack of synchronization indicates irregular, chaotic motion. Thus, there appears a clear correlation between the states of synchronization and desynchronization and the values of Lyapunov exponent. This dependence allows the use of the phenomenon of synchronization for the detection of chaos and estimation of the largest Lyapunov exponent of any dynamical system.

Lyapunov exponents in a form useful for dynamical systems were introduced by Russian mathematician V. I. Oseledec in the year 1968 [81]. They denote

the number describing the average behaviour of the derivative along the phase trajectories, which are a logarithmic measure of the sensitivity of dynamical system for arbitrarily small changes in initial conditions. These numbers represent a qualitative and quantitative illustration of the stability criterion of dynamical systems [78], formulated by the Russian scientist A. M. Lyapunov.

In general, the concept of Lyapunov exponents can be represented by equation (3.3). Let's assume that the initial distance of two infinitely close phase trajectories is $\varepsilon(0)$. After a time τ distance is given by the following formula

$$\varepsilon(\tau) = \varepsilon(0)\, e^{\lambda \tau}, \tag{3.3}$$

where λ is the Lyapunov exponent. From depending (3.3) it follows that close phase trajectories diverge only when $\lambda > 0$. However, if $\lambda \leq 0$ phenomenon of sensitivity to initial conditions does not occur, and it is characteristic of most dynamical systems. Lyapunov exponents determined for both representations with discrete time ($n \in \mathfrak{N}$), described by differential equations, as well as for data streams phase differential equations, in which time is continuous ($\tau \in \mathfrak{R}$).

From a mathematical point of view Lyapunov exponents can be considered as a generalized concept of the eigenvalues at the critical point [82]. Let us consider a dynamical system defined by differential equation

$$\frac{d\mathbf{x}}{d\tau} = \mathbf{f}(\mathbf{x},\, a), \tag{3.4}$$

where

$$\mathbf{x} = [x_1,\, x_2,\, \ldots,\, x_k]^T, \tag{3.5a}$$

$$\mathbf{f} = [f_1,\, f_2,\, \ldots,\, f_k]^T \tag{3.5b}$$

is a differentiable function which depends on the parameter a and $x \in \mathfrak{D}$ ($\mathfrak{D}$ is an open set in the phase space $\mathfrak{R}^k$).

The solution of Eq. (3.4) for the initial condition $\mathbf{x}(0) = \mathbf{x}_0$ can be written as follows

$$\mathbf{x}(\tau) = \mathbf{T}(\tau)\, \mathbf{x}_0, \tag{3.6}$$

where $\mathbf{T}(\tau)$ is a mapping describing time evolution of all points in the phase space.

Let $\mathbf{y}(\tau)$ be a particular solution of system Eq. (3.4). After expanding Eq. (3.4) into a Taylor series in the neighbourhood of particular solution $\mathbf{y}(\tau)$ and neglecting all terms of order higher then one, we obtain

$$\frac{d\mathbf{x}}{d\tau} - \frac{d\mathbf{y}}{d\tau} = \frac{\mathbf{f}[\mathbf{y}(\tau)]}{\mathbf{x}} \left[\mathbf{x}(\tau) - \mathbf{y}(\tau)\right]. \tag{3.7}$$

For the analysis of stability of the solution $\mathbf{y}(\tau)$. Let's introduce a new variable $\mathbf{z}(\tau)$ which represents a difference between the disturbed solution $\mathbf{x}(\tau)$ and the particular one $\mathbf{y}(\tau)$ in the form

$$\mathbf{z}(\tau) = \mathbf{x}(\tau) - \mathbf{y}(\tau). \tag{3.8}$$

Substitution of the Eq. (3.8) into Eq. (3.7) gives the linearised equation in the following form

$$\frac{d\mathbf{z}}{d\tau} = \mathbf{J}\left(\mathbf{y}(\tau)\right)\, \mathbf{z}, \tag{3.9}$$

and

$$\mathbf{J}\left(\mathbf{y}(\tau)\right) = \frac{\mathbf{f}[\mathbf{y}(\tau)]}{\mathbf{x}} \tag{3.10}$$

is the Jacobian defined in the point $\mathbf{y}(\tau)$. Linearisation in the neighbourhood of particular solution described above was made in the way similar to linearisation in the neighbourhood of the critical point. Note, that in this case $\mathbf{y}(\tau)$ is not a constant function and $\mathbf{J}\left(\mathbf{y}(\tau)\right)$ is not a matrix with constant coefficients.

Let's assume that

$$\mathbf{y}(\tau = 0) = \mathbf{y}_0$$

is an initial point of the solution $\mathbf{y}(\tau)$, and

$$\mathbf{z}(0) = \mathbf{z}_0$$

the initial value of the disturbance introduced to the system. There exists a fundamental set of solutions for Eq. (3.9), which is composed of k linearly independent solutions of the equation

$$\frac{d\mathbf{Z}(\tau, \mathbf{y}_0)}{d\tau} = \mathbf{J}\left(\mathbf{y}(\tau)\right)\, \mathbf{Z}(\tau, \mathbf{y}_0). \tag{3.11}$$

Hence, the solution of Eq. (3.9) can be written as

$$\mathbf{z}(\tau) = \mathbf{Z}(\tau, \mathbf{y}_0)\, \mathbf{z}_0, \tag{3.12}$$

where $\mathbf{Z}(\tau, \mathbf{y}_0)$ is a fundamental matrix of solution to Eq. (3.9).

Definition 3.3 (Lyapunov exponent) *The Lyapunov exponent of linearised Eq. (3.9) is the number defined as*

$$\lambda_i = \lim_{\tau\to\infty} \frac{1}{\tau} \ln \parallel z^i(\tau,\, y_0,\, e^i) \parallel, \tag{3.13}$$

where $z^i(\tau,\, y_0,\, e^i)$ is the i-th fundamental solution of the system described by Eq. (3.9), e^i is i-th unit vector, and $\parallel . \parallel$ stand for any norm in the space $\Re^k$. Lyapunov exponent can be also defined by equality

$$\lambda_i = \lim_{\tau\to\infty} \frac{1}{\tau} \ln \parallel m_i(\tau) \parallel, \tag{3.14}$$

where $m_i(\tau)$ are eigenvalues of solution Eq. (3.12).

From the above considerations result that in the dynamical system given by equation (3.4) there exists a set of k Lyapunov exponents, i.e. their number is equal to the dimension of the phase space of the system. This collection $\{\lambda_i\}$ $(i = 1,\, 2,\, 3, \ldots,\, m)$ of real numbers ordered from largest to smallest is called the spectrum of Lyapunov exponents of the phase trajectory $y(\tau)$. The largest of them called $\{\lambda_i\}$ will be referred to the maximum. The set of Lyapunov exponents λ_1 may also be written as an ordered set of symbols: $+$, 0, $-$, which correspond to positive, zero and negative values of the Lyapunov exponent λ_i. From the properties of Lyapunov exponents results that their sum is equal to the divergence of the phase stream [82]. Thus, the volume of phase space $V(\tau)$, which evolves perturbed solution $x(\tau)$ ambient $y(\tau)$ is expressed as follows

$$V(\tau) = V(0)e^{\tau\sum_{i=1}^{k}\lambda_i}, \tag{3.15}$$

where $V(0)$ is initial volume of phase space. From equation (3.15) and under the divergence theorem [82] for dissipative dynamical systems can save

$$\sum_{i=1}^{n} \lambda_i < 0. \tag{3.16}$$

This dependence is always satisfied when in the systems where dissipation occurs.

When all Lyapunov exponents are negative ($\lambda_i < 0$), the solution of the system is a critical point which is the attractor. In the case of a periodic solution, while the attractor is stable limit cycle, the maximum exponent is zero ($\lambda_1 = 0$, $\lambda_i < 0$,

$i = 2, 3, \ldots, k$), and the attractor is quasi-periodic torus when is characterized by a pair of zeros maximum Lyapunov exponents ($\lambda_1 = 0,\ \lambda_2 = 0,\ \lambda_i < 0$, $i = 3, 4, \ldots, k$). In contrast, if the largest Lyapunov exponent is positive ($\lambda_i > 0$), the trajectory $y(\tau)$ for all $\tau > 0$ evolves in a limited set of phase space, called a strange, chaotic attractor. Such a set is defined by the trajectory Lyapunov instability, but is stable in the sense of Poisson limitations due to the solutions of equation (3.4).

Analytical calculation of Lyapunov exponents is possible only when dealing with simple dynamical systems. In the case of systems described with nonlinear differential equations numerical methods are used. The first robust algorithms for calculating the spectrum of Lyapunov exponents have been developed by Benettin et al. [83] as well as Shimada and Nagashima [84]. These approaches are based on the Oseledec theorem and can be applied for the system given by continuous and differentiable ODEs. The first numerical algorithm analysing the dynamics of dynamical systems, in terms of divergence closely phase trajectories, was presented by Henon and Heiles [85]. The algorithm for calculating the complete spectrum of Lyapunov exponents basing on Oseledec theorem was formed by Wolf [86, 87]. In subsequent years there have been algorithms for systems with discontinuities or time delay [88, 89, 90, 91, 92, 93].

3.3. Transversal Lyapunov exponents - Master Stability Function

During the research of the nonlinear systems dynamics, noted the need to redefine the idea of classical Lyapunov exponent to the current needs. In this way, concept of transversal Lyapunov exponents (TLEs) describing the stability of the synchronization manifold was introduced [94]. Especially noteworthy here is a concept of the MSF proposed by Pecora and Carroll [72], which can be treated as the representative one among the stability criterions based on the eigenvalue spectrum of the connectivity matrix.

In order to explain this concept let us take under consideration system

$$\dot{\mathbf{x}} = \mathbf{F}(\mathbf{x}) + \sigma[\mathbf{G} \otimes \mathbf{H}] \times \mathbf{x}, \tag{3.17}$$

where $\mathbf{x} = [\mathbf{x}_1,\ \mathbf{x}_2, \ldots,\ \mathbf{x}_N]^T \in \Re^m$, $\mathbf{F}(\mathbf{x}) = [\mathbf{f}(\mathbf{x}_1),\ \mathbf{f}(\mathbf{x}_2), \ldots,\ \mathbf{f}(\mathbf{x}_N)]^T$, σ is an overall coupling strength, $\mathbf{G}$ is a connectivity matrix and $\mathbf{H}$ is an output (linking) function.

As a tool for testing the stability of synchronous state, we have applied Lyapunov exponents. These quantities determine the divergence of nearby trajectories in directions transverse to the synchronization manifold ($\mathbf{x}_1 = \mathbf{x}_2 = \cdots = \mathbf{x}_N$), so they are called transversal Lyapunov exponents (TLEs – λ^T) [95]. Therefore, it requires separating the transverse modes from the longitudinal one in the variational equation. Deriving system (3.17), we obtain

$$\dot{\boldsymbol{\zeta}} = [D\mathbf{f} + \sigma \mathbf{G} \otimes D\mathbf{H}] \times \boldsymbol{\zeta}, \tag{3.18}$$

where $\boldsymbol{\zeta}_i$ represents an m-dimensional perturbation of the i-th node, $D\mathbf{f}$ is the Jacobi matrix of any node, i.e., the derivative with respect to the first argument of the function $\mathbf{f}(\mathbf{x}_i)$, the same for all oscillators on the synchronization manifold, and $D\mathbf{H}$ is the Jacobian of the linking function $\mathbf{H}$.

The next stage is a diagonalization of Eq. (3.18). Such block diagonalization leads to the uncoupling of variational Eq. (3.18) into blocks like in a mode analysis. After such a block diagonalization of the variational equation, there appear N separated blocks

$$\dot{\zeta}_k = [D\mathbf{f} + \sigma \gamma_k D\mathbf{H}]\zeta_k, \tag{3.19}$$

where ζ_k represents different transverse modes of a perturbation from the synchronous state and γ_k represents a k-th eigenvalue of the connectivity matrix $\mathbf{G}$, $k = 0,\ 1,\ 2, \ldots,\ N-1$. An orientation of the set of coordinates in the phase space of system (3.17) before and after the diagonalization is depicted in Fig. 3.1. For $k = 0$ we have $\gamma_0 = 0$ and Eq. (3.19) is reduced to the variational equation of the separated node system

$$\dot{\zeta} = D\mathbf{f}\zeta_k, \tag{3.20}$$

corresponding to the longitudinal direction located within the synchronization manifold (the coordinate $x_1^{\perp}$ in Fig. 3.1). All other k-th eigenvalues correspond to transverse eigenvectors (the coordinate $x_2^{\perp}$ in Fig. 3.1).

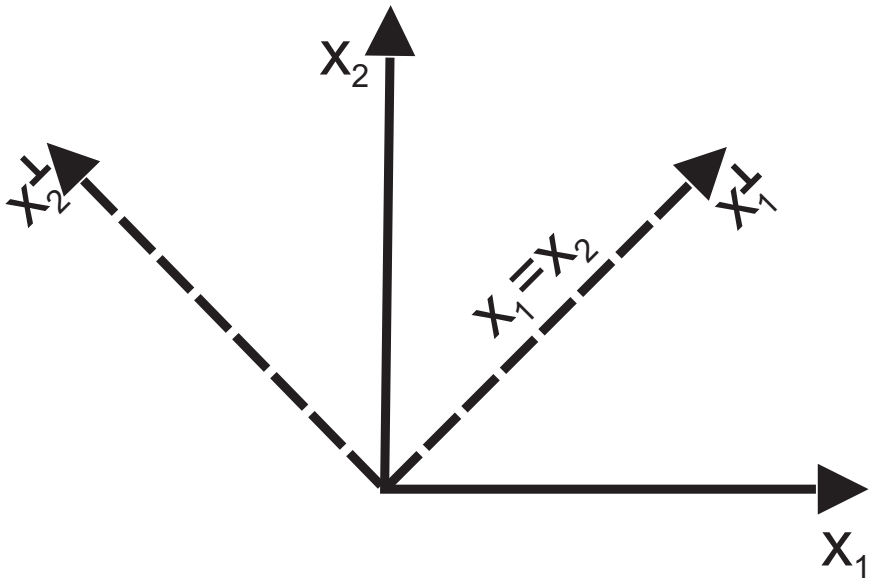

Figure 3.1: Orientation of the space coordinate systems of the phase space of system (3.17) before (continuous line) and after (broken line) the diagonalization.

In accordance with the MSF concept, a tendency to synchronization of the network is a function of the eigenvalues γ_k. Substituting $\sigma\gamma = \alpha + i\beta$, where $\alpha = \sigma Re(\gamma)$, $\beta = \sigma Im(\gamma)$ and γ represents an arbitrary value of γ_k, we obtain the generic variational equation

$$\dot{\zeta} = [D\mathbf{f} + (\alpha + i\beta)D\mathbf{H}]\zeta, \tag{3.21}$$

where ζ symbolizes an arbitrary transverse mode. The connectivity matrix $\mathbf{G}$ satisfies a zero row-sum ($\sum_{j=1}^{N} G_{ij} = 0$), so that the synchronization manifold $\mathbf{x}_1 = \mathbf{x}_2 = \cdots = \mathbf{x}_N$ is invariant and all the real parts of eigenvalues γ_k associated with transversal modes are negative ($Re(\gamma_{k\neq 0}) < 0$). Hence, we obtain the following spectrum of the eigenvalues of $\mathbf{G}$: $\gamma_0 = 0 \geq \gamma_1 \geq \gamma_{N-1}$. Now, we can define the MSF as a surface representing the largest TLE λ^T, calculated for generic variational equation (Eq. (3.21)), over the complex numbers plane (α, β). Obviously, the calculation of the MSF requires a simultaneous integration of the node system $d\mathbf{x}_i/dt = \mathbf{f}(\mathbf{x}_i)$. If an interaction between each pair of nodes is mutual

and symmetrical, then a real coupling of oscillators takes place (Subsec. 2.1.4), i.e., $\beta_k = 0$. In such a case, the MSF is reduced to a form of the curve representing the largest TLE as a function of the real number α (see Fig. 3.2) fulfilling the equation

$$\alpha = \sigma\gamma. \tag{3.22}$$

If all the eigenmodes corresponding to the discrete spectrum of eigenvalues $\sigma\gamma_k$ can be found in the ranges of negative TLE (Fig. 3.2a), then the synchronous state is stable for the considered configuration of couplings. On the other hand, if even only one of the eigenvalues is located in the area of positive TLE (Fig. 3.2b), then the global synchronization of all network nodes is unstable but, e.g., an appearance of the cluster synchronization is possible.

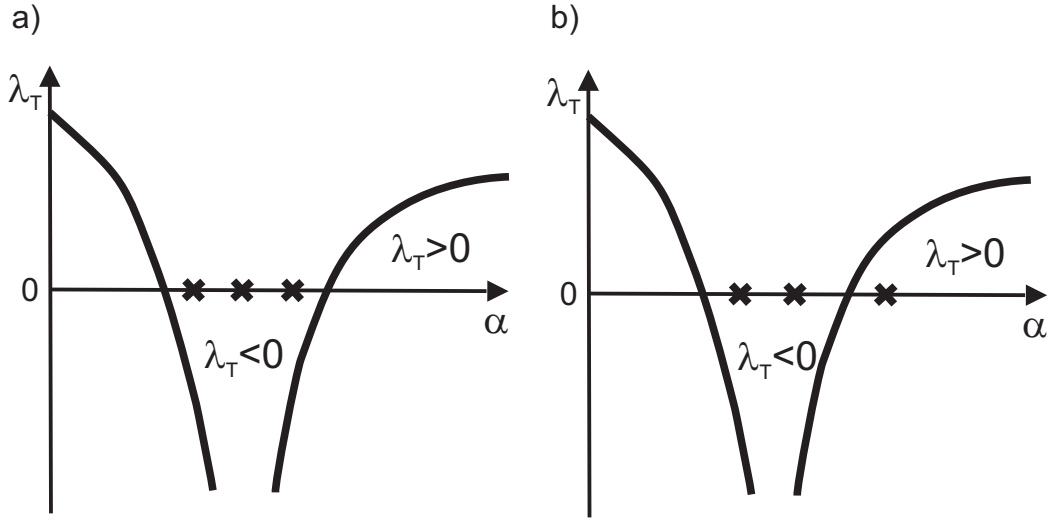

Figure 3.2: Visualization of any discrete spectrum of real eigenvalues of connectivity matrix on the background of the exemplary MSF plot $\lambda_T(\alpha)$ representing the synchronous (a) and desynchronous (b) tendency of the network oscillators.

3.4. Conditional Lyapunov exponents

The idea of TLEs has been mentioned as a criterion for stability of the synchronous state. This tool is especially useful in the case of the direct, e.g., diffusive coupling between the oscillators via connecting components. Such

a connection often causes the transversal (with respect to the synchronization manifold) convergence of trajectories in the phase space. However, in the case of a master-slave connection in decomposed or externally driven systems, the mechanism of synchronization is slightly different. Namely, the synchronization of response oscillators is possible if they forget their initial conditions [14]. Such a situation takes place when the Lyapunov exponents corresponding to response subsystems are negative. These exponents have been called conditional Lyapunov exponents (CLEs) or response Lyapunov exponents (RLEs).

3.4.1 Decomposed systems

Let us come back to the example of the decomposed Rössler system from Sec. 2.3 given by equations (2.23) and (2.24). As the drive (2.23) in this system, the x variable is applied. The uncoupled linearised sub-block yz is in the form

$$\begin{pmatrix} a & 0 \\ 0 & x-c \end{pmatrix}, \tag{3.23}$$

Hence, the CLEs are Lyapunov exponents of the uncoupled sub-block yz can be calculated from the Jacobian of the yz sub-block (3.23). In the classical Rössler system, the parameter a is positive and x is usually much smaller than c. Thus, the maximum CLE of the sub-block $\dot{\mathbf{x}}_i = \mathbf{f}(\mathbf{x}_i) + \sum_{i=1}^{n} G_{ij}(t)\ \mathbf{H}\ \mathbf{x}_j$, where $i = 0, 1, 2, \ldots, N$ and $G_{ij}(t)$ represents potentially time-varying components of the connectivity matrix $\mathbf{G}$, is also positive because it is equal to a. Therefore, the subsystems of x-driven Rössler oscillators cannot synchronize.

Consider now the y-driven Rössler systems as follows

$$\begin{aligned} \dot{x} &= -y - z \\ \dot{y} &= x - ay \\ \dot{z} &= b + z(x-c), \\ \dot{x}' &= -y - z' \\ \dot{z}' &= b + z'(x-c). \end{aligned} \tag{3.24}$$

where the uncoupled linearised sub-block xz is

$$\begin{pmatrix} 0 & -1 \\ z & x-c \end{pmatrix}, \tag{3.25}$$

The eigenvalues of Jacobian (3.25) approximating the CLEs are

$$\lambda_{1,2} = \frac{1}{2}\left(x - c \pm \sqrt{(c-x)^2 - 4z}\right). \tag{3.26}$$

The variable z in the system under consideration is almost always non-negative. Hence, for x much smaller than c, the real part of the eigenvalues (Eq. (3.26)) is negative. Consequently, the CLEs of y-driven subsystems of the Rössler oscillator are negative, so their synchronization is possible.

3.4.2 Externally driven oscillators

The general description of the systems with a common external drive is given in Sec. 2.2 in the block matrix form (Eqs. (2.18) and (2.19)). Here, the synchronization mechanism in these systems is explained. This mechanism is described in a version for continuous-time systems (Eq. (2.18)).

In order to investigate the synchronizability of the array of externally excited oscillators, the properties of the GS have been employed [29, 30, 35]. We have assumed that all response oscillators are identical. The dynamics of each individual driven oscillator ($x = x_i$, $i = 1, 2, \ldots, N$) is expressed by the following equations

$$\dot{\mathbf{e}} = \mathbf{g}(\mathbf{e}), \tag{3.27a}$$

$$\dot{\mathbf{x}} = \mathbf{f}(\mathbf{x}) + q\mathbf{h}(\mathbf{e}). \tag{3.27b}$$

The solution to the response system (Eq. (3.27b)) can be assumed in the following form

$$\mathbf{x}(t) = \mathbf{\Phi}[\mathbf{x}(t), \mathbf{x}_0] + \mathbf{\Psi}[\mathbf{e}(t)], \tag{3.28}$$

where $\mathbf{\Phi}$ and $\mathbf{\Psi}$ represent the functional parts of the solution, which are dependent on and independent of the response subsystem, respectively.

In order to examine the synchronization tendency of the response oscillators, let us consider two of them, arbitrarily chosen from system (3.27a), i.e., $\mathbf{x}_i$ and $\mathbf{x}_{i+1}$. The time evolution of the trajectory separation between them (synchronization error) is described by the equation

$$\dot{\mathbf{x}}_i - \dot{\mathbf{x}}_j = \mathbf{f}(\mathbf{x}_i) - \mathbf{f}(\mathbf{x}_{i+1}), \tag{3.29}$$

resulting from Eq. (3.27b). The linearisation of Eq. (3.29) leads to the following variational equation

$$\dot{\boldsymbol{\zeta}} = D\mathbf{f}[\mathbf{x}(t), \mathbf{x}_0]\boldsymbol{\zeta}, \tag{3.30}$$

where $D\mathbf{f}[\mathbf{x}(t), \mathbf{x}_0]$ is the Jacobi matrix of the response system. On the basis of Eq. (3.30), the CLEs of systems (3.27a) and (3.27b) can be calculated. From Eqs. (3.29) and (3.30) it results that the synchronization error tends to zero and the synchronous state is stable if all the CLEs are negative:

$$\lambda_j^C < 0, \tag{3.31}$$

where $j = 1, 2, \ldots, m$. Then, the component of solution (3.28) associated with the response of the system $\boldsymbol{\Phi}[\mathbf{x}(t), \mathbf{x}_0]$ tends to zero and there appears a functional relation between the drive and the response systems analogous to Eq. (1.4). Thus, the GS of systems (3.27a) and (3.27b) takes place because the external drive results in the response, forgetting its initial condition.

Chapter 4

Modelling and numerical results

In this chapter detailed models of the system under consideration, its components (pendulum, mass - spring oscillator) and results of numerical simulations are presented.

4.1. Physical pendulum

The pendulum is a well known object and remain relatively common in the research [96, 97, 98, 99, 100, 101, 102]. The pendulum's attraction and interest is associated with the familiar regularity of its swings, and as the consequence its relation to the fundamental natural force of gravity. The history of the pendulum might be begin with a recall of the tale of Galileo's observation of the swinging bronze chandelier in the cathedral of Pisa, using his pulse as a timer. Galileo was one of the first of the modern scientists and the pendulum was among the first objects of scientific enquiry.

There is a wide range of pendulum. A physical pendulum is simply a rigid object which swings freely about some pivot point. Neglecting the energy loss factors, there is no need for energizing this device through the forcing mechanisms. We have one generalized coordinate φ, so we want to write the Lagrange's equation in terms of φ and $\dot{\varphi}$.

The kinetic energy is

$$T = \frac{1}{2}[B_S + (m+\mu)\, b^2]\, \dot{\varphi}^2. \tag{4.1}$$

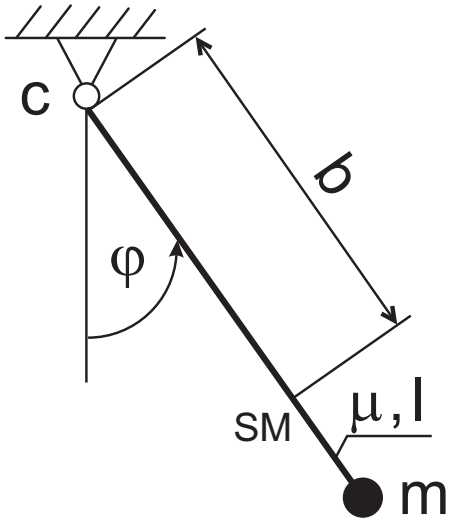

Figure 4.1: The physical pendulum: m – mass concentrated at the point in the end of the rod, μ, l – mass and length of the rod, c – damping factor at the node.

The potential energy is

$$V = (m+\mu)\, gb\, \cos\varphi. \tag{4.2}$$

The Rayleigh's dissipation function is given by the following formula

$$D = \frac{1}{2}\, c\, \dot{\varphi}^2. \tag{4.3}$$

Using the Lagrange's equations

$$\frac{d}{dt}\frac{\partial T}{\partial \dot{\varphi}} - \frac{\partial T}{\partial \varphi} + \frac{\partial V}{\partial \varphi} = 0 \tag{4.4}$$

the equations of the motion for the physical pendulum were formulated.

$$B\, \ddot{\varphi} + c\, \dot{\varphi} + (m+\mu)\, gb\, \sin\varphi = 0, \tag{4.5}$$

where m is the mass concentrated at the point in the end of the rod, μ is the mass of the rod, l is the length of the rod, c is the damping factor at the node, B_S is the inertia moment of the mass and b is the distance from the center of the mass to the center of rotation of the rod and mass, given by

$$B_S = \frac{1}{12}\mu l^2 + m(l-b)^2 + \mu(b-\frac{1}{2}l)^2, \tag{4.6a}$$

$$b = \frac{(m+\frac{1}{2}\mu)l}{(m+\mu)}, \tag{4.6b}$$

$$B = B_S + (m+\mu)\, b^2, \tag{4.6c}$$

respectively.

4.2. Oscillator

The majority of the oscillatory systems that we meet in everyday life suffer some sort of irreversible energy loss whilst they are in motion, which is due, for instance, to frictional or viscous heat generation. We would therefore expect oscillations excited in such systems to eventually be damped away.

Let us examine a damped oscillatory system. The oscillator consists of a mass M suspended on a spring with stiffness k. The system is viscously damped with a factor d and externally excited with x_z which is transmitted by the spring of stiffness k.

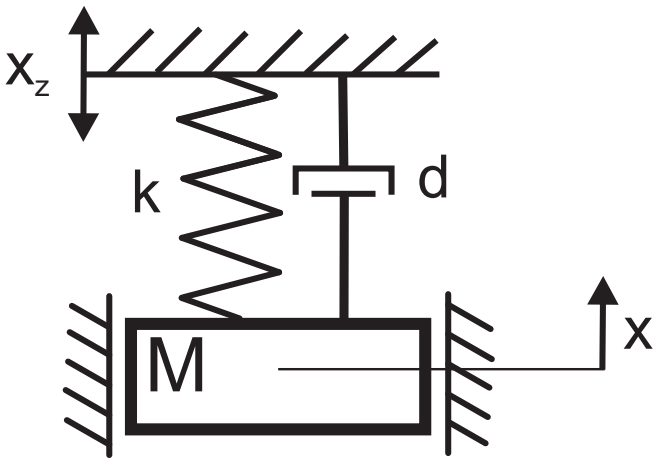

Figure 4.2: The linear oscillator.

We have one generalized coordinate x, so we want to write the Lagrangian in terms of x and $\dot{x}$.
The kinetic energy is

$$T = \frac{1}{2} M \dot{x}^2. \tag{4.7}$$

The potential energy is the elastic potential energy

$$V = \frac{1}{2} k (x - x_z)^2. \tag{4.8}$$

The Rayleigh's dissipation function is given by the following formula

$$D = \frac{1}{2} d \dot{x}^2. \tag{4.9}$$

Using the Lagrange's formula the equations of motion for the physical pendulum can be written in the form

$$M\,\ddot{x} + d\,\dot{x} + k\,(x - x_z) = 0. \tag{4.10}$$

4.3. Mass with physical pendulum

In this section the analysis of more complex system is presented. By adding the pendulum (Fig. 4.1) to the mass (Fig. 4.2), we obtain kinematically excited mass-pendulum oscillator shown in Fig. 4.3. This system has two degrees of freedom: the vertical displacement x and the angle φ.

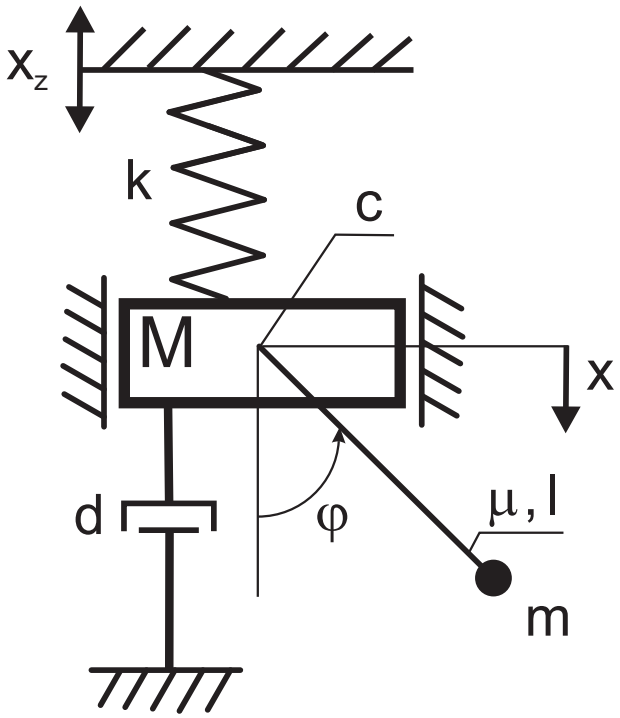

Figure 4.3: The elastically supported mass with physical pendulum.

We have two generalized coordinates φ and x, so we are able to formulate the Lagrangian in terms of φ, x, $\dot{\varphi}$ and $\dot{x}$.

The kinetic energy is

$$T = \frac{1}{2}\,(M + m + \mu)\,\dot{x}^2 + (m + \mu)\,b\,\dot{x}\,\dot{\varphi}\,\sin\varphi + \frac{1}{2}[B_S + (m + \mu)\,b^2]\,\dot{\varphi}^2, \tag{4.11}$$

where B_S is the inertia moment of the mass and b is distance from the center of mass to the center of rotation of the rod and mass, given by formulas

$$B_S = \frac{1}{12}\mu l^2 + m(l-b)^2 + \mu(b-\frac{1}{2}l)^2, \tag{4.12a}$$

$$b = \frac{(m+\frac{1}{2}\mu)l}{(m+\mu)}. \tag{4.12b}$$

The potential energy is

$$V = \frac{1}{2}k\,(x-x_w)^2 + (m+\mu)\,gb\,(1-\cos\varphi). \tag{4.13}$$

The Rayleigh's dissipation function is given by the following formula:

$$D = \frac{1}{2}\,c\,\dot{\varphi}^2 + \frac{1}{2}\,d\,\dot{x}^2. \tag{4.14}$$

Using the Lagrange's method the equations of motion for the elastically supported mass with physical pendulum and sinusoidal external forcing (Fig. 4.3) were formulated in the following form

$$B\,\ddot{\varphi} + A\,\ddot{x}\,\sin\varphi + A\,g\,\sin\varphi + c\,\dot{\varphi} = 0 \tag{4.15a}$$

$$(M+m+\mu)\,\ddot{x} + A\,(\ddot{\varphi}\,\sin\varphi + \dot{\varphi}^2\,\cos\varphi) + d\,\dot{x} + k\,(x - z\,\sin(\Omega t)) = 0 \tag{4.15b}$$

where

$$B = B_S + (m+\mu)\,b^2,$$

$$A = (m+\mu)\,b,$$

M – mass of the oscillator $[kg]$, m – mass concentrated at the point in the end of rod $[kg]$, μ – mass of the rod $[kg]$, l – length of the rod $[m]$, k – spring stiffness $[N/m]$, c – damping factor at the node $[Nms]$, d – viscous damping $[Ns/m]$ and x_z is a signal of excitation which is transmitted by the spring of stiffness k. The derivatives in Eq. (4.16) are calculated with respect to dimensionless time τ.

Introducing $\omega = \sqrt{\frac{k}{M+m+\mu}}$ (the natural frequency), $x_S = \frac{M+m+\mu}{k}$ and dividing Eq. (4.15) by bkx_S and Eq. (4.15a) by kx_S we obtain the dimensionless equations

$$\alpha\,\ddot{\varphi} + \beta\sin\varphi\,\ddot{x} + \zeta\dot{\varphi} + \gamma\sin\varphi = 0 \tag{4.16a}$$

$$\varepsilon\,\ddot{x} + \rho(\sin\varphi\,\ddot{\varphi} + \cos\varphi\,\dot{\varphi}^2) + \delta\,\dot{x} + \kappa(x - z\sin(\eta\tau)) = 0 \tag{4.16b}$$

where

$$\alpha = \frac{B}{(M+m+\mu)\, b\, x_S}, \quad \beta = \frac{A}{(M+m+\mu)\, b\, x_S}, \quad \gamma = \frac{A}{(M+m+\mu)\, b}, \quad \zeta = \frac{c}{\omega\, (M+m+\mu)\, b\, x_S},$$
$$\varepsilon = \frac{(M+m+\mu)}{(M+m+\mu)}, \quad \rho = \frac{A}{(M+m+\mu)\, x_S}, \quad \delta = \frac{d}{\omega\, (M+m+\mu)\, x_S}, \quad \kappa_1 = \frac{k_1}{k_1\, x_S},$$
$$Z = \frac{z}{x_S}, \quad \eta = \frac{\Omega}{\omega}$$

are dimensionless parameters and

$$x = \frac{1}{x_S}\frac{dx}{d\tau}, \quad \varphi = \frac{d\varphi}{d\tau}, \quad \tau = \omega\, t$$

are dimensionless variables.

4.3.1 Numerical results for mass with physical pendulum

Among the variety of numerical integration methods one of the most accurate and also the most commonly used by many authors, is the classical method proposed by Runge – Kutta. Near the internal and external resonances depending on a selection of physical system parameters the frequencies of external excitation of both coupled bodies may exhibit various responses x and pendulum are periodic or multiperiodic vibrations, but sometimes the motion of the pendulum is chaotic.

In our numerical simulations we consider the system described by Eq. (4.15) with the following parameter values

$$\begin{aligned} &M = 0.5[kg], && k = 1000[N/m], \\ &m = 0.2[kg], && a = 0.01[m], \\ &\mu = 0.1[kg], && c = 0.01[Nms], \\ &b = 0.1375[m], && d = 5[Ns/m], \\ &B = 0.65625 \cdot 10^{-3}[kg\, m^2], && g = 9.81[N/kg]. \end{aligned} \tag{4.17}$$

The frequancy of harmonic forcing Ω is a control parameter. Having a dimensionless form of Eq. (4.15), we obtain Eq. (4.16) and following values of dimensionless parameters

$$\begin{aligned} &\alpha = 28.0, && \varepsilon = 2.0, \\ &\gamma = 27.8, && \zeta = 0.527, \\ &\delta = 0.204, && A = 1.85, \end{aligned} \tag{4.18}$$

and η is a control parameter. As an external excitation, we have chosen a sinusoidal signal. The system is released from the initial conditions: $\varphi = 3.0$, $\dot{\varphi} = 0.0$, $x = 0.05$, $\dot{x} = 0.0$. Exemplary results, for the above values of parameters are presented in the diagrams (Figs. 4.4 and 4.5), where vertical displacement of the mass and angular position of the pendulum versus frequency of excitation are shown.

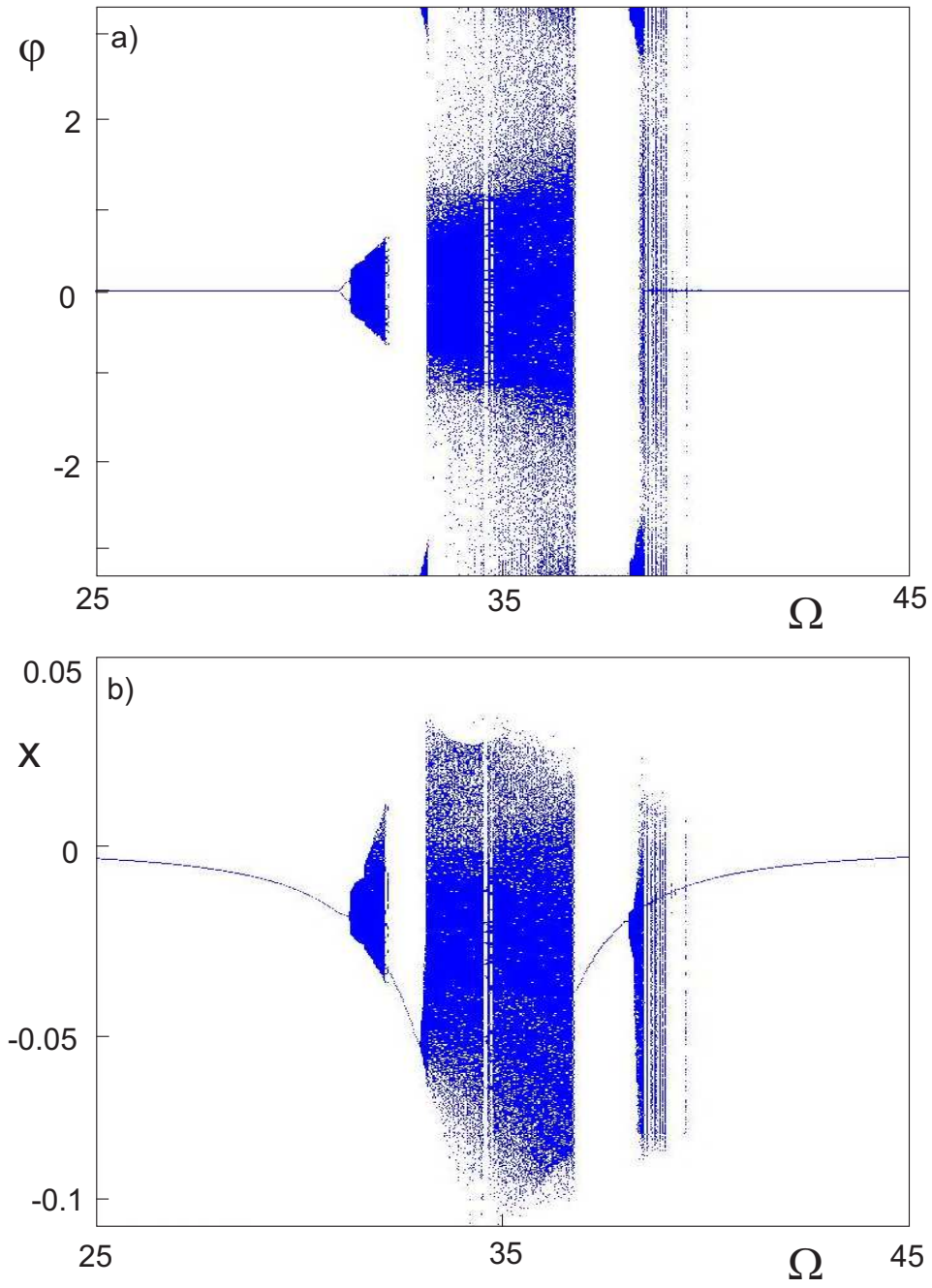

Figure 4.4: Bifurcation diagrams for φ (a) and x (b) versus Ω.

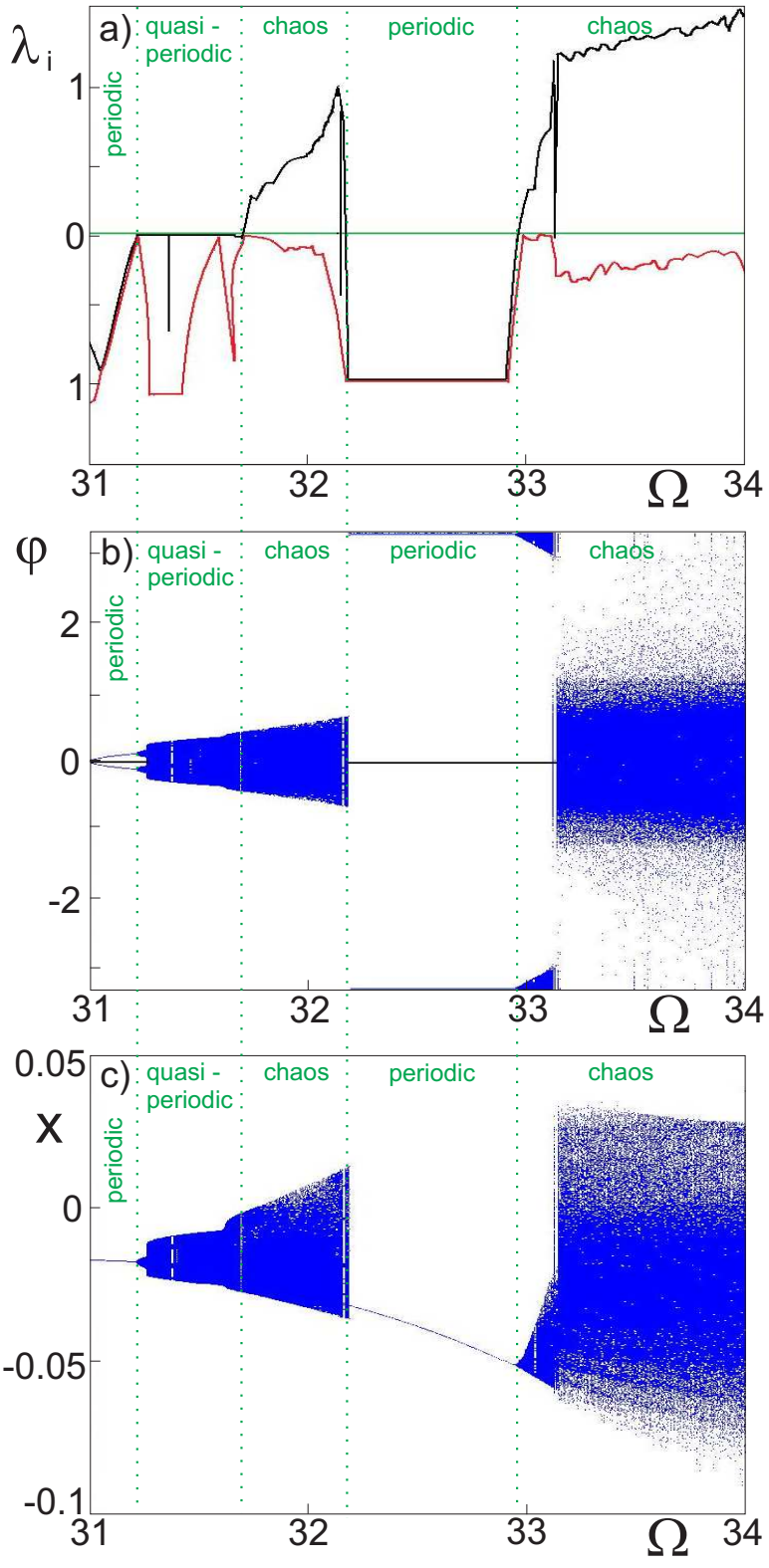

Figure 4.5: Lyapunov exponents λ (a) and bifurcation diagrams for φ (b) and x (c) versus Ω. Enlarged scope of Fig. 4.4.

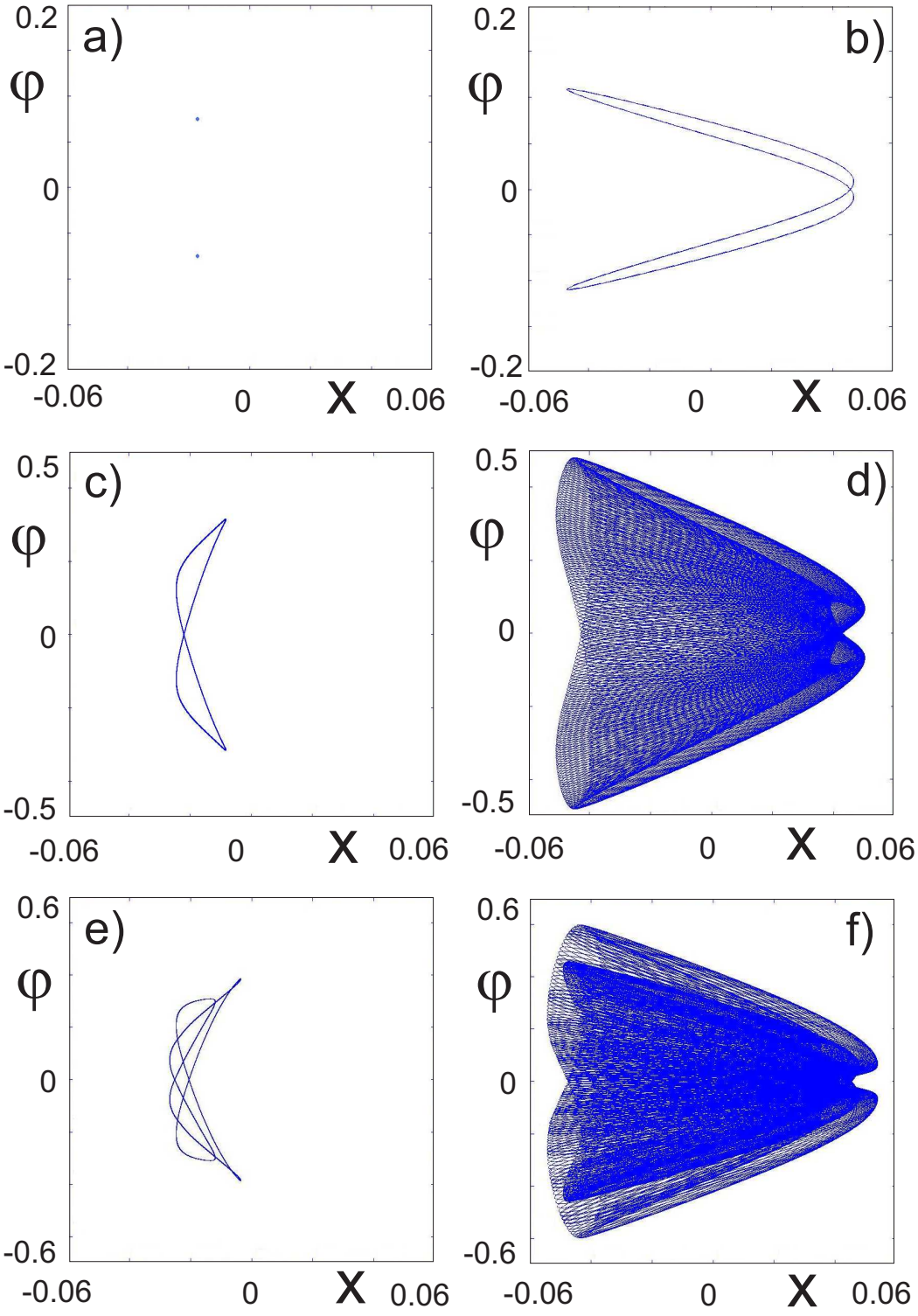

Figure 4.6: Poincaré maps (left column) and phase portraits (right column) for Ω =31.10 $[\frac{rad}{s}]$ (a, b), $\Omega = 31.50\ [\frac{rad}{s}]$ (c, d) and $\Omega = 31.65\ [\frac{rad}{s}]$ (e, f).

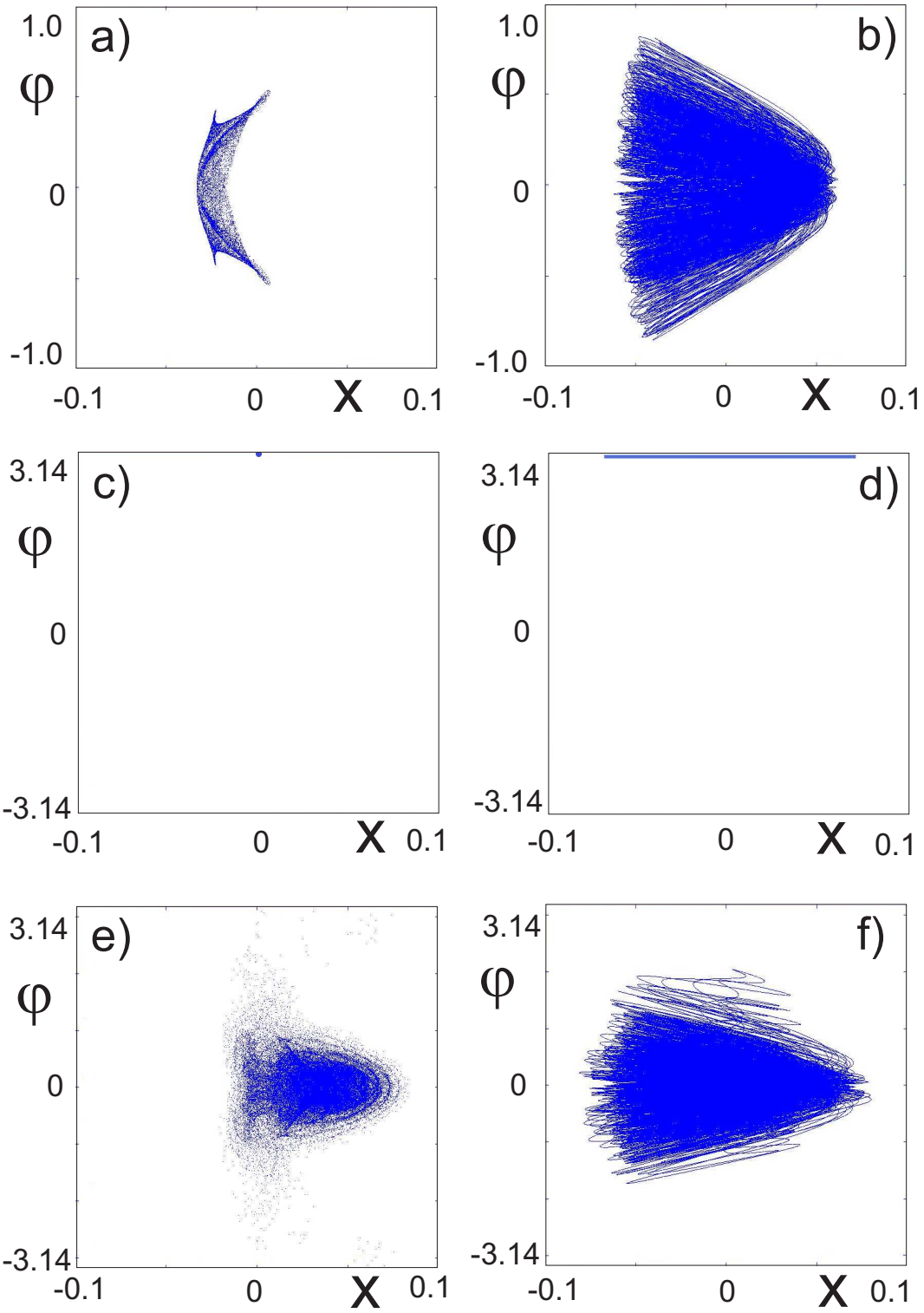

Figure 4.7: Poincaré maps (left column) and phase portraits (right column) for $\Omega = 32.00\ [\frac{rad}{s}]$ (a, b), $\Omega = 32.20\ [\frac{rad}{s}]$ (c, d) and $\Omega = 33.20\ [\frac{rad}{s}]$ (e, f).

Analysing bifurcation diagrams demonstrated in Figs. 4.4a–b we can see that motion of the pendulum is activated only in the range $\Omega \in (31.0; 39.00)$ $[\frac{rad}{s}]$ directly surrounding the value of natural frequency $\Omega = 34.64$ $[\frac{rad}{s}]$, i.e., in the neighbourhood of the resonance. Outside of this range forced harmonic oscillations of the mass with angularly immoveable pendulum are observed.

In Figs. 4.5a–c the narrowed range of Ω is depicted – $\Omega \in (31.0; 39.0)$ $[\frac{rad}{s}]$, in which interesting dynamical behaviour of the pendulum occurs. The corresponding three largest Lyapunov exponents are shown in Fig. 4.5a. One of them of zero value, represented by green line, is connected with external forcing. Periodic (the largest Lyapunov exponent equal to zero) or quasi-periodic motion (two largest Lyapunov exponent of zero value) is interwoven with chaotic behaviour of the pendulum (Ω - ranges of positive the largest Lyapunov exponent).

Results shown in bifurcation diagrams (Fig. 4.5) are confirmed with phase portraits and Poincaré maps generated numerically for chosen values of control parameter (frequency of forcing Ω) - see Figs. 4.6 and 4.7. The phase portraits and Poincaré maps show φ versus x. Increasing frequency Ω causes transition via period doubling (Fig. 4.6a–b) and Hopf bifurcation to quasi-periodic solution (Fig. 4.6c–d). Further increase of Ω leads to the chaotic solution (Fig. 4.7a–b) via torus period-doubling (Fig. 4.6e–f). Next, for value of the excitation frequency from the interval $32.17 < \Omega < 32.95$ $[\frac{rad}{s}]$ we can see the pendulum stabilized in the upper equilibrium position during periodic vibration of the mass (Fig. 4.7c–d). Starting from $\Omega > 32.95$ $[\frac{rad}{s}]$ there appear chaotic oscillations around the upper equilibrium position passing into sequences of chaotic rotations and oscillations (Fig. 4.7e–f).

4.4. Mass with two pendulums ($n = 1$)

One oscillator node consists of mechanical oscillator (mass) and two physical pendulums suspended on both sides of the mass, which is presented in Fig. 4.8. This system has three degrees of freedom: the vertical displacement x_1 and the angles φ_{11} and φ_{12}.

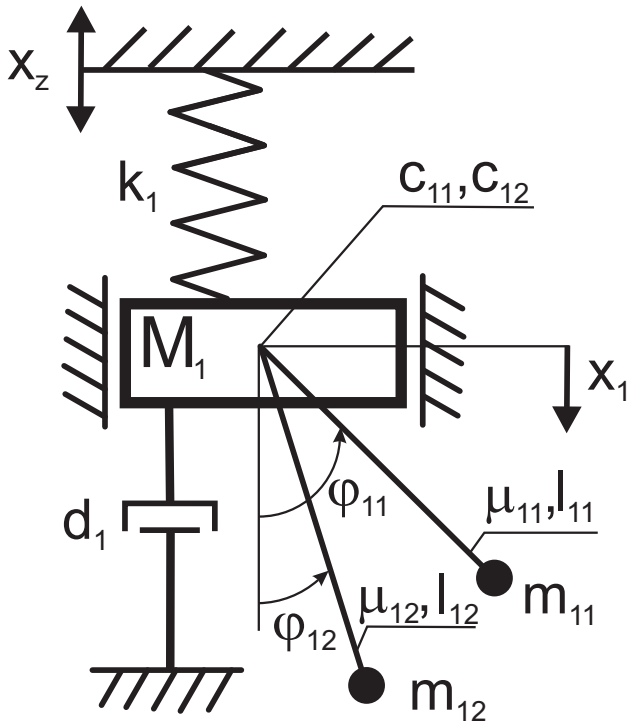

Figure 4.8: The elastically supported mass with two physical pendulums.

Lagrange's equations for analysed system are as follows

$$B_{11}\,\ddot{\varphi}_{11} + A_{11}\,\ddot{x}_1\,\sin\varphi_{11} + A_{11}\,g\,\sin\varphi_{11} + c_{11}\,\dot{\varphi}_{11} = 0 \tag{4.19a}$$

$$B_{12}\,\ddot{\varphi}_{12} + A_{12}\,\ddot{x}_1\,\sin\varphi_{12} + A_{12}\,g\,\sin\varphi_{12} + c_{12}\,\dot{\varphi}_{12} = 0 \tag{4.19b}$$

$$\begin{aligned} M_1\,\ddot{x}_1 + A_{11}\,(\ddot{\varphi}_{11}\,\sin\varphi_{11} + \dot{\varphi}_{11}^2\,\cos\varphi_{11}) + A_{12}\,(\ddot{\varphi}_{12}\,\sin\varphi_{12} + \dot{\varphi}_{12}^2\,\cos\varphi_{12}) \\ + d_1\,\dot{x}_1 + k_{11}\,(x_1 - z\,\sin(\Omega t)) = 0, \end{aligned} \tag{4.19c}$$

where

$$B_{11,\,12} = B_{S1,\,S2} + (m_{11,\,12} + \mu_{11,\,12})\,b_{11,\,12}{}^2,$$

$$A_{11,\,12} = (m_{11,\,12} + \mu_{11,\,12})\,b_{11,\,12},$$

$$M_1 = M_{b1} + m_{11} + \mu_{11} + m_{12} + \mu_{12},$$

and M_{b1} – mass of the oscillator $[kg]$, $m_{11,12}$ – mass concentrated at the end point of the rod $[kg]$, $\mu_{11,12}$ – mass of the rod $[kg]$, $l_{11,12}$ – length of the rod $[m]$, $B_{11,12}$ is the inertia moment of the mass $[kg\,m^2]$ given by

$$B_{S1,S2} = m_{11,12}(l_{11,12} - b_{11,12})^2 + \frac{1}{12}\mu_{11,12}l_{11,12}^2 + \mu_{11,12}(b_{11,12} - \frac{1}{2}l_{11,12})^2 \tag{4.20}$$

and

$$b_{11,12} = \frac{(m_{11,12} + \frac{1}{2}\mu_{11,12})l}{(m_{11,12} + \mu_{11,12})} \tag{4.21}$$

is distance from the center of mass to the center of rotation of the rod and mass $m_{11,12}$, k_{11} – spring stiffness $[N/m]$, $c_{11,12}$ – damping factor at the node $[Nms]$, $\Delta c_1 = c_{11} - c_{12}$ – damping factor mismatch at the node, d_1 – viscous damping $[Ns/m]$ and x_z is a signal of excitation which is transmitted by the spring with a stiffness k_{11}.

Matrix form of Eqs.(4.19 a-c) is as follows

$$\begin{bmatrix} B_{11} & 0 & A_{11}\,\sin\varphi_{11} \\ 0 & B_{12} & A_{12}\,\sin\varphi_{12} \\ A_{11}\,\sin\varphi_{11} & A_{12}\,\sin\varphi_{12} & M_1 \end{bmatrix} \begin{pmatrix} \ddot{\varphi}_{11} \\ \ddot{\varphi}_{12} \\ \ddot{x}_1 \end{pmatrix} + \begin{pmatrix} A_{11}\,g\,\sin\varphi_{11} + c_{11}\,\dot{\varphi}_{11} \\ A_{12}\,g\,\sin\varphi_{12} + c_{12}\,\dot{\varphi}_{12} \\ A_{11}\dot{\varphi}_{11}^2\cos\varphi_{11} + A_{12}\dot{\varphi}_{12}^2\cos\varphi_{12} + d_1\dot{x}_1 + k_{11}x_1 \end{pmatrix} = \begin{pmatrix} 0 \\ 0 \\ k_{11}\,z\,\sin(\Omega t) \end{pmatrix}. \tag{4.22}$$

Such representation of the system under consideration gives clear illustration of the inertial coupling between its components - inertial matrix (quadratic parenthesis) with non-diagonal elements.

Introducing $\omega = \sqrt{\frac{k_{11}}{M_1}}$ (the natural frequency), $x_S = \frac{M_1\,g}{k_{11}}$ and dividing Eq. (4.19a) by $b_{11,12}k_{11}x_S$ and Eq. (4.19b) by $k_{11}x_S$ we obtain the dimensionless equations:

$$\alpha_{11}\,\ddot{\varphi}_{11} + \beta_{11}\,\ddot{x}_1\,\sin\varphi_{11} + \gamma_{11}\,\sin\varphi_{11} + \zeta_{11}\,\dot{\varphi}_{11} = 0 \tag{4.23a}$$

$$\alpha_{12}\,\ddot{\varphi}_{12} + \beta_{12}\,\ddot{x}_1\,\sin\varphi_{12} + \gamma_{12}\,\sin\varphi_{12} + \zeta_{12}\,\dot{\varphi}_{12} = 0 \tag{4.23b}$$

$$\varepsilon_1\,\ddot{x}_1 + \rho_{11}\,(\sin\varphi_{11}\,\ddot{\varphi}_{11} + \cos\varphi_{11}\,\dot{\varphi}_{11}^2) + \rho_{12}\,(\sin\varphi_{12}\,\ddot{\varphi}_{12} + \cos\varphi_{12}\,\dot{\varphi}_{12}^2) + \delta_1\,\dot{x}_1 + \kappa_{11}(x_1 - Z\sin(\eta\tau)) = 0, \tag{4.23c}$$

where

$$\alpha_{11,\,12} = \frac{B_{11,\,12}}{M_1\,b_{11}\,x_S}, \quad \beta_{11,\,12} = \frac{A_{11,\,12}}{M_1\,b_{11}\,x_S}, \quad \gamma_{11,\,12} = \frac{A_{11,\,12}}{M_1\,b_{11}}, \quad \zeta_{11,\,12} = \frac{c_{11,\,12}}{\omega\,M_1\,b_{11}\,x_S},$$
$$\varepsilon_1 = \frac{M_1}{M_1}, \quad \rho_{11,\,12} = \frac{A_{11,\,12}}{M_1\,x_S}, \quad \delta_1 = \frac{d_1}{\omega\,M_1}, \quad \kappa_{11} = \frac{k_{11}}{k_{11}},$$
$$Z = \frac{z}{x_S}, \quad \eta = \frac{\Omega}{\omega}$$

are dimensionless parameters and

$$\varphi_{11,\,12} = \frac{d\varphi_{11,\,12}}{d\tau}, \quad x_1 = \frac{1}{x_S}\frac{dx_1}{d\tau}, \quad \tau = \omega\, t$$

are dimensionless variables. The derivatives in Eqs. (4.23) are calculated with respect to dimensionless time τ.

4.4.1 Numerical results for $n = 1$

In this research, to integrate the differential equations Eq. (4.19) 4th order Runge – Kutta method with fixed time step was used. The time step is $T/3600$, where T is the period of excitation. Near the internal and external resonances depending on a selection of physical system parameters the frequencies of external forcing of both coupled bodies may relate to different motions: x_1 and pendulum are periodic or quasi-periodic vibrations, but sometimes the motion of the pendulums is chaotic or they are located in stabilized position (upper or lower). Two cases of the system for $n = 1$ are analysed: the system consisting of identical pendulums or pendulums with parameter's mismatch, i.e., having slightly different damping factor at the node.

Identical pendulums

In the numerical simulations of the system described by Eq. (4.19) with the following parameter values for identical pendulums was considered:

$M_{b1} = 0.2\ [kg]$	$M_1 = 0.5\ [kg]$	$k_{11} = 600\ [\frac{N}{m}]$
$m_{11,12} = 0.1\ [kg]$	$A_{1,\,2} = 0.01875\ [kgm]$	$c_{11,12} = 0.01\ [Nms]$
$\mu_{11,12} = 0.05\ [kg]$	$B_{11,12} = 0.002625\ [\frac{kg}{m^2}]$	$d_1 = 1.5\ [\frac{Ns}{m}]$
$l_{11,12} = 0.15\ [m]$	$b_{11,12} = 0.125\ [m]$	$z = 0.01\ [m]$

and frequency Ω is a control parameter. Above values correspond to real parameters measured and estimated on the experimental rig. Damping coefficients were approximated with classical free vibrations probe. On the other hand, they were established in order to make possible the comparison of the results with the case considered in the previous Sec. 4.4 (mass with the single pendulum).

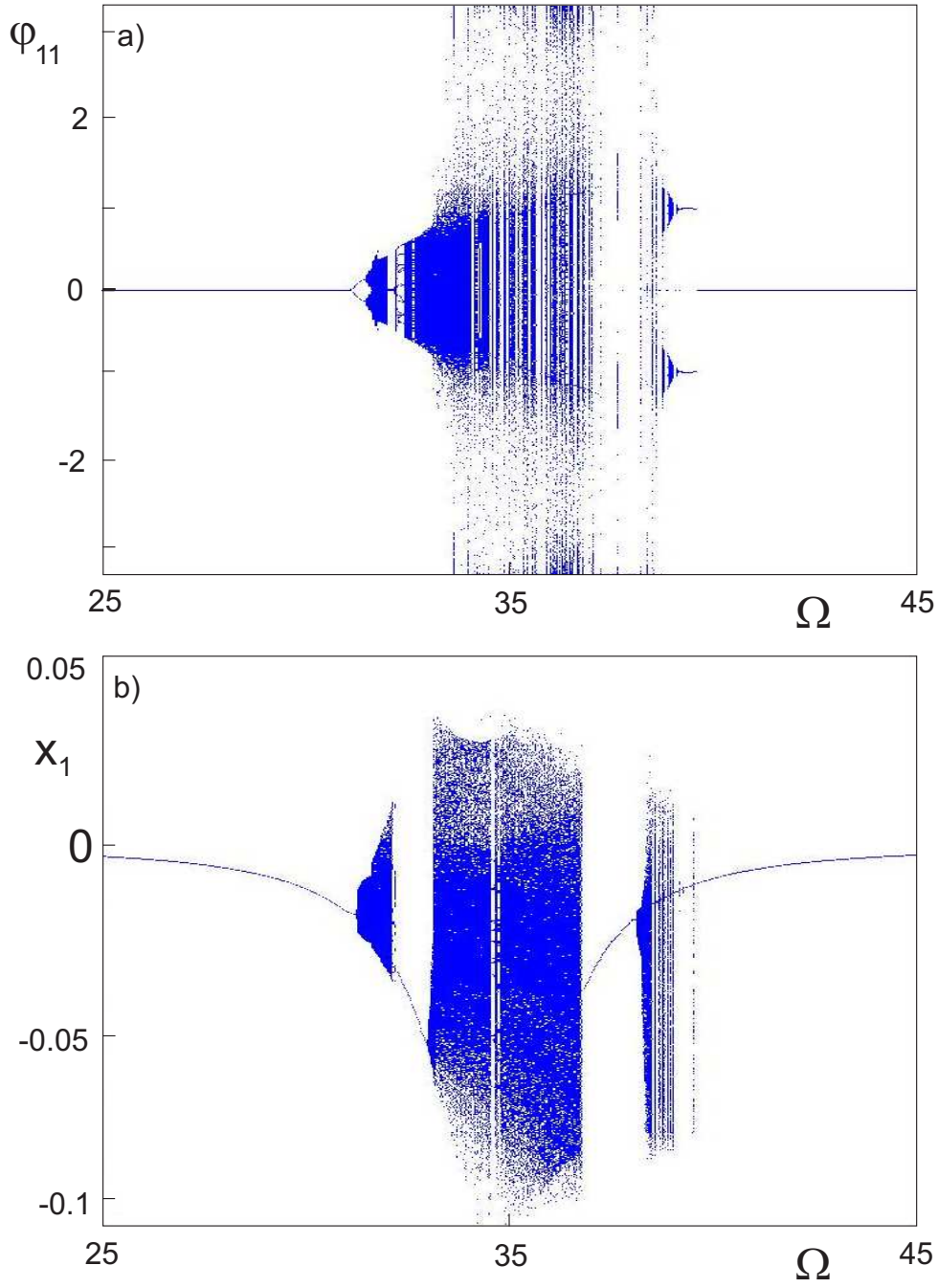

Figure 4.9: Bifurcation diagrams for the case of identical pendulums Eq. (4.19): a) pendulum angle φ_{11}, b) mass displacement x_1 versus Ω.

Therefore, the mass of this single pendulum was divided symmetrically between both pendulums in Eq. (4.19). Remaining parameters were left unchanged. The pendulums are released from the initial conditions $\varphi_{11} = 3.0$, $\dot{\varphi}_{11} = 0.0$, $\varphi_{12} = 2.0$, $\dot{\varphi}_{12} = 0.0$, $x_1 = 0.05$, $\dot{x}_1 = 0.0$. Dimensionless parameters of the system are as

follows:

$$\alpha_{11,\,12} = 5.14, \quad \beta_{11,\,12} = 36.70, \quad \gamma_{11,\,12} = 0.30, \quad \zeta_{11,\,12} = 0.56,$$
$$\varepsilon_1 = 1.00, \quad \rho_{11,\,12} = 4.59, \quad \delta_1 = 0.09, \quad \kappa_{11} = 1.00,$$

where η is dimensionless control parameter. As an external excitation, we have chosen a sinusoidal signal with amplitude $z = 0.01\ [m]$ (dimensionless value of amplitude is $Z = 1.22$).

In Figs. 4.9 and and their enlargements in Figs. 4.10 bifurcation diagrams of mass and pendulums positions versus driving frequency are demonstrated. We can see that, as in the case of mass-single pendulum system, nonlinear oscillations are activated near the dominant resonance frequency $\omega = \sqrt{\frac{k_{11}}{M_1}}$. In Figs. 4.11 corresponding (to Figs. 4.10) course of largest Lyapunov exponents (Fig. 4.11a) and bifurcation diagrams depicting an occurrence of complete (Fig. 4.11b) and combined in phase and in anti-phase synchronization (Fig. 4.11c) are demonstrated. These diagrams clearly illustrate the sequence of bifurcations, dominant solutions and their correlation with the synchronization of pendulums. For the frequency $\Omega = 31.22\ [\frac{rad}{s}]$ we can see the tendency of pendulums to stabilize in the lower stationary position (Figs. 4.10a–b). Period – doubling bifurcation at $\Omega = 31.22\ [\frac{rad}{s}]$ stimulate periodic, completely synchronized response of the pendulums within the interval $31.22 < \Omega < 31.53\ [\frac{rad}{s}]$ In this range all the values of Lyapunov exponents are negative ($\lambda_i < 0$). Further increase of driving frequency in the interval under consideration (up to $\Omega = 34.00\ [\frac{rad}{s}]$) results in alternately appearing intervals of periodic, quasi-periodic, chaotic (one positive Lyapunov exponent - see Fig. 4.11a) and finally hyperchaotic (two positive Lyapunov exponents - see Fig. 4.11a) states.

Comparison of synchronous intervals in Figs. 4.11b and 4.11c indicates coexistence of phase and anti-phase synchronization of pendulums. In Figs. 4.12 and 4.13 Poincaré maps demonstrating the pendulum dynamics (left column) and corresponding synchronization tendency (right column) are shown. We can see that pendulums desynchronization is typical for hyperchaos (Figs. 4.12a–b, 4.13c–d) or can an effect of attractor's coexistence, i.e., first pendulum is closed in stationary position while the second one oscillates quasi-periodically (Fig. 4.12c–d). On the other hand, the synchronous behaviour is possible

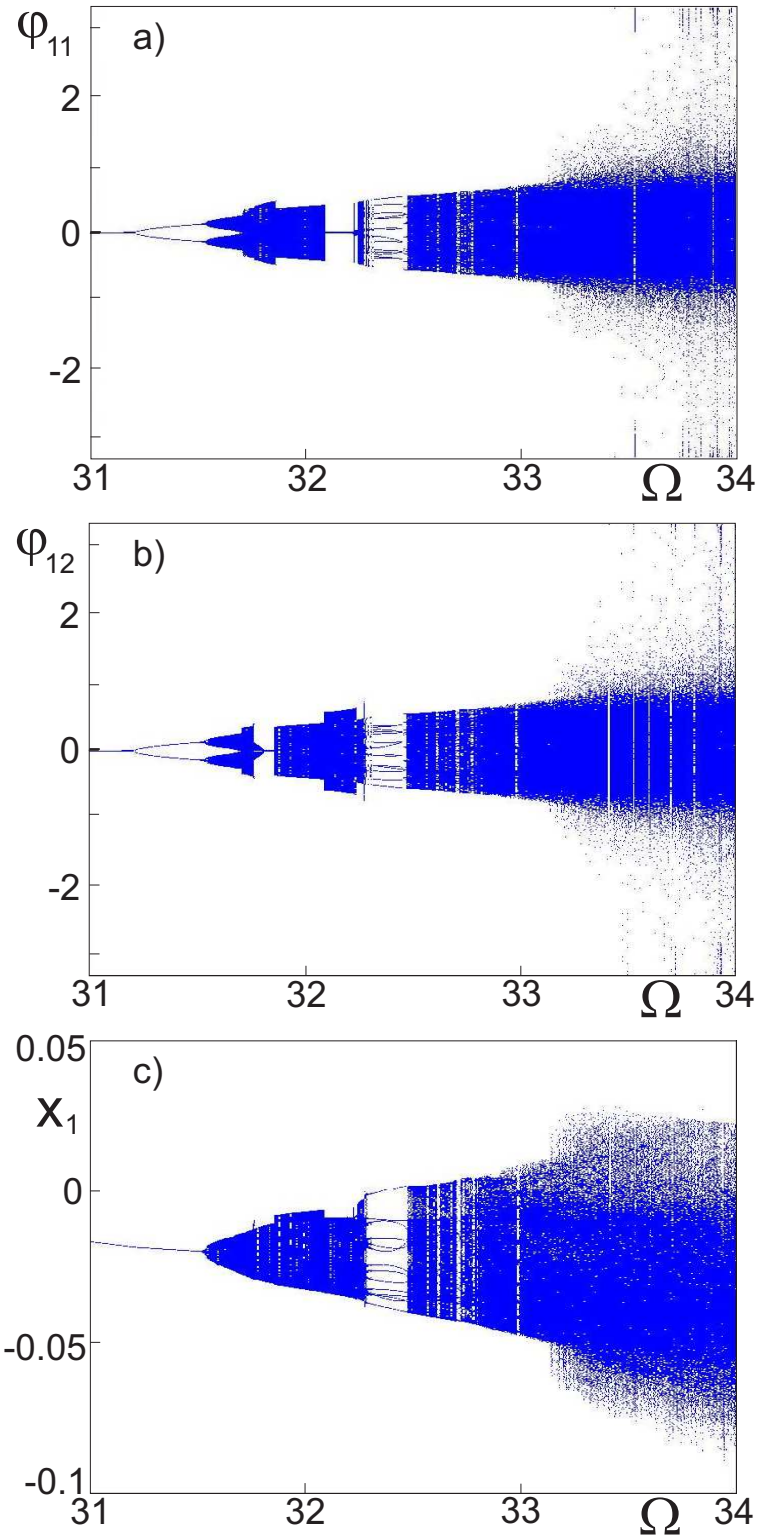

Figure 4.10: Zoom of bifurcation diagrams from Fig. 4.9.

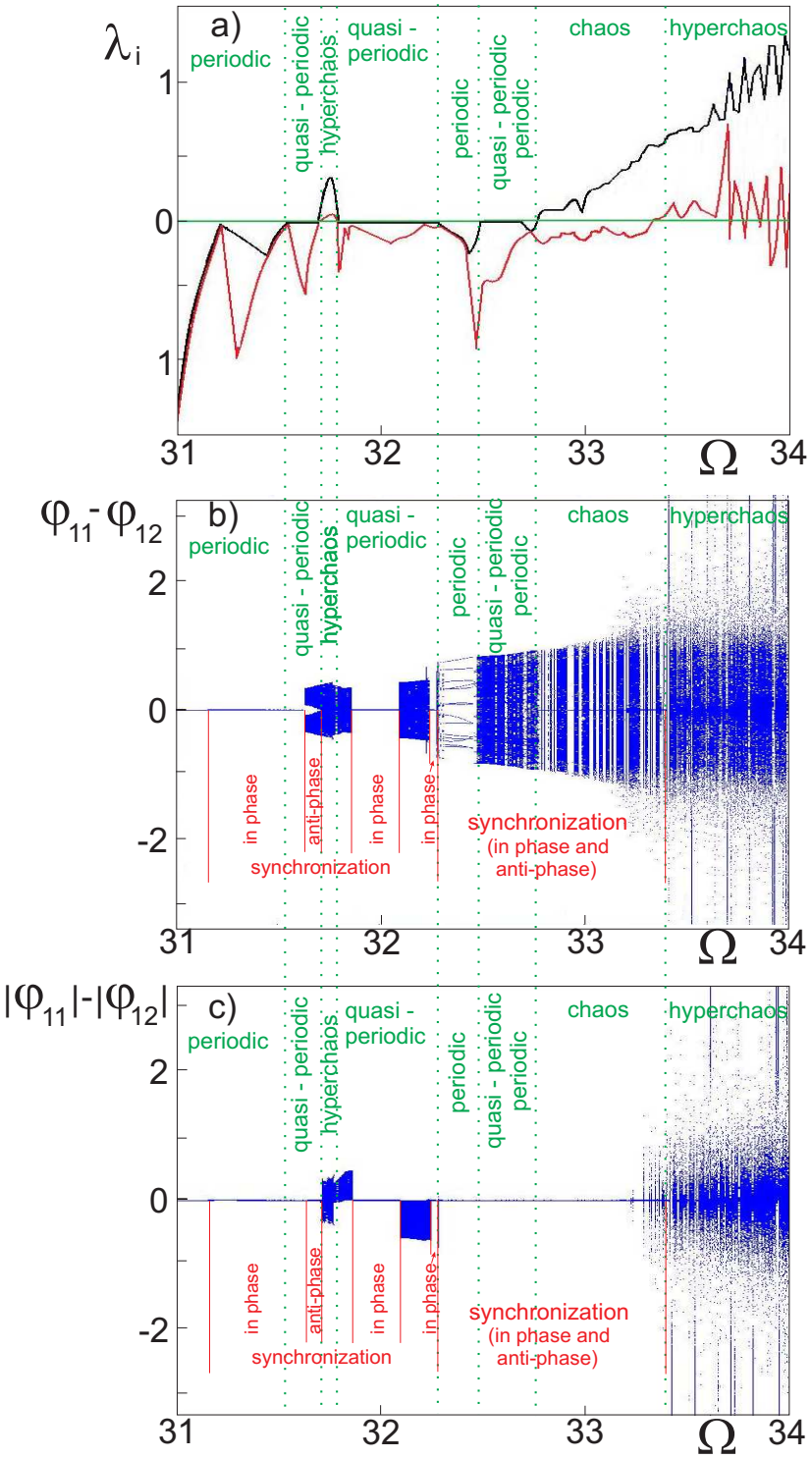

Figure 4.11: Diagram of Lyapunov exponents λ_1, λ_2, λ_3 (the green one is equal to zero) versus Ω and corresponding bifurcation diagrams presenting the occurrence of synchronization $\varphi_{11} - \varphi_{12}$, $|\varphi_{11}| - |\varphi_{12}|$.

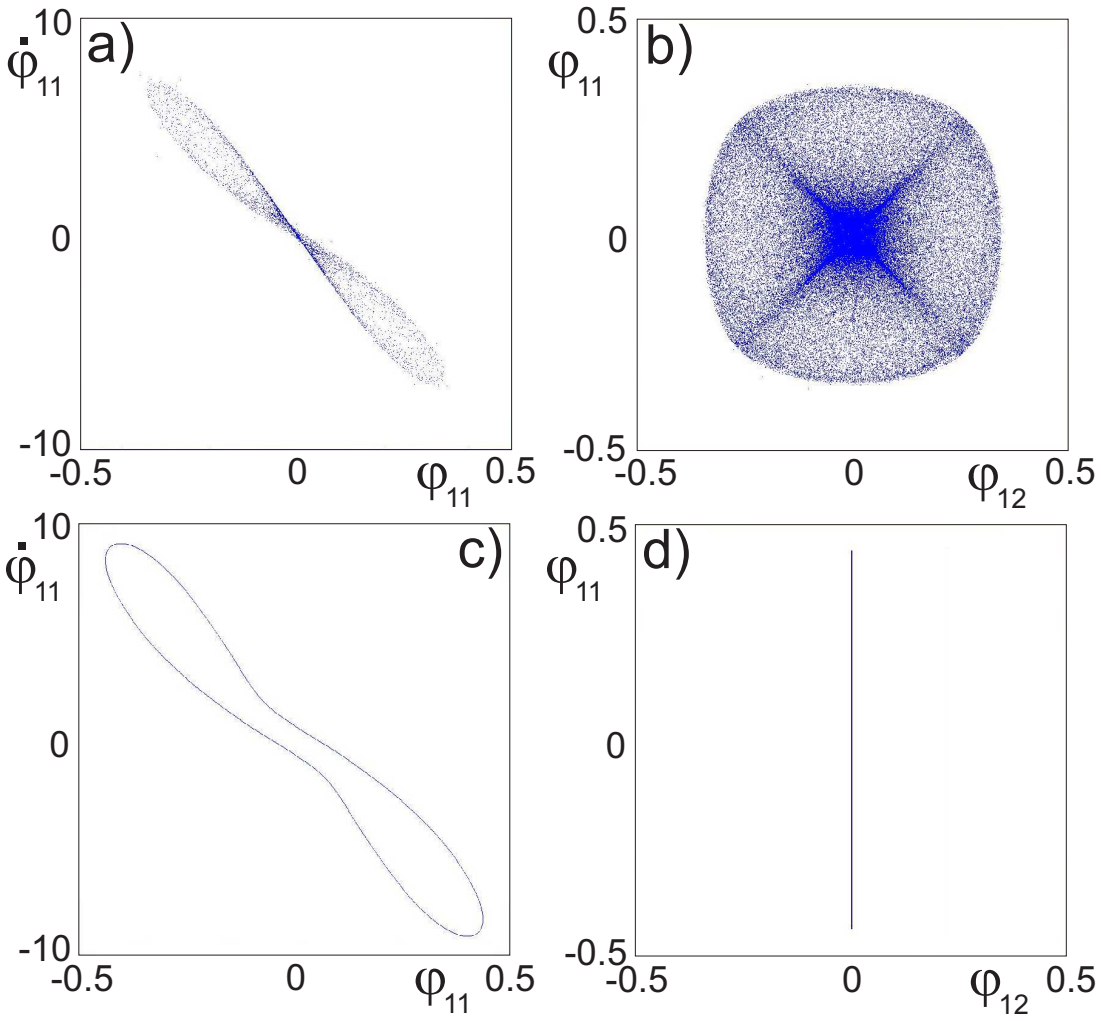

Figure 4.12: Poincaré maps (left column) and synchronization diagrams (right column) for identical pendulums for $\Omega = 31.75\ [\frac{rad}{s}]$ (a, b) and for $\Omega = 31.85\ [\frac{rad}{s}]$ (c, d).

in chaotic regime of pendulums oscillation (Fig. 4.13a–b). Such phenomena of chaotic synchronization is verified by comparison of Figs. 4.11a and 4.11c where in-phase or anti-phase synchronization range (Fig. 4.11c) is corresponding to the scope of one positive Lyapunov exponent (Fig. 4.11a). In-phase and anti-phase synchronous regimes in the system under consideration are demonstrated with time series in Figs. 4.14 and 4.15, respectively.

In the next stage of numerical analysis an increased value of the mass M_1 has been taken in calculation. This increase corresponds to the experiment (see Sec. 5.2) and can be treated as as an equivalent mass of the beam m_e. Hence,

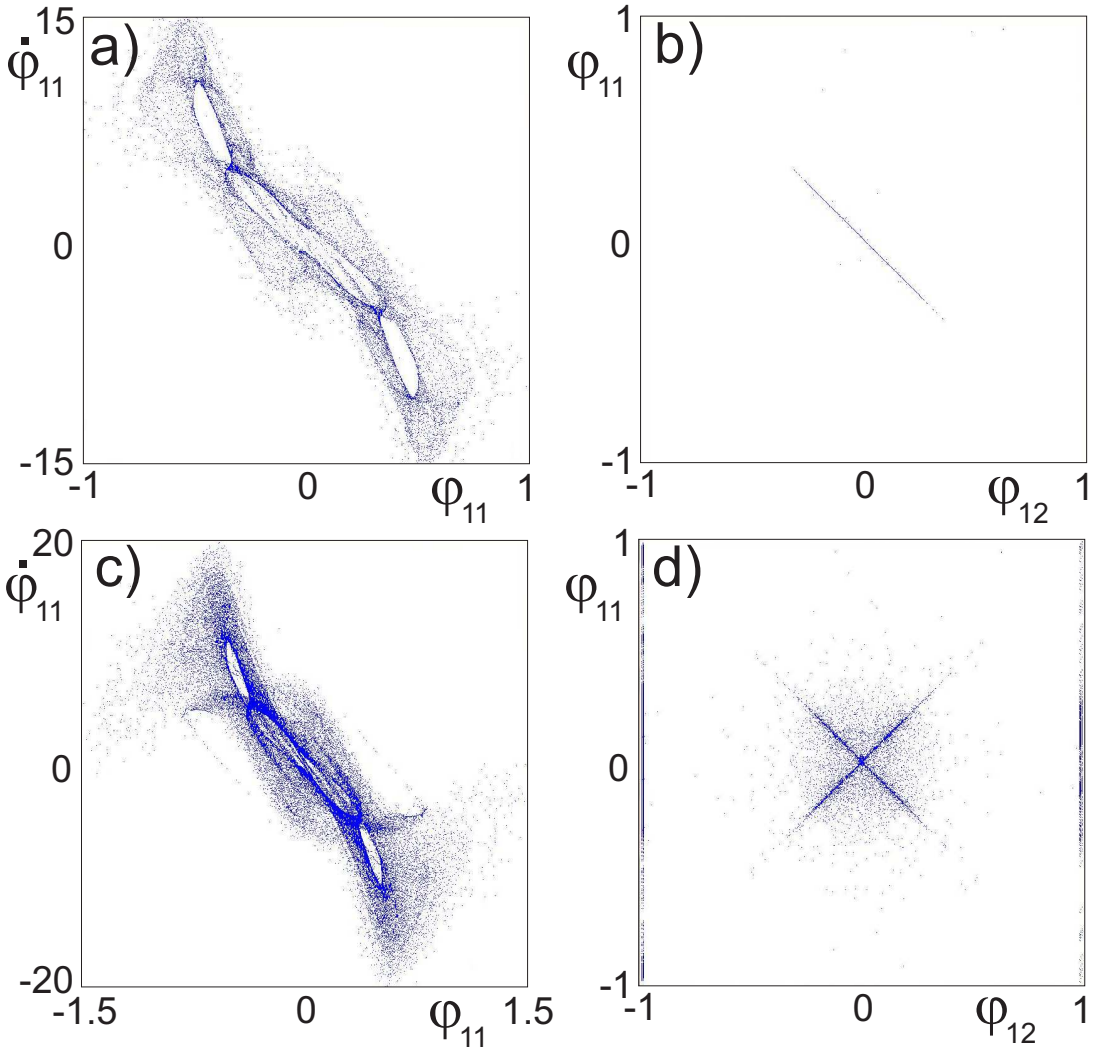

Figure 4.13: Poincaré maps (left column) and synchronization diagrams (right column) for identical pendulums for $\Omega = 32.20\ [\frac{rad}{s}]$ (a, b) and for $\Omega = 33.20\ [\frac{rad}{s}]$ (c, d).

the increased rate of M_1 is now given by the sum

$$M_1 = M_{b1} + m_{11} + \mu_{11} + m_{12} + \mu_{12} + m_e. \tag{4.24}$$

For the case of the beam which is fixed on both ends we have $m_e = 0.375\ m_b$. Taking into account the mass of experimental beam $m_b = 0.64\ [kg]$, we have $m_e = 0.24\ [kg]$ and consequently $M_1 = 0.44\ [kg]$.

In Figs. 4.16a–b bifurcation diagram illustrating an occurrence of combined in phase and in anti-phase synchronization (Fig. 4.16a) corresponding largest Lyapunov exponents (Fig. 4.16b) versus frequency of excitation, are presented.

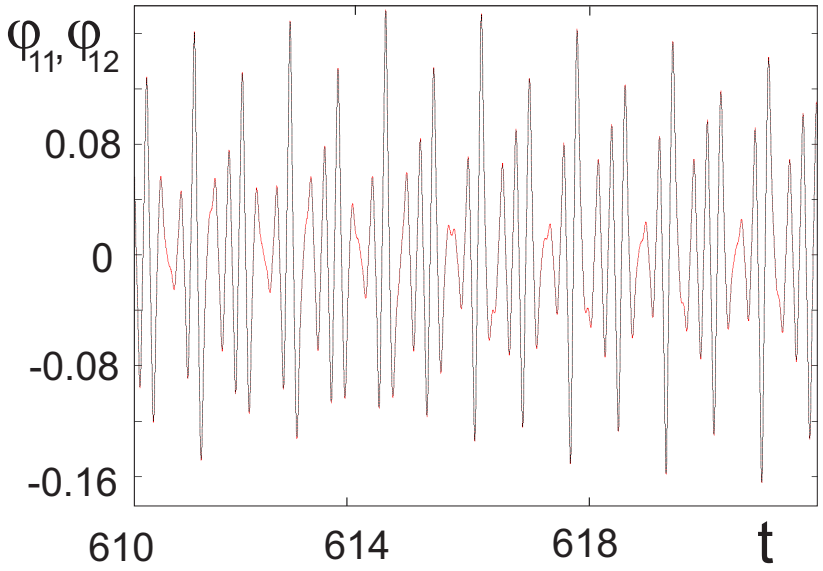

Figure 4.14: Time diagram for identical pendulums φ_{11}, φ_{12} for $\Omega = 32.93\ [\frac{rad}{s}]$ – pendulums in phase (complete synchronization).

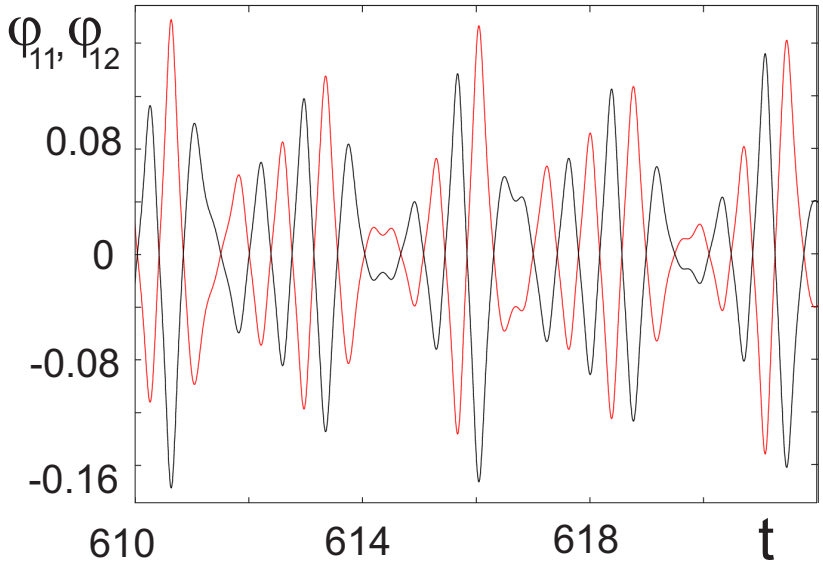

Figure 4.15: Time diagram for identical pendulums φ_{11}, φ_{12} for $\Omega = 32.20\ [\frac{rad}{s}]$ – pendulums in anti-phase (anti-phase synchronization).

It is evident that increased mass M_1 causes lack of synchronization in ranges of chaotic (one positive Lyapunov exponent) and hyperchaotic (two positive Lyapunov exponents) ranges of control parameter. Synchronous behaviour of pendulums is visible only in intervals of their regular motion, where Lyapunov exponents are non-positive.

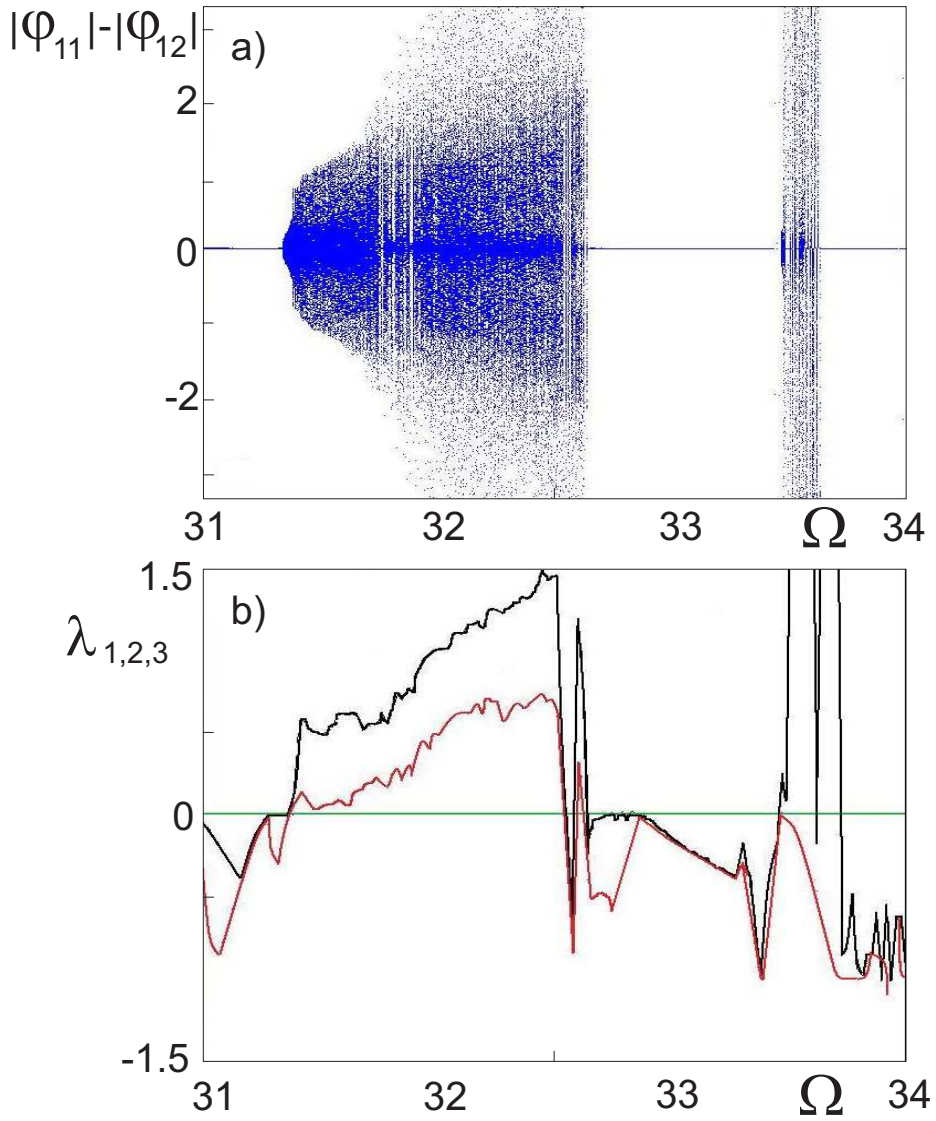

Figure 4.16: Bifurcation diagram $|\varphi_{11}| - |\varphi_{12}|$ (a) and corresponding Lyapunov exponents λ_1, λ_2, λ_3 (b) versus Ω.

Noidentical pendulums

In order to verify stability of synchronous state in the experimental case a parameter's mismatch, which is unavoidable in real systems, has to be taken under consideration. Hence, let us introduce to analysed system (Eq. (4.19)) parameter's mismatch of pendulums damping $\Delta c_1 = 3\%$. The other values of parameters are the same as those of identical pendulums.

Results shown in Fig. 4.17 correspond to Fig. 4.11 but there is taking into account the parameter's mismatch Δc_1. Comparing both cases we can

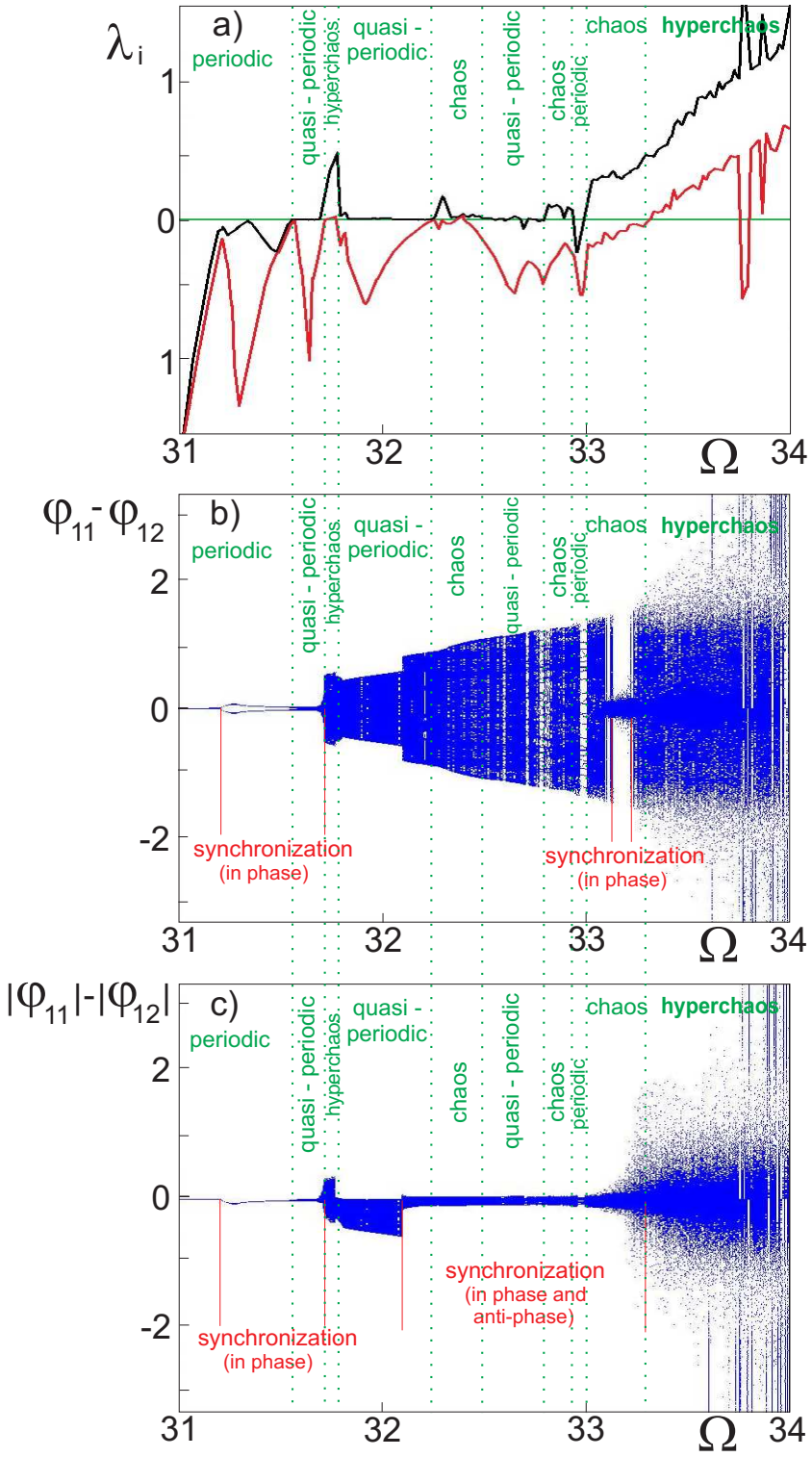

Figure 4.17: Diagram of Lyapunov exponents λ_1, λ_2, λ_3 and bifurcation diagrams $\varphi_{11} - \varphi_{12}$ versus Ω for $\Delta c_1 = 3\%$.

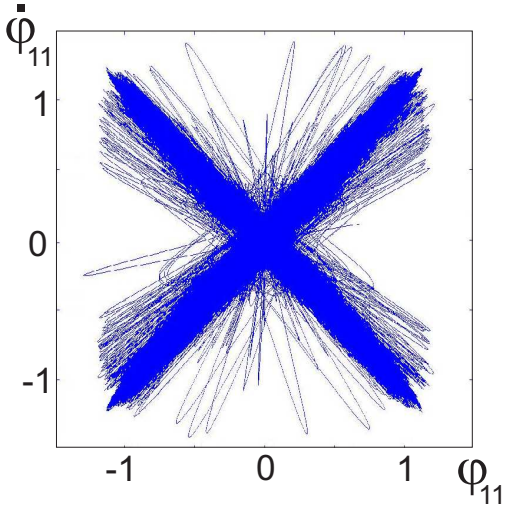

Figure 4.18: Poincaré map for φ_{11} versus $\dot{\varphi}_{11}$ for $\Delta c_1 = 3\%$ for $\Omega = 33.20\ [\frac{rad}{s}]$.

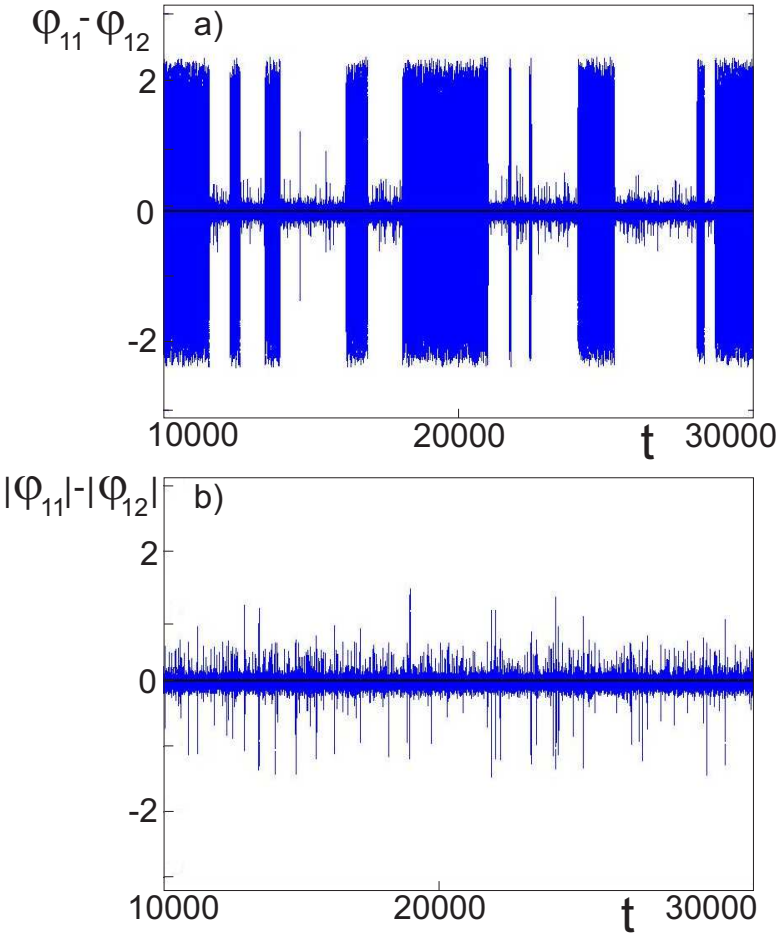

Figure 4.19: Time diagrams for $\Omega = 33.20$ for a) $\varphi_{11} - \varphi_{12}$ and b) $|\varphi_{11}| - |\varphi_{12}|$ for $\Delta c_1 = 3\%$.

estimate its influence on the pendulums synchronization stability. Significant similarity of Lyapunov exponents values (see Figs. 4.11a and 4.17a) indicates a slight disturbation of the synchronous state. This observation is borne out in Figs. 4.17b–c. Imperfect complete synchronization (small distance $\varphi_{11} - \varphi_{12}$) is observed in narrow interval of control parameter (Fig. 4.17b), but imperfect complete phase or anti-phase synchronization, i.e. a difference of absolute values $|\varphi_{11}| - |\varphi_{12}|$ if limited to a small distance, we can see in wide range of periodic, quasi-periodic and chaotic response of the system (Fig. 4.17c). Especially interesting result is presented in Figs. 4.18 and 4.19, where alternated states of chaotic synchronization in-phase and anti-phase are depicted for the range $\Omega \in (32.76; 33.40)\ [\frac{rad}{s}]$ – pendulums transit permanently from phase to anti-phase oscillations (see Fig. 4.18). We called this phenomenon intermittent in phase – anti-phase synchronization. The essence of this phenomenon is illustrated in time diagrams in Figs. 4.19a-b. In Fig. 4.19a we can observe synchronous intervals (imperfect complete synchronization) broken by bursting desynchronous periods. However, in these periods φ_{11} approaches $-\varphi_{12}$ (see time diagram 4.19b), what indicates an occurrence of the anti-synchronous regime. It is clearly visible that transitions between both synchronous states are sudden and not smooth. This property is typical for the phenomenon of intermittency.

4.5. Three masses with six pendulums ($n = 3$)

In the current subsection the dynamics of 6 physical pendulums located on (coupled through) an elastic structure is considered. The numerical study of a realistic model of identical pendulums suspended on an elastic beam is presented. The pendulums are externally excited by a periodic signal. The excitation in the position of mass M_{bn} is expressed by the formula $x_{ex\,n} = x_{z1} + \frac{l_n}{l_b}\,(x_{z2} - x_{z1})$, where l_b is a total length of the elastic beam. In the present case, the driving on both sides of the elastic beam are the same $x_{z1} = x_{z2} = x_z = z\,\sin(\Omega t)$, therefore we have $x_{ex\,1} = x_{ex\,3}$. The analysed system is presented in Fig. 4.20.

Equations of motion for the system shown in Fig. 4.20 were formulated using

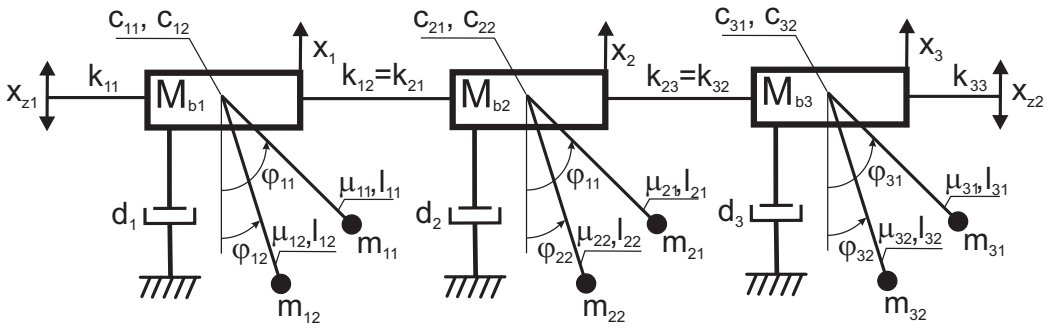

Figure 4.20: System of 6 physical pendulums located on (coupled through) an elastic structure.

the Lagrange's equations:

$$B_{11}\,\ddot{\varphi}_{11} + A_{11}\,\ddot{x}_1\,\sin\varphi_{11} + A_{11}\,g\,\sin\varphi_{11} + c_{11}\,\dot{\varphi}_{11} = 0 \tag{4.25a}$$

$$B_{12}\,\ddot{\varphi}_{12} + A_{12}\,\ddot{x}_1\,\sin\varphi_{12} + A_{12}\,g\,\sin\varphi_{12} + c_{12}\,\dot{\varphi}_{12} = 0 \tag{4.25b}$$

$$\begin{aligned} &M_1\,\ddot{x}_1 + A_{11}\,(\ddot{\varphi}_{11}\,\sin\varphi_{11} + \dot{\varphi}_{11}^2\,\cos\varphi_{11}) + A_{12}\,(\ddot{\varphi}_{12}\,\sin\varphi_{12} + \dot{\varphi}_{12}^2\,\cos\varphi_{12}) \\ &\quad + d_1\,\dot{x}_1 + k_{11}\,(x_1 - x_{ex\,1}) + k_{12}\,(x_2 - x_{ex\,2}) + k_{13}\,(x_3 - x_{ex\,3}) = 0 \end{aligned} \tag{4.25c}$$

$$B_{21}\,\ddot{\varphi}_{21} + A_{21}\,\ddot{x}_2\,\sin\varphi_{21} + A_{21}\,g\,\sin\varphi_{21} + c_{21}\,\dot{\varphi}_{21} = 0 \tag{4.25d}$$

$$B_{22}\,\ddot{\varphi}_{22} + A_{22}\,\ddot{x}_2\,\sin\varphi_{22} + A_{22}\,g\,\sin\varphi_{22} + c_{22}\,\dot{\varphi}_{22} = 0 \tag{4.25e}$$

$$\begin{aligned} &M_2\,\ddot{x}_2 + A_{21}\,(\ddot{\varphi}_{21}\,\sin\varphi_{21} + \dot{\varphi}_{21}^2\,\cos\varphi_{21}) + A_{22}\,(\ddot{\varphi}_{22}\,\sin\varphi_{22} + \dot{\varphi}_{22}^2\,\cos\varphi_{22}) \\ &\quad + d_2\,\dot{x}_2 + k_{21}\,(x_1 - x_{ex\,1}) + k_{22}\,(x_2 - x_{ex\,2}) + k_{23}\,(x_3 - x_{ex\,3}) = 0 \end{aligned} \tag{4.25f}$$

$$B_{31}\,\ddot{\varphi}_{31} + A_{31}\,\ddot{x}_3\,\sin\varphi_{31} + A_{31}\,g\,\sin\varphi_{31} + c_{31}\,\dot{\varphi}_{31} = 0 \tag{4.25g}$$

$$B_{32}\,\ddot{\varphi}_{32} + A_{32}\,\ddot{x}_3\,\sin\varphi_{32} + A_{32}\,g\,\sin\varphi_{32} + c_{32}\,\dot{\varphi}_{32} = 0 \tag{4.25h}$$

$$\begin{aligned} &M_3\,\ddot{x}_3 + A_{31}\,(\ddot{\varphi}_{31}\,\sin\varphi_{31} + \dot{\varphi}_{31}^2\,\cos\varphi_{31}) + A_{32}\,(\ddot{\varphi}_{32}\,\sin\varphi_{32} + \dot{\varphi}_{32}^2\,\cos\varphi_{32}) \\ &\quad + d_3\,\dot{x}_3 + k_{31}\,(x_1 - x_{ex\,1}) + k_{32}\,(x_2 - x_{ex\,2}) + k_{33}\,(x_3 - x_{ex\,3}) = 0 \end{aligned} \tag{4.25i}$$

where (for $i,\ j = 1,\ 2,\ 3$)

$$B_{i1,\,i2} = B_{i\,S1,i\,S2} + (m_{i1,\,i2} + \mu_{i1,\,i2})\,{b_{i1,\,i2}}^2,$$

$$A_{i1,\,i2} = (m_{i1,\,i2} + \mu_{i1,\,i2})\,b_{i1,\,i2},$$

$$M_i = M_{bi} + m_{i1} + \mu_{i1} + m_{i2} + \mu_{i2},$$

and M_{bi} – mass of the oscillator $[kg]$, $m_{i1,i2}$ – mass concentrated at the point in the end of rod $[kg]$, $\mu_{i1,i2}$ – mass of the rod $[kg]$, $l_{i1,i2}$ – length of the rod $[m]$,

$B_{i\,S1,i\,S2}$ is the inertia moment of the mass $[kg\,m^2]$ given by

$$B_{i\,S1,i\,S2} = m_{i1,i2}(l_{i1,i2} - b_{i1,i2})^2 + \frac{1}{12}\mu_{i1,i2}l_{i1,i2}^2 + \mu_{i1,i2}(b_{i1,i2} - \frac{1}{2}l_{i1,i2})^2 \quad (4.26)$$

and

$$b_{i1,i2} = \frac{(m_{i1,i2} + \frac{1}{2}\mu_{i1,i2})l}{(m_{i1,i2} + \mu_{i1,i2})} \quad (4.27)$$

is distance from the center of mass to the center of rotation of the rod and mass $m_{i1,i2}$, k_{ji} – spring stiffness $[N/m]$, $c_{i1,i2}$ – damping factor at the node $[Nms]$, d_i – viscous damping $[Ns/m]$. The derivatives in Eq. (4.28) are calculated with respect to nondimensional time τ.

Introducing $\omega = \sqrt{\frac{k_{11}}{M_1}}$ (the natural frequency), $x_S = \frac{M_1 g}{k_{11}}$ and dividing Eqs. (4.25a), (4.25b), (4.25d), (4.25e), (4.25g), (4.25h) by $l_1\ k_{11}\ x_S$ and Eqs. (4.25c), (4.25f), (4.25i) by $k_{11}\ x_S$ we obtain the dimensionless equations:

$$\alpha_{11}\ \ddot{\varphi}_{11} + \beta_{11}\ \ddot{x}_1\ \sin\varphi_{11} + \gamma_{11}\ \sin\varphi_{11} + \zeta_{11}\ \dot{\varphi}_{11} = 0 \quad (4.28a)$$

$$\alpha_{12}\ \ddot{\varphi}_{12} + \beta_{12}\ \ddot{x}_1\ \sin\varphi_{12} + \gamma_{12}\ \sin\varphi_{12} + \zeta_{12}\ \dot{\varphi}_{12} = 0 \quad (4.28b)$$

$$\varepsilon_1\ \ddot{x}_1 + \rho_{11}\ (\sin\varphi_{11}\ \ddot{\varphi}_{11} + \cos\varphi_{11}\ \dot{\varphi}_{11}^2) + \rho_{12}\ (\sin\varphi_{12}\ \ddot{\varphi}_{12} + \cos\varphi_{12}\ \dot{\varphi}_{12}^2)$$
$$+ \delta_1\ \dot{x}_1 + \kappa_{11}(x_1 - X_{ex\,1}) + \kappa_{12}(x_2 - X_{ex\,2}) + \kappa_{13}(x_3 - X_{ex\,3}) = 0 \quad (4.28c)$$

$$\alpha_{21}\ \ddot{\varphi}_{21} + \beta_{21}\ \ddot{x}_2\ \sin\varphi_{21} + \gamma_{21}\ \sin\varphi_{21} + \zeta_{21}\ \dot{\varphi}_{21} = 0 \quad (4.28d)$$

$$\alpha_{22}\ \ddot{\varphi}_{22} + \beta_{22}\ \ddot{x}_2\ \sin\varphi_{22} + \gamma_{22}\ \sin\varphi_{22} + \zeta_{22}\ \dot{\varphi}_{22} = 0 \quad (4.28e)$$

$$\varepsilon_2\ \ddot{x}_2 + \rho_{21}\ (\sin\varphi_{21}\ \ddot{\varphi}_{21} + \cos\varphi_{21}\ \dot{\varphi}_{21}^2) + \rho_{22}\ (\sin\varphi_{22}\ \ddot{\varphi}_{22} + \cos\varphi_{22}\ \dot{\varphi}_{22}^2)$$
$$+ \delta_2\ \dot{x}_2 + \kappa_{21}(x_1 - X_{ex\,1}) + \kappa_{22}(x_2 - X_{ex\,2}) + \kappa_{23}(x_3 - X_{ex\,3}) = 0 \quad (4.28f)$$

$$\alpha_{31}\ \ddot{\varphi}_{31} + \beta_{31}\ \ddot{x}_3\ \sin\varphi_{31} + \gamma_{31}\ \sin\varphi_{31} + \zeta_{31}\ \dot{\varphi}_{31} = 0 \quad (4.28g)$$

$$\alpha_{32}\ \ddot{\varphi}_{32} + \beta_{32}\ \ddot{x}_3\ \sin\varphi_{32} + \gamma_{32}\ \sin\varphi_{32} + \zeta_{32}\ \dot{\varphi}_{32} = 0 \quad (4.28h)$$

$$\varepsilon_3\ \ddot{x}_3 + \rho_{31}\ (\sin\varphi_{31}\ \ddot{\varphi}_{31} + \cos\varphi_{31}\ \dot{\varphi}_{31}^2) + \rho_{32}\ (\sin\varphi_{32}\ \ddot{\varphi}_{32} + \cos\varphi_{32}\ \dot{\varphi}_{32}^2)$$
$$+ \delta_3\ \dot{x}_3 + \kappa_{31}(x_1 - X_{ex\,1}) + \kappa_{32}(x_2 - X_{ex\,2}) + \kappa_{33}(x_3 - X_{ex\,3}) = 0 \quad (4.28i)$$

where (for $i,\ j = 1,\ 2,\ 3$)

$$\alpha_{i1,\,i2} = \frac{B_{i1,\,i2}}{M_1\,b_{11}\,x_S},\quad \beta_{i1,\,i2} = \frac{A_{i1,\,i2}}{M_1\,b_{11}\,x_S},\quad \gamma_{i1,\,i2} = \frac{A_{i1,\,i2}}{M_1\,b_{11}},\quad \zeta_{i1,\,i2} = \frac{c_{i1,\,i2}}{\omega\,M_1\,b_{11}\,x_S},$$
$$\varepsilon_i = \frac{M_i}{M_1},\qquad \rho_{i1,\,i2} = \frac{A_{i1,\,i2}}{M_1\,x_S},\qquad \delta_i = \frac{d_i}{\omega\,M_1},\qquad \kappa_{ji} = \frac{k_{ji}}{k_{11}},$$
$$X_{ex\,j} = \frac{x_{ex\,j}}{x_S},\qquad Z = \frac{z}{x_S},\qquad \eta = \frac{\Omega}{\omega}$$

are dimensionless parameters and

$$\varphi_{i1,\,i2} = \frac{d\varphi_{i1,\,i2}}{d\tau},$$
$$x_i = \frac{1}{x_S}\frac{dx_i}{d\tau},$$
$$\tau = \omega\, t$$

are dimensionless variables. The derivatives in Eqs. (4.28) are calculated with respect to nondimensional time τ.

4.5.1 Numerical results for $n = 3$

In the numerical analysis we assumed the mass of each oscillator $M_{bi} = 0.2\ [kg]$ and the following dimensional parameters of the system (4.25) with mismatches $\Delta m_i \leq 1\%$, $\Delta\mu_i \leq 1\%$ and $\Delta l_i \leq 1\%$:

$$m_{11,21,31} = 0.1\ [kg] \quad m_{12,22} = 0.101\ [kg] \quad m_{32} = 0.099\ [kg]$$
$$\mu_{11,12,32} = 0.05\ [kg] \quad \mu_{21} = 0.0505\ [kg] \quad \mu_{22} = 0.0504\ [kg] \quad \mu_{31} = 0.0495\ [kg]$$
$$l_{11,21,31} = 0.15\ [m] \quad l_{12} = 0.1515\ [m] \quad l_{22} = 0.1512\ [m] \quad l_{32} = 0.1485\ [m]$$
$$z = 0.01\ [m] \quad d_i = 2.0\ [\tfrac{Ns}{m}] \quad c_{i1,i2} = 0.0003\ [Nms].$$

We took Ω to be a bifurcation parameter. We assumed that the oscillators were located symmetrically on the beam and we calculated $[k_{ji}]$:

$$\begin{bmatrix} k_{11} & k_{12} & k_{13} \\ k_{21} & k_{22} & k_{23} \\ k_{31} & k_{32} & k_{33} \end{bmatrix} = \begin{bmatrix} 1202.98 & -1157.07 & 472.882 \\ -1157.07 & 1691.59 & -1157.07 \\ 472.882 & -1157.07 & 1202.98 \end{bmatrix}.$$

Parameters of the beam: length $l_b = 1.0\ [m]$, height $h = 0.002\ [m]$ and width $a = 0.03\ [m]$, modulus of elasticity $E = 0.74\, e^{11}\ [N/m^2]$, the inertial momentum of cross-section $I\ [m^4]$ and $EI = 1.48\ [Nm^2]$.

Results for the following parameter values and initial conditions

$$\varphi_{11,32} = 3.11\ [rad] \quad \varphi_{12,21,22,31} = -3.11\ [rad]$$
$$\varphi_{11,21,32} = 1.5\ [\tfrac{rad}{s}] \quad \varphi_{12,22,31} = -1.5\ [\tfrac{rad}{s}]$$
$$x_{1,3} = 0.01\ [m] \quad x_2 = 0.014\ [m]$$
$$\dot{x}_{1,3} = 1.0\ [\tfrac{m}{s}] \quad \dot{x}_2 = 1.0\ [\tfrac{m}{s}]$$

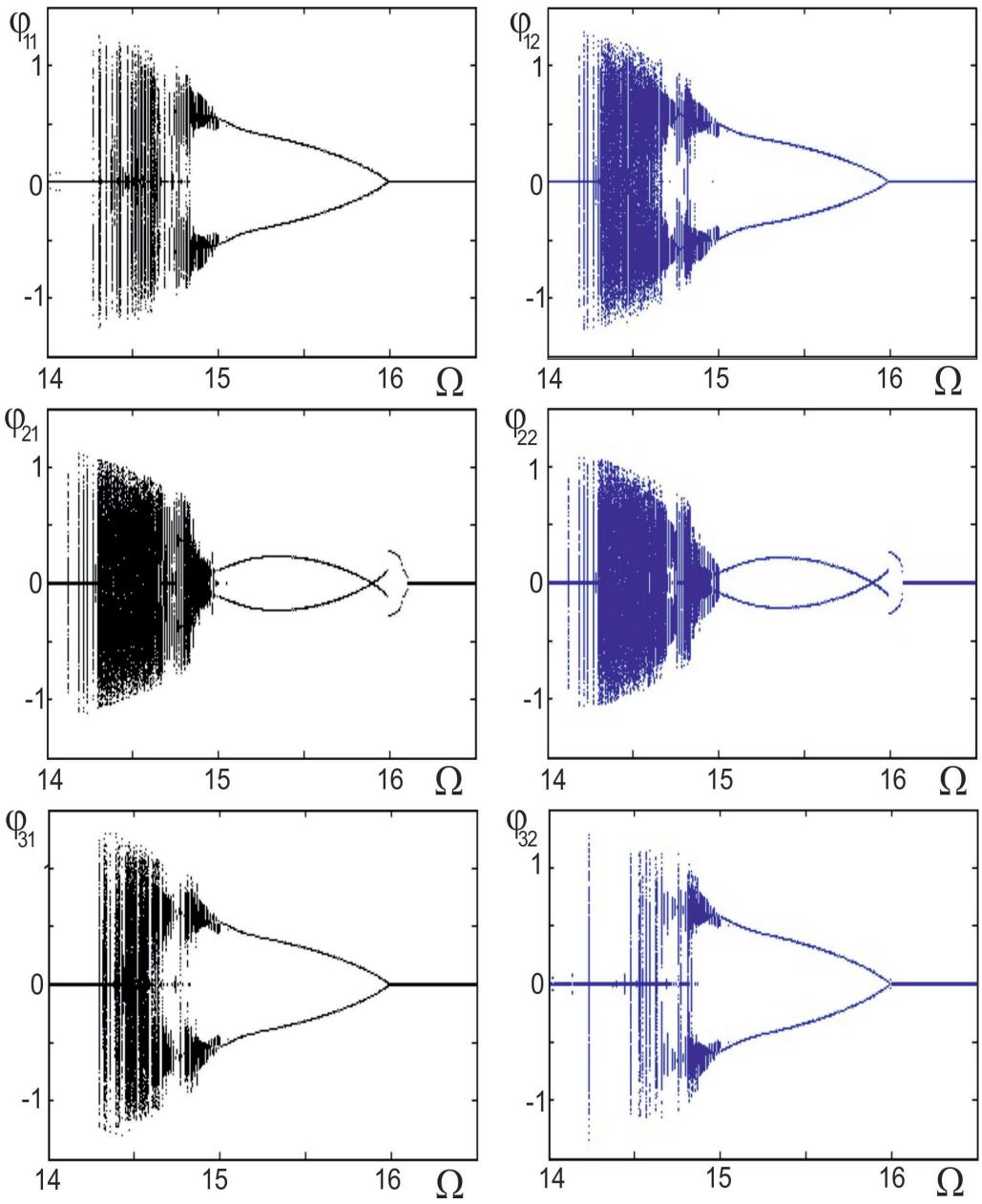

Figure 4.21: Numerical results for $n = 3$ oscillator nodes.

are presented in the diagrams in Figs. 4.21, 4.22 and 4.23.

Performed numerical simulations shown that dynamics of the system Eq. (4.25) is extremely sensitive to initial conditions. This property seems to be significant, especially in context of experimental research. The analysis of this system was concentrated on the responses of pendulums and their possible collective behaviour. In Figs. 4.21a–f bifurcation diagrams of angular displacement of all six pendulums versus frequency of excitation

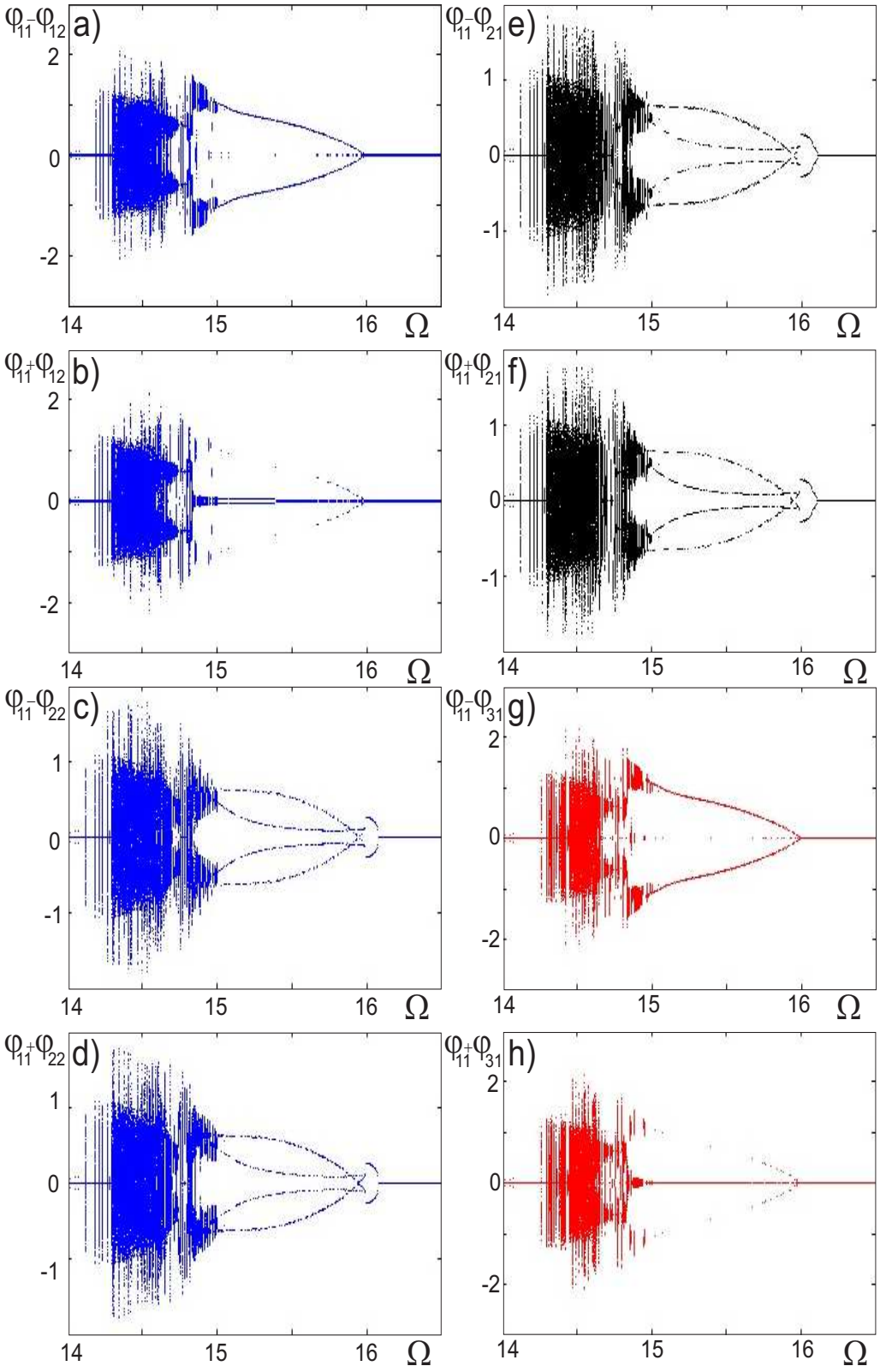

Figure 4.22: Numerical results for $n = 3$ oscillator nodes. Diagram $\varphi_{11} - \varphi_{ij}$.

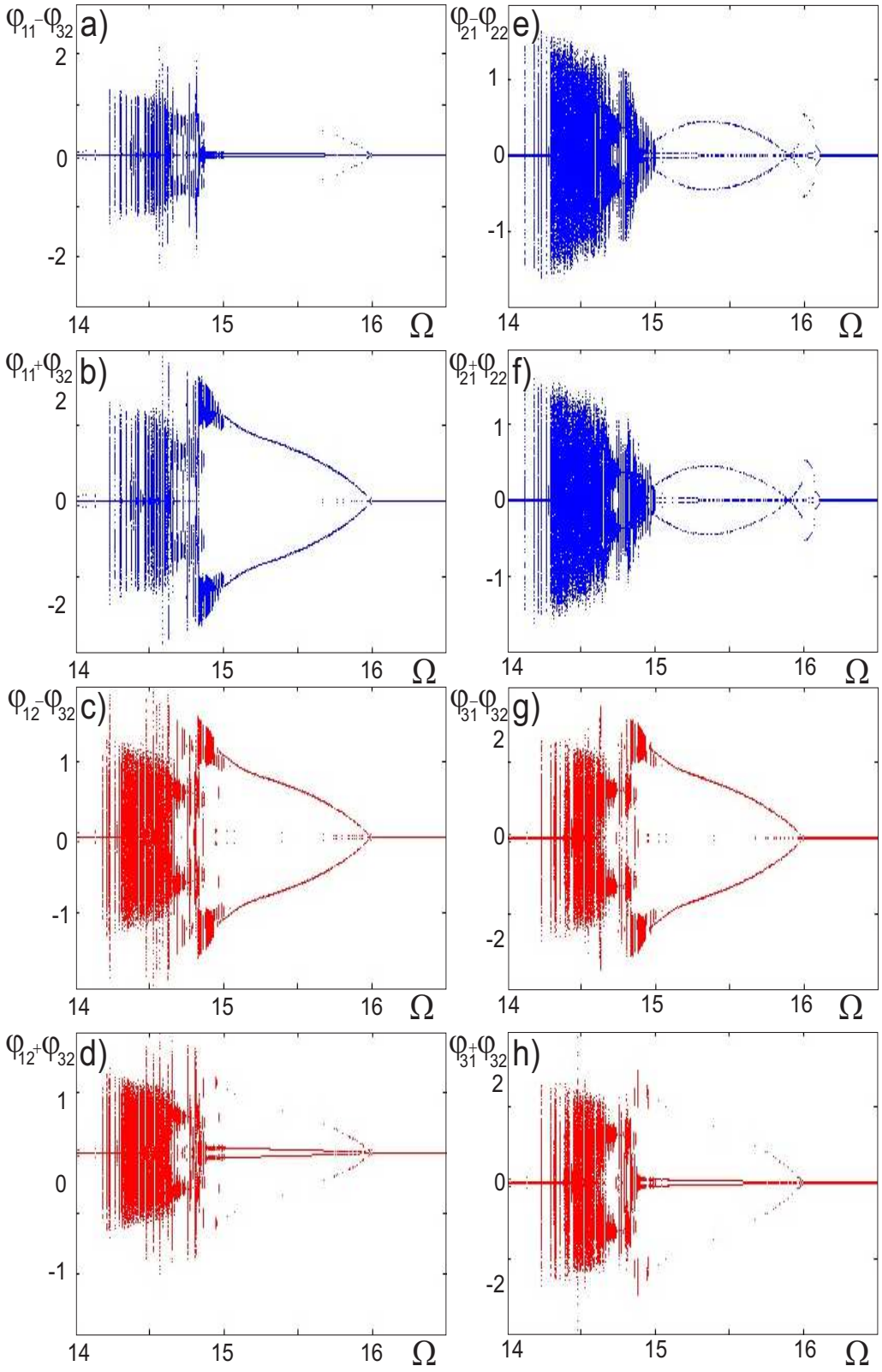

Figure 4.23: Numerical results for $n = 3$ oscillator nodes.

are demonstrated. Overall shape of bifurcation courses shows synchronization possibility in each i-th pair of pendulums as well as between symmetrically located pendulums, i.e., in nodes 1 and 3. Verification of pendulums synchronizability is illustrated in Figs. 4.22a–h and 4.23a–h for arbitrarily chosen pairs of pendulums, i.e. collected from the same or different nodes. Complete (in-phase) synchronization tendency is represented by bifurcation diagrams of angles subtraction (Figs. 4.22 b, f, d, h and 4.23 b, f, d, h) while anti-phase synchronization can be detected by means of sum of angles (Figs. 4.22 a, e, c, g and 4.23 a, e, c, g). Presented results, representative for our research, shown occurrence of synchronous states in ranges of periodic oscillations (Figs. 4.22 b, h, 4.23 a, d, h). Chaotic synchronization was not observed.

Chapter 5

Experiment

5.1. Experimental rig

Coupled dynamical systems whose elements can be treated as mathematical or physical pendulum, are widely used technical and engineering devices. They may be parts of machines, such as components of cranes and port crane, where the pendulum plays the role of a crane arm. Also each suspension element, which during motion of the machine varies, can be considered as the pendulum, e.g., the engine suspension system for an aircraft wing. Furthermore, pendulums are increasingly used to eliminate the vibrating components of bridges, tall chimneys and towers. Oscillating systems of multiple degree of freedom, comprising of pendulums, may exhibit the phenomenon of energy transfer between the degrees of freedom as a result of various types of couplings.

The flow of energy can be partial or complete, and it depends on the choice of parameters. It turns out that the total energy transfer occurs when the ratio of self-oscillation frequency is equal to the ratio of the integers, i.e., when this frequencies are commensurate. In the literature, this phenomenon is called an internal resonance. The nature of the flow of energy can be diversified. The conjugated elastic phenomena may lead to beats, and conjugated inertia – to autoparametric resonance. If we have damping in the system, then the internal resonance of the vibration with one frequency or the vibration in the type of beats (with superimposed at least two frequencies) may occur. Therefore, it is important

to know the feedback, because their character may be different.

In systems with many degrees of freedom with inertial coupling the parametric vibration may appear. Parametric vibration problem is quite complex, and solutions are only known for a specific form of the equations in the case of equations with one degree of freedom. The phenomenon of excited of auto-parametric vibration have been observed in the thirties of the last century by Gorelik and Witt [103] and many others [104]. They studied the mathematical pendulum suspended on a spring system and described by two second order differential equations coupled with a nonlinear element. They reported as the first the transfer of energy between the principal modes of vibration (longitudinal and rotational pendulum) in relation to the case where the frequency of vibration of the pendulum is doubled along the rotational vibration frequency of the pendulum. The analysis of this system can be found in the monographs [105, 106, 107].

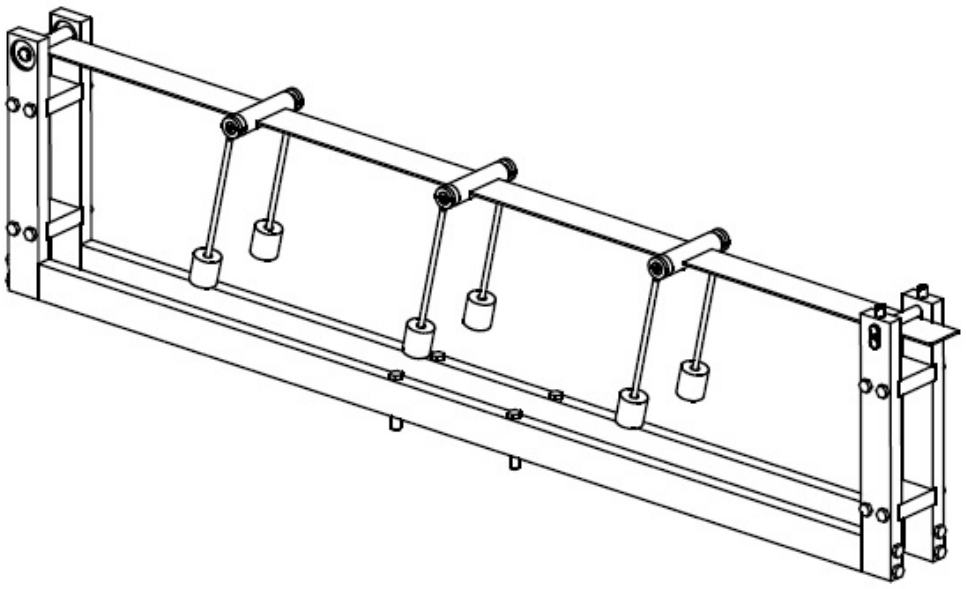

Figure 5.1: Experimental rig consisting of three nodes of oscillators.

In our experiments, we have used the rig with the set of three pairs of double pendulums shown in schematic Fig. 5.1 and Fig. 5.2 and with one pair of double pendulums shown in Fig. 5.3. The vertical oscillations can be seen here as a blurry contour of the rig frame. Before numerical simulations and experiments some basic measurements of the individual pendulums have been carried out.

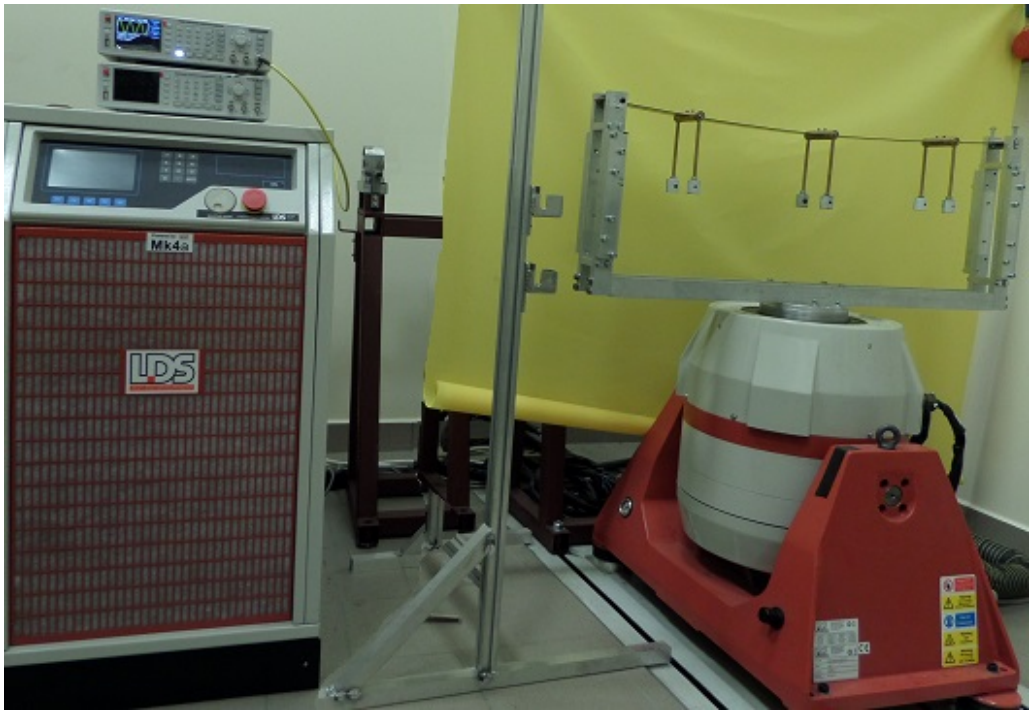

Figure 5.2: Complete experimental rig consisting of the beam with pendulums mounted on the electrodynamic shaker.

In order to verify the numerical results in practice, the experimental study has been conducted. Real parameters of experimental rig approach (with the mismatch not exceeding 3%) nominally identical values assumed in numerical simulations. Parameters of pendulums: lengths $l_{i1} = l_{i2} = 0.15$ $[m]$, masses of the rods $\mu_{i1} = \mu_{i2} = 0.05$ $[kg]$ with masses $m_{i1} = m_{i2} = 0.10$ $[kg]$, masses at the end $M_{bi} = 0.2$ $[kg]$, $i = 1, 2, \ldots, n$. Parameters of the beam: mass $m_b = 0.64$ $[kg]$, length $l_b = 1.0$ $[m]$, height $h = 0.002$ $[m]$ and width $a = 0.03$ $[m]$, modulus of elasticity $E = 0.74e^{11}$ $[N/m^2]$, the inertial momentum of cross-section I $[m^4]$ and $EI = 1.48$ $[Nm^2]$. Two cases were investigated experimentally: $n = 1$ and $n = 3$. The rig has been mounted on the shaker LDS V780 Low Force Shaker (basic data are as follows: sine force peak 5120 $[N]$; max random force (rms) 4230 $[N]$; max acceleration sine peak $g_n = 0.111$ $[m]$; system velocity sine peak 1.9 $[m/s]$; displacement pk-pk $g_n = 0.254$ $[m]$; moving element mass 4.7 $[kg]$). The shaker introduces kinematic periodic excitation $z\cos\Omega t$, where z and Ω are the amplitude and the frequency of the excitation, respectively. At initial moments of the lower pendulum have been assumed to be in the upper position $\varphi_{ij} = \pi \pm \pi/36$

for $i = 1,\ 2, \ldots,\ n,\ j = 1,\ 2$. We fix the value of the excitation amplitude $z = 0.0082 \pm 0.004\ [m]$ and consider excitation frequency Ω as a control parameter. The rig was excited around its resonance frequency Ω in the approximated range between 5 and 7 $[Hz]$, i.e. approximately $30 - 40\ [rad/s]$.

The amplitude of external excitation $z = 0.0082\ [m]$ was calculated from following formula

$$z = \frac{\sum_{i=1}^{n} z_{max}^{i} - z_{min}^{i}}{n} \tag{5.1}$$

where n is a number of peaks.

In designing the rig, we deliberately chosen identical masses and length of elements (the differences in masses and length are about 1% between the maximum and the minimum values). Our goal was to check if the theoretically predicted synchronization of the nominally identical pendulums can be observed experimentally.

Dynamics of the system has been video recorded and the beam and pendulum's trajectories have been determined using image analysis software *Kinovea*.

5.2. Mass with two pendulums ($n = 1$)

In Fig. 5.3 experimental rig consisting of one mass-pendulums ($n = 1$) component is presented, whereas, in Figs. 5.4 a-b we see pictures documenting synchronous behaviour of the pendulums - in phase and in anti-phase, respectively, observed during the experiment.

In general, carried out experimental tests brought a variety of interesting dynamical behaviours of pendulums, e.g. chaotic rotation of the first pendulum while the second remains in the top position of equilibrium or anti-phase synchronization of the quasi-periodic behaviour of pendulums.

An exemplary analysis of experimental results is demonstrated in Figs. 5.5 and 5.6. The measurement equipment allows us to detect a position of the pendulum in an orthogonal coordinate system $(x_{ij},\ y_{ij})$ as shown in Fig. 5.5. Hence, angular

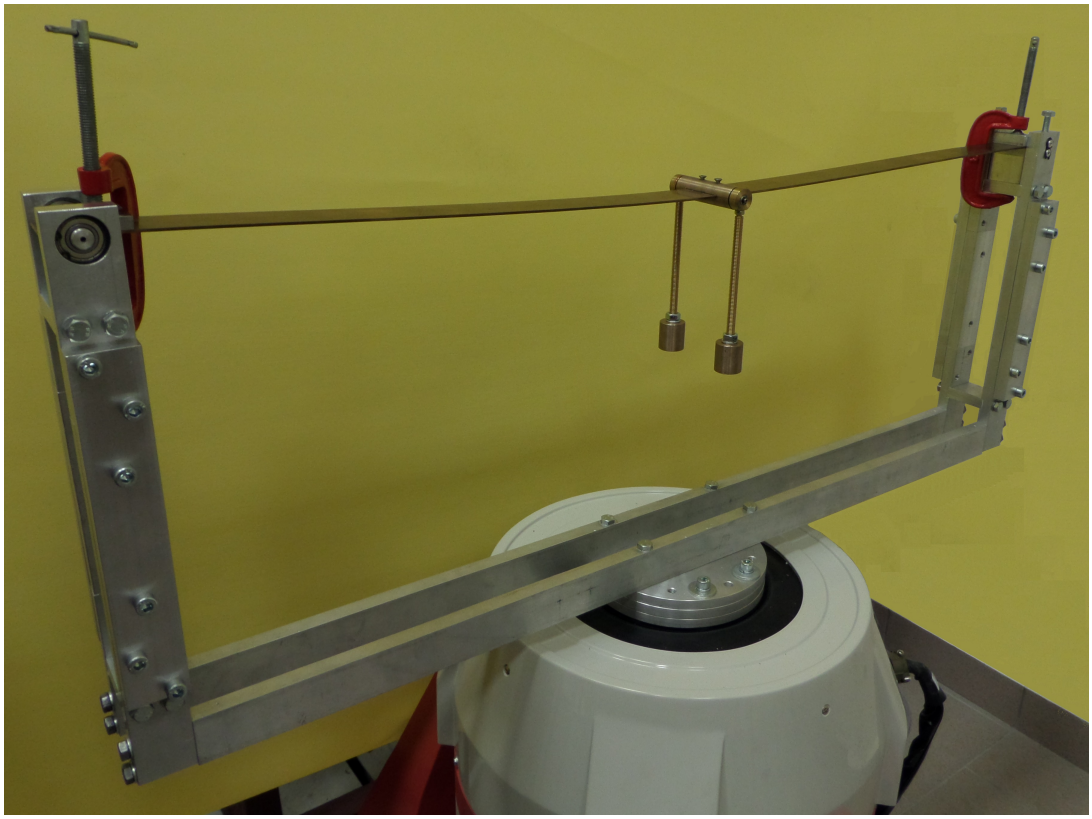

Figure 5.3: Experimental rig consisting of one oscillator node ($n = 1$).

displacement can be determined from obvious relation

$$\tan(\varphi_{ij}) = \frac{y_{ij}}{x_{ij}}. \tag{5.2}$$

In Fig. 5.6 a diagram illustrating the synchronization tendency of both pendulums (i.e., vertical position x_{11} and x_{12} of pendulums), corresponding to Fig. 5.5, is shown. Due to applied method of collecting the experimental data in orthogonal directions, trajectories shown in Figs. 5.5 and 5.6 seem to represent a case of irregular motion. However, we have to remember that collected signal also contain the vertical displacement of the beam with the mass. Thus, in fact pendulum's oscillations are periodic. This is one of the most interesting cases, where imperfect complete synchronization in phase (Fig. 5.4a and in anti-phase (Fig. 5.4b) is observed during periodic motion of pendulums (Fig. 5.5). One can observe intermittent transition between the synchronization in phase and in anti-phase - Fig. 5.6, which was also obtained in the computer simulations. On the other hand, the synchronization of chaotic pendulums has not been observed experimentally.

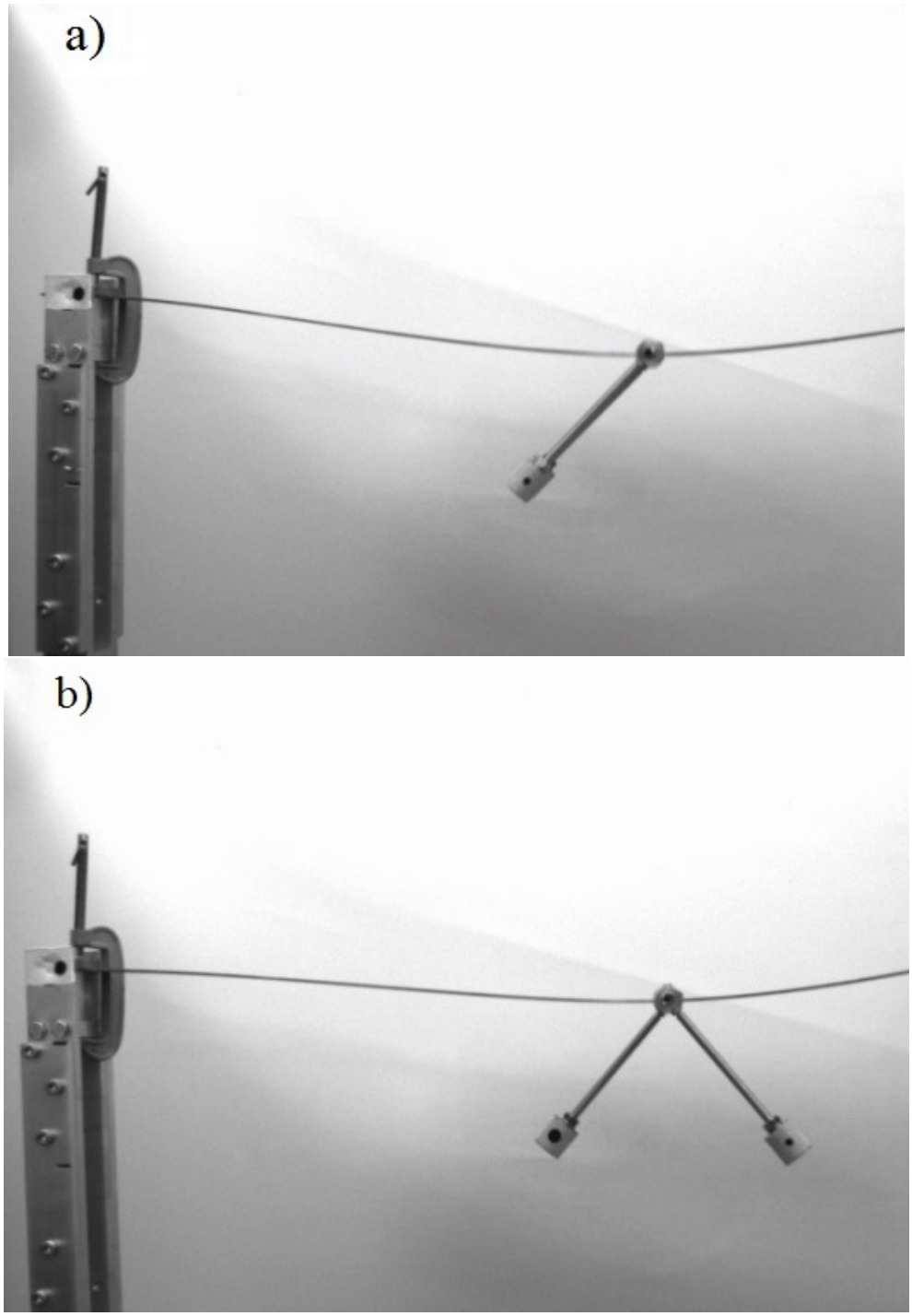

Figure 5.4: Experiment: a) phase synchronization (practical): $\varphi_{11} = \varphi_{12}$, b) anti-phase synchronization: $\varphi_{11} = -\varphi_{12}$ for $\Omega = 36\ [rad/s]$.

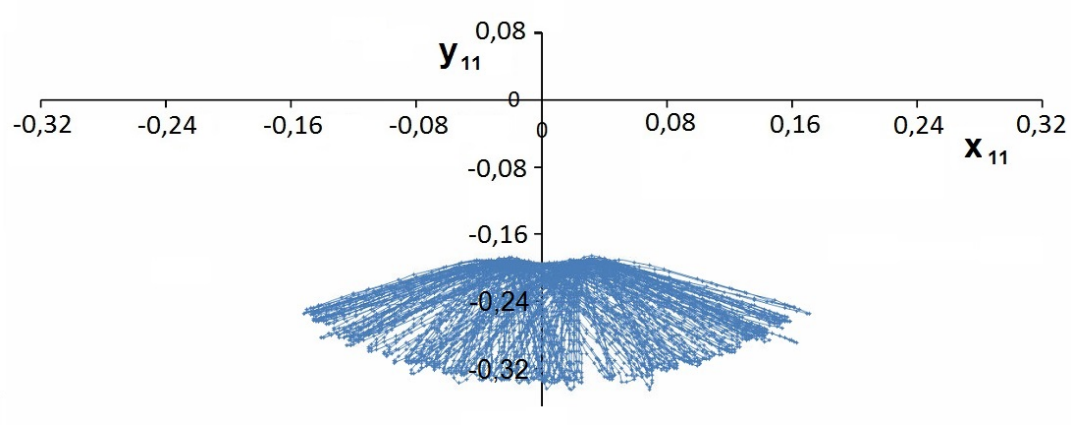

Figure 5.5: Trajectory of the motion of pendulum described by angle φ_{11} at the plane $(x_{11},\ y_{11})$ for $\Omega = 36\ [rad/s]$.

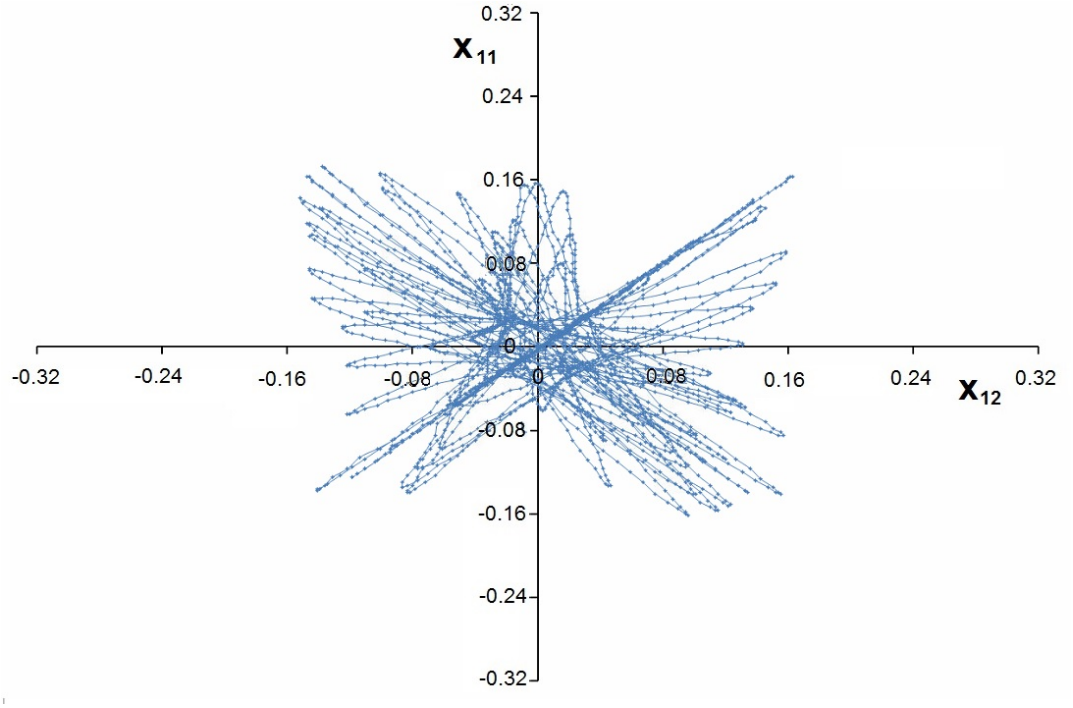

Figure 5.6: Experiment: coexistence of phase synchronization (practical) – $\varphi_{11} = \varphi_{12}$ and anti-phase synchronization – $\varphi_{11} = -\varphi_{12}$ for $\Omega = 36\ [rad/s]$.

5.3. Three masses with six pendulums ($n = 3$)

In Fig. 5.7 experimental rig containing of three mass-pendulums oscillators is presented. The mass-pendulums components are symmetrically suspended on the beam.

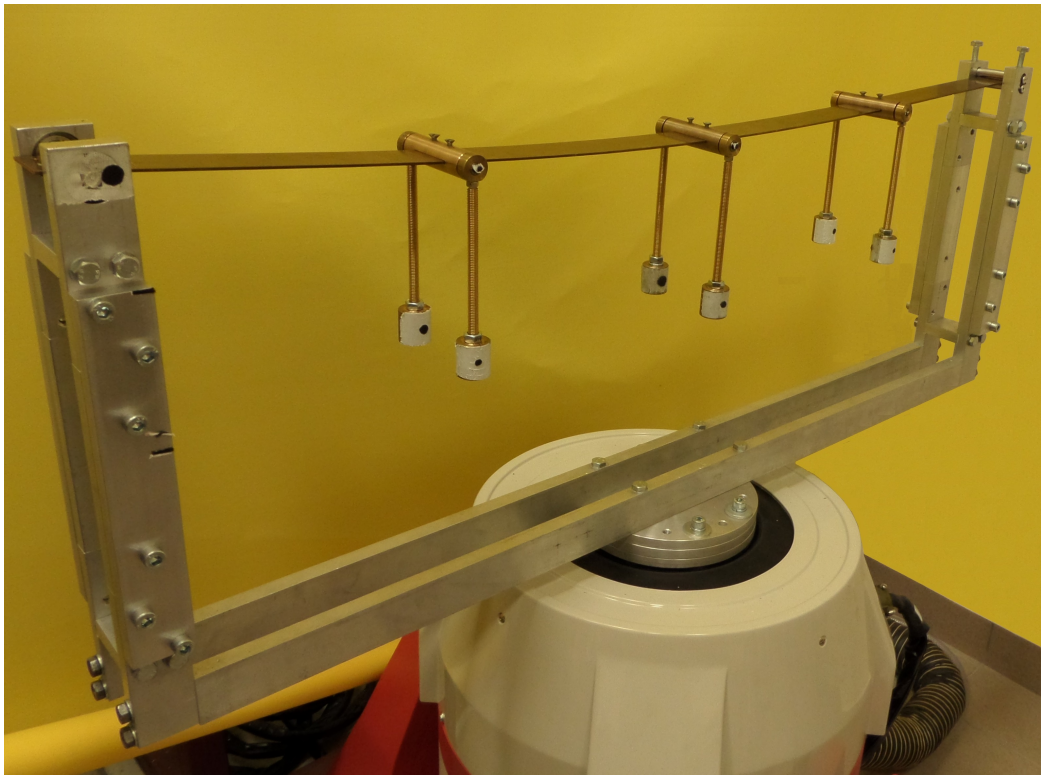

Figure 5.7: Experimental rig for $n = 3$.

Relatively large number of degrees of freedom leads to a rich spectrum of dynamical responses, especially in context of pendulum's synchronization. Among a variety of detected responses of the system under consideration the most interesting are cases when rotations of some pendulums coexist with oscillations of others. In this case, one can observe various types of pendulums synchronization. Two distinguished examples of different types of synchronization are shown in Figs. 5.8a-b, where arrows indicate the direction of motion (rotation or oscillation). In Fig. 5.8a presents the case when two pendulums rotate in the same direction (φ_{11}, φ_{32}) and when the rest four pendulums swing in phase (φ_{12}, φ_{31}) and anti-phase (φ_{21}, φ_{22}). The pendulum's displacements fulfil the relations $\varphi_{11} - \varphi_{32} = \pi$, $\varphi_{12} + \varphi_{31} = 0$, $\varphi_{21} + \varphi_{22} = 0$. In Fig. 5.8b, one observes the synchronous motion when two pendulums (φ_{11}, φ_{32}) rotate with the same direction, while the four pendulums swing in the anti-phase in pairs φ_{12}, φ_{31} and φ_{21}, φ_{22}. From these observations one can conclude the presence of the synchronized clusters: 1) φ_{11}, φ_{32}, 2) φ_{12}, φ_{31} and 3) φ_{21}, φ_{22}.

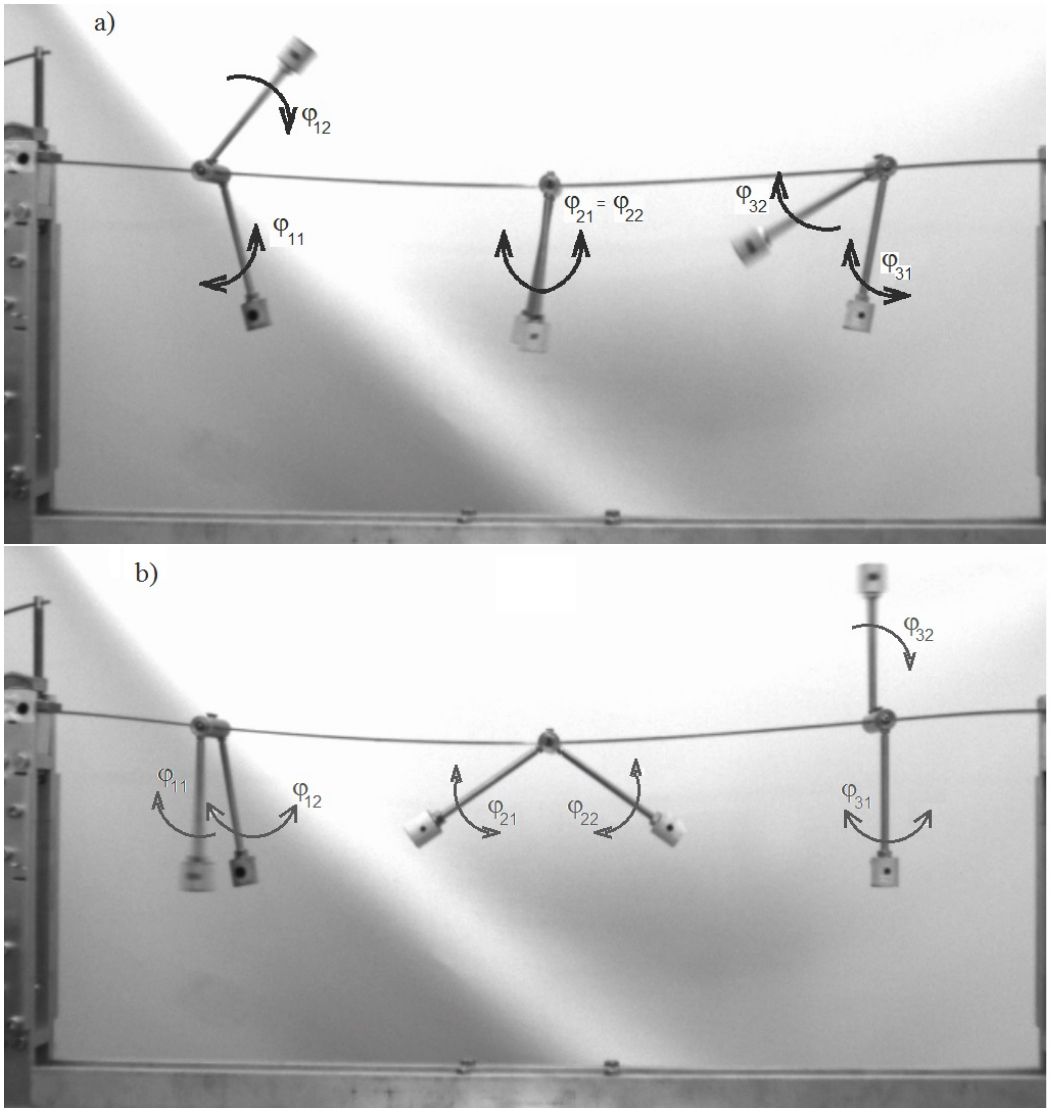

Figure 5.8: Experiment: a) phase synchronization: $\varphi_{11} = \varphi_{32} + \pi$, $\varphi_{21} = \varphi_{22}$, anti-phase synchronization: $\varphi_{12} = -\varphi_{31}$, b) phase synchronization: $\varphi_{11} = \varphi_{32} + \pi$, anti-phase synchronization: $\varphi_{21} = \varphi_{22}$, $\varphi_{12} = -\varphi_{31}$.

In Figs. 5.9 – 5.12 exemplary analysis of synchronous responses for chosen experimental results is demonstrated. Shifted in phase rotation regime (phase shift approaching π) between two pendulums on the side nodes (φ_{11} and φ_{32}), rotating in the same direction, is demonstrated in Figs. 5.9 - 5.10. Trajectories of both pendulums in orthogonal coordinates are shown in Fig. 5.9a. Corresponding time (Fig. 5.10) and synchronization (Fig. 5.9b) diagrams, respectively, prove that shifted in phase synchronous rotations are stable.

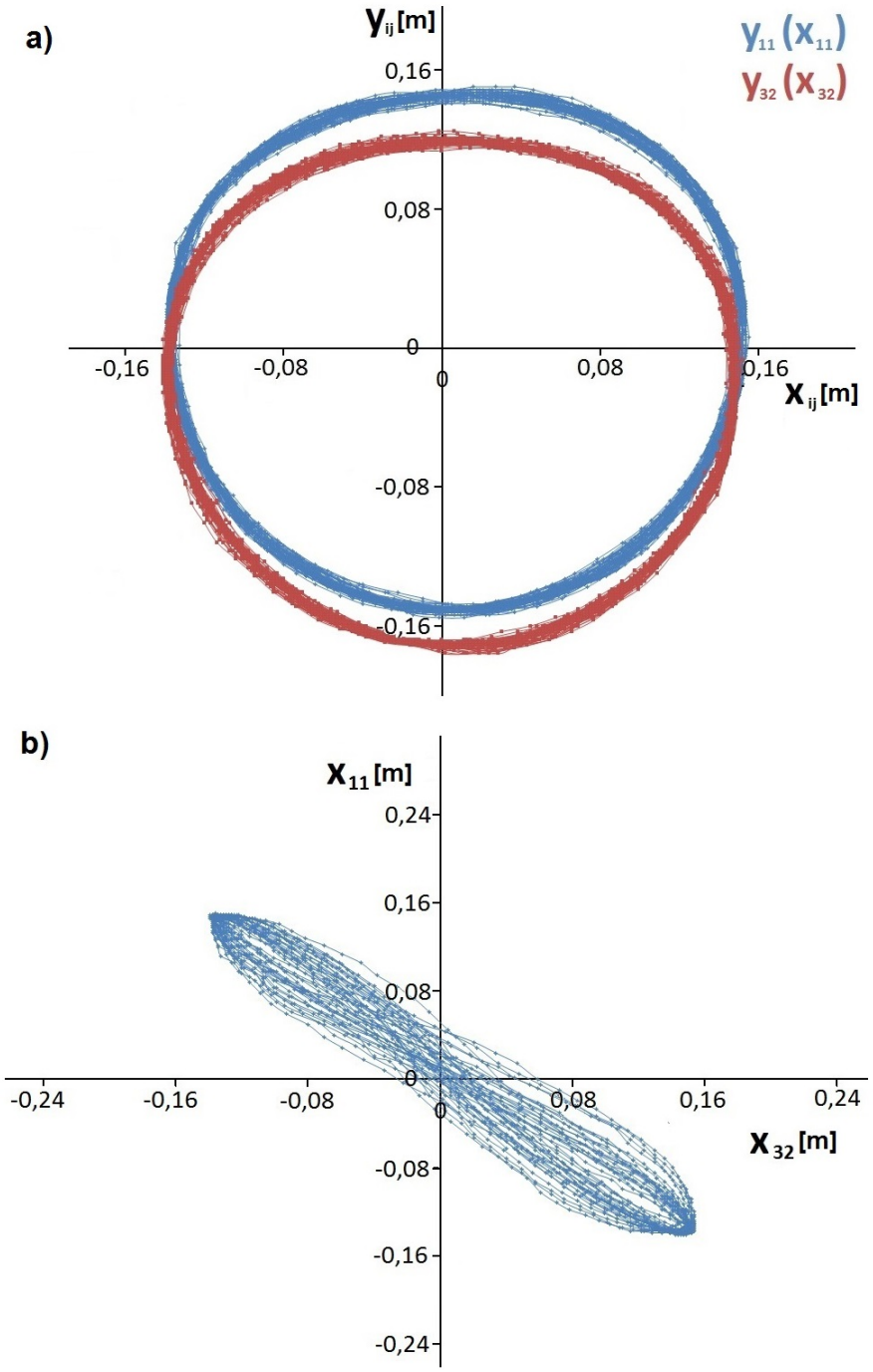

Figure 5.9: a) Experimental trajectories of rotating pendulums ($\Omega = 37.5\ [\frac{rad}{s}]$) for the zero initial velocity and different initial displacements, showing phase shifts of pendulum's rotation, b) Synchronization diagram of $x_{11}(x_{32})$ - shifted in phase synchronization (delayed by π), x_{11} and x_{32} are coordinates of φ_{11} and φ_{32}, respectively.

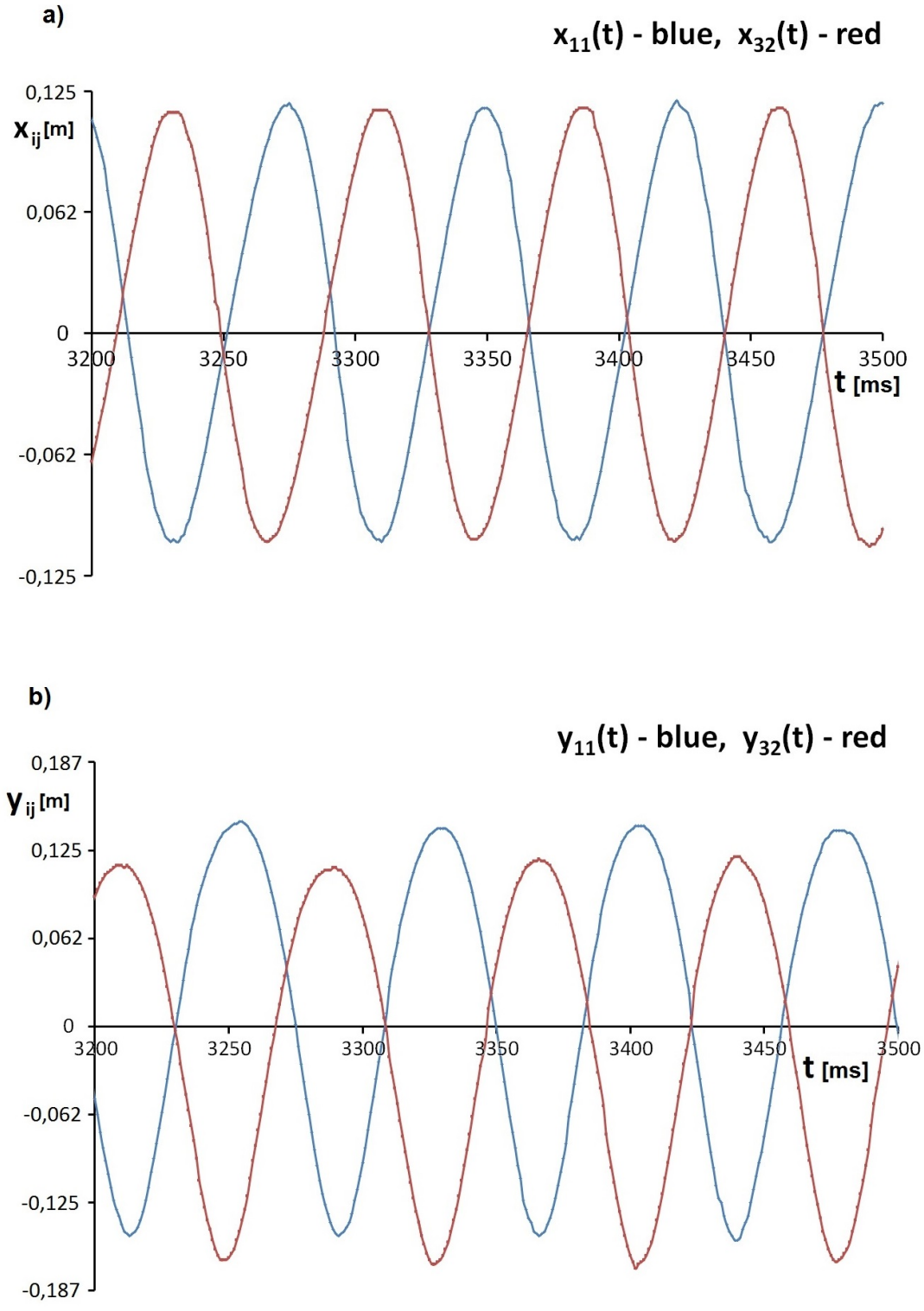

Figure 5.10: Time diagrams of motion of φ_{11} and φ_{32}.

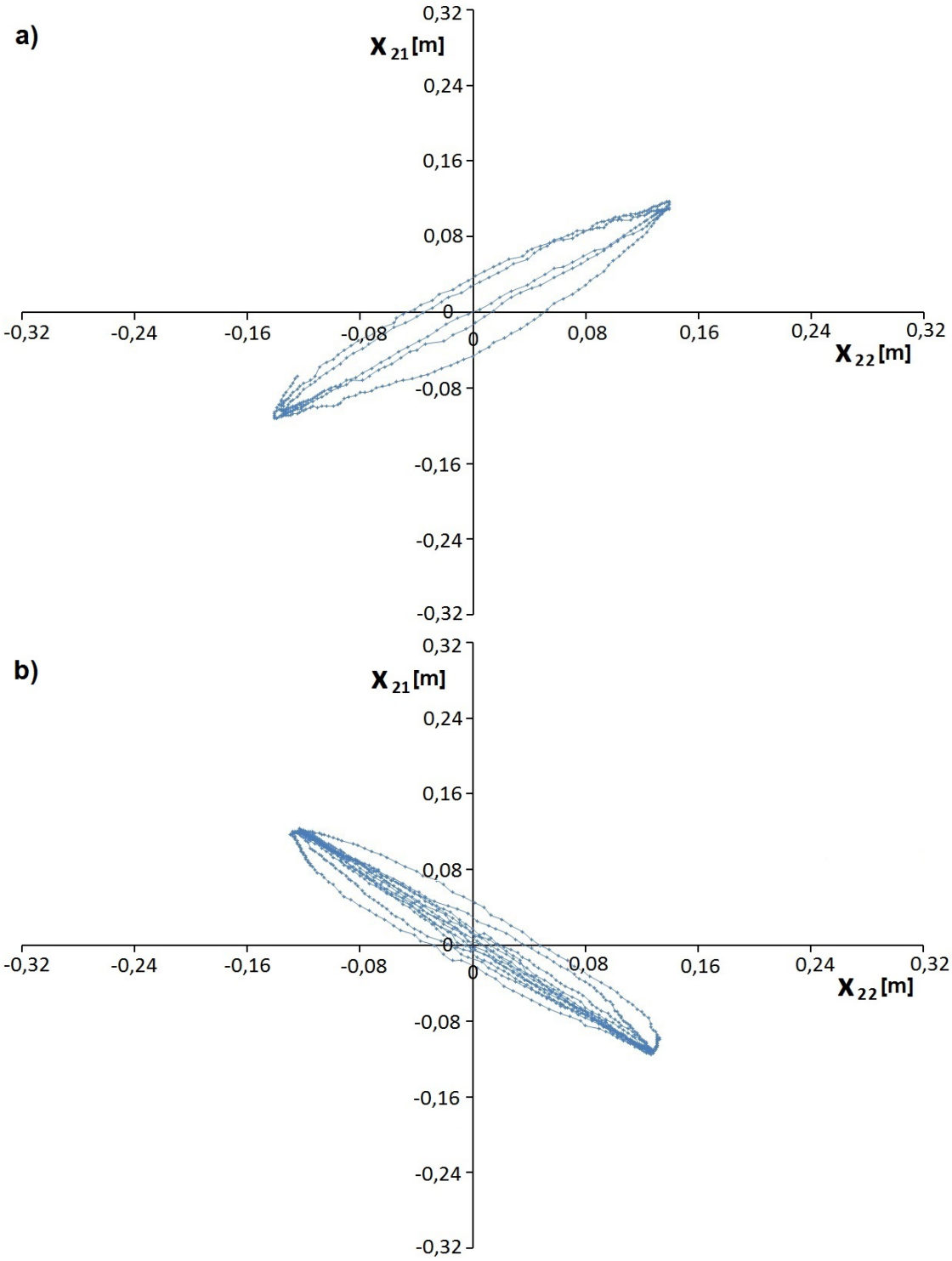

Figure 5.11: Diagram of a) $x_{21}(x_{22})$ – in phase synchronization, b) $x_{21}(x_{22})$ – in anti-phase synchronization. x_{21} and x_{22} are coordinates of φ_{21} and φ_{22}, respectively.

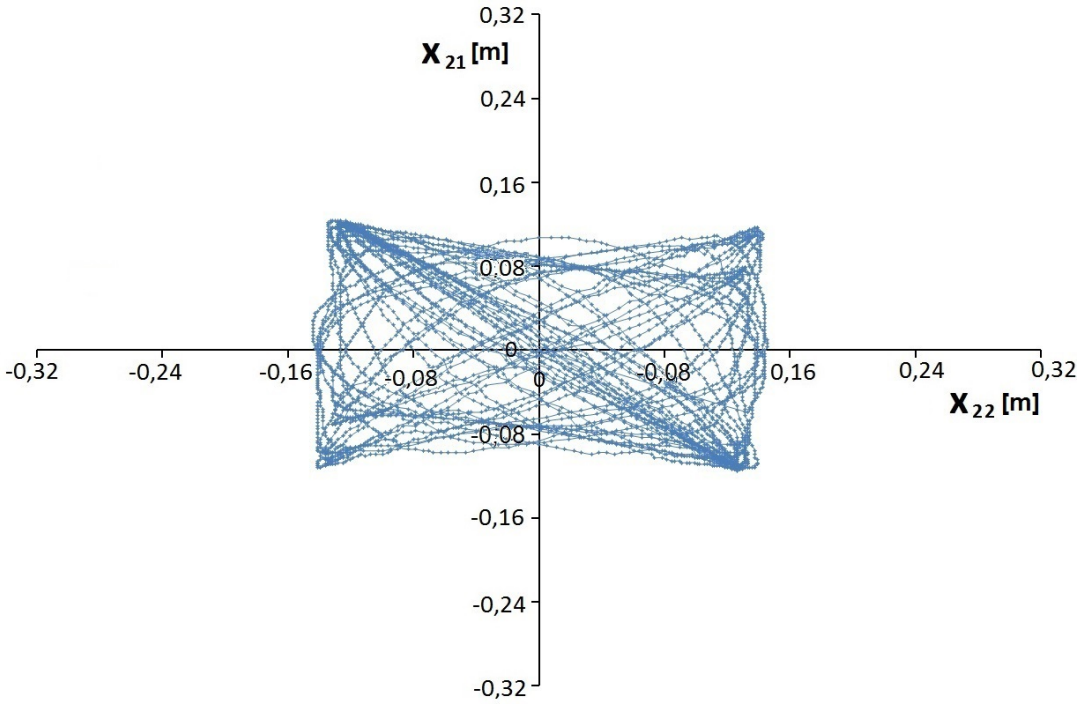

Figure 5.12: Synchronization diagram of $x_{21}(x_{22})$ - intermittent in phase and in anti-phase synchronization. x_{21} and x_{22} are coordinates of φ_{21} and φ_{22}, respectively.

On the other hand, in Figs. 5.11 – 5.12 the results of experimental synchronization analysis of pendulums suspended in the middle node of the beam, are demonstrated. These results correspond to the view of the middle pendulums (in that moment they are in anti-phase) depicted in Fig. 5.8. Intermittent in phase and in anti-phase synchronization (Fig. 5.12) or stabilized synchronization states, i.e., only in phase (Fig. 5.11a) or only in anti-phase (Fig. 5.11b) can be observed. In general presented experimental results correspond to their numerical equivalents (Chapter 4)

Chapter 6

Final remarks and conclusions

To summarize the analysis of the results presented in this dissertation one can conclude that its main objectives and thesis have been realized and confirmed. During the analysis, particular attention was paid to study the phenomenon of synchronization between pendulums suspended on the elastic beam. This phenomenon has been detected both in numerical simulations and during the experiment. Moreover, it has been observed in the simplest case of one 3DoF oscillator (mass with two pendulums, $n = 1$) as well as for three such oscillators (9DoF system, $n = 3$) located on the beam.

Especially noteworthy here is the chaotic synchronization of pendulums revealed in case of $n = 1$ (Eqs. (4.19), (4.22) and (4.23)) - see Sec. 4.4. This fact can be treated as an original and scientifically valuable result of this dissertation. Occurrence of synchronization is common for periodic or quasi-periodic system's response (Figs. 4.11, 4.16 and 4.17). On the other hand, chaotic systems are characterized by sensitivity on initial condition which should exclude synchronization of pendulums in system (4.19a-c). However, an introduction of some kind of coupling between the subsystems can result in their synchronization in chaotic regime. Crucial question for an explanation of chaotic synchronization mechanism in the system (4.19a-c) is to identify the nature of coupling between the pendulums. A complexity of this coupling is visualized by matrix form given by Eq. (4.22). Possible synchronous responses, also in chaotic regime, are an effect of direct inertial (first component with inertial coupling matrix), nonlinear diffusive coupling (second component representing

nonlinear vector) or they can be also caused by external forcing (right side of Eq. (4.22)). As a result, there appear complex form of the interaction between the pendulums which can lead to chaos synchronization. Characteristic for this coupling configuration is a mutual interaction between vibrating mass and pendulums, so independent subsystem cannot be extracted (isolated) from this structure of the oscillator. Therefore, this scheme of coupling cannot be treated either as a master-slave unidirectional connection (Subsec. 2.1.2) or as an autonomous driver (Sec. 2.3) or active-passive (Sec. 2.4) decomposition.

Numerical analysis of the system (4.19a–c) presented in Sec. 4.4 demonstrates that due to vertical direction of forcing, angular oscillations and rotations of pendulums are activated only in the direct neighbourhood of principal resonance frequency of the system (Fig. 4.9). Outside this range of excitation frequency we observe an extinction of angular osculations of pendulums and system (4.19a–c) is reduced to 1DoF linear oscillator executing vertical vibration. However, close to resonance high amplitude of the mass excites nonlinear response of pendulums and transition nonlinear dynamics takes place. The Ω-interval of chaotic synchronization is clearly depicted in Figs. 4.11 and 4.17. This is complete synchronization in phase or in anti-phase, which are equivalent coexisting solutions. Chaotic synchronization state is characterized with one positive Lyapunov exponent (see Fig. 4.11a). Loss of stability of chaotic synchronization is caused by chaos-hyperchaos transition when second Lyapunov exponent becomes positive. Thus, this exponent play a rule of transversal (Sec. 3.3) or conditional (Sec. 3.4) Lyapunov exponent quantifying the stability of synchronous regime. Other reason of observed desynchronization can be possible coexistence of attractors, even in the Ω-range of regular motion, e.g., one pendulum oscillates while the second is stabilized in upper or lower position (see Figs. 4.12c-d). On the other hand, for increased mass of main oscillator chaotic synchronization of pendulums does not occur (see Fig. 4.16). Possible explanation is that increasing mass influences for decrease of coupling terms in the system under consideration, because after transformation the Eq. 4.22) by diagonalization of the inertial coupling matrix value of mass is located in the denominator of coupling terms. Hence, coupling rate is reduced when the mass grows.

Then pendulums ”lose mutual contact” which manifests with independent chaotic or hyperchaotic motion of both pendulums.

Equally remarkable is numerical analysis of the system (4.19) with introduced parameter's mismatch (Fig. 4.17) which results in interesting type of synchronous behaviour manifesting with alternately appearing and disappearing states of chaotic synchronization in-phase and anti-phase. This effect was called intermittent phase – anti-phase synchronization (see Figs. 4.17 and 4.18). Such dynamical behaviour can be explained by a presence of a specific memory of the principal modes of vibration. In phase and in anti-phase oscillations are typical principal modes of linearised system. Some attracting trace of this solution can be embedded in the skeleton of chaotic attractor. It is only a conjecture.

Numerical results for $n = 1$ have been verified experimentally qualitatively and in general quantitatively. Phenomena of in phase (Fig. 5.4a), in anti-phase (Fig. 5.4b) and intermittent phase – anti-phase transition (Fig. 5.6) have been observed, registered and analysed during experimental study. Comparison of numerical (Subsec. 4.5.1) and experimental (Sec. 5.3) outcomes for $n = 3$ (Eqs. (4.25a-i)) also demonstrates a qualitative their agreement. In this augmented system chaotic synchronization of pendulums has not been detected in numerical simulations (Figs. 4.22 - 4.20) and in experiment (Figs. 5.8 - 5.12). However, various synchronous configuration have been observed, e.g., those depicted in Figs. 5.8a-b. These results indicate existence of cluster synchronization between pairs of pendulums.

Concluding, experimental studies have confirmed the results obtained numerically, which proves the correctness of the adopted model. In the future it is planned to extend the numerical investigations into $n > 3$ oscillator nodes in order to look for new types of synchronization, especially in cluster configuration.

Bibliography

[1] I. I. Blekhman, *Synchronization in Science and Technology*, ASME Press, New York (1988).

[2] A. Pikovsky, M. Rosenblum, J. Kurths, *Synchronization: A Universal Concept in Nonlinear Sciences*, Cambrige University Press, Cambrige (2001).

[3] L.M. Pecora, T.L. Carroll, G.A. Johnson, D.J. Mar, J.F. Heagy, *Fundamentals of synchronization in chaotic systems, concepts, and applications*, Chaos **7**, 520 (1997).

[4] G. D. Birkhoff, *Dynamical Systems*, AMS Colloquium Publications, Providence, 305 (1927).

[5] C. Huygens, *The Pendulum Clock*, Iowa State University Press, Ames (1986).

[6] J. Pena-Ramirez, R. H. B. Fey, H. Nijmeijer, *An experimental study on synchronization of nonlinear oscillators with Huygens' coupling*, Nonlinear Theory and its Applications, IEICE **3** (2), 128 (2012).

[7] J. Pena-Ramirez, R. H. B. Fey, and H. Nijmeijer. In-phase and anti-phase synchronization of oscillators with Huygens' coupling. Cybernetics and Physics, 1(1):58-66, 2012.

[8] M. Kapitaniak, K. Czolczynski, P. Perlikowski, A. Stefanski, T. Kapitaniak, *Synchronization of clocks*, Physics Reports **517** (1-2), 1 (2012).

[9] K. Czolczynski, P. Perlikowski, A. Stefanski, T. Kapitaniak, *Huygens' odd sympathy experiment revisited*, International Journal of Bifurcations and Chaos **21** (7), 2047 (2011).

[10] R. Dilao, *Anti-phase and in-phase synchronization of nonlinear oscillators: The Huygens's clocks system*, Chaos: An Interdisciplinary Journal of Nonlinear Science **19** (2), 023118 (2009).

[11] L. M. Pecora, T. S. Carroll, *Synchronization in chaotic systems*, Phys. Rev. Lett. **64**, 821 (1990).

[12] T. Kapitaniak, *Controlling Chaos*, Academic Press, London (1996).

[13] G. Chen, *Controlling Chaos and Bifurcations*, CRC Press, Boca Raton (1999).

[14] S. Boccaletti, J. Kurths, G. Osipov, D. L. Valladares, C. S. Zhou, *The synchronization of chaotic systems*, Physics Reports **366**, 1 (2002).

[15] A. Rodrigues - Angeles, H. Nijmeijer, *Coordination of two robot manipulators based on position measurements only*, International Journal of Control **74**, 1311 (2001).

[16] Y. - H. Liu, Y. Xu, M. Bergerman, *Coordination control of multiple manipulators with passive joints*, IEEE Transactions on Robotics and Automation **15**, 258 (1999).

[17] A. Yu. Pogromsky, Y. Xu,V. N. Belykh, H. Nijmeijer, *Controlled synchronization of pendula*, Proceedings of the 42nd IEEE Conference on Design and Control, Maui, Hawaii 4381 (2003).

[18] F. Han, Q. - S. Lu, M. Wiercigroch, Q. - B. Ji, *Complete and phase synchronization in a heterogeneous small-world neuronal network*, Chinese Physics B **18** (2), 482 (2009).

[19] M. Rosenblum, A. S. Pikovsky, J. Kurths, *Phase synchronization of chaotic oscillators*, Phys. Rev. Lett. **76**, 1804 (1996).

[20] A. S. Pikovsky, *On the interaction of strange attractors*, Zeitschrift Physik B **55**, 149 (1984).

[21] H. Fujisaka, T. Yamada, *Stability theory of synchronized motion in coupled oscillator systems*, Prog. Theor. Phys. **69**, 32 (1983).

[22] H. Fujisaka, T. Yamada, *Stability theory of synchronized motion in coupled-oscillator systems. ii - the mapping approach*, Prog. Theor. Phys. **70** (1983).

[23] E. R. Rosa, E. Ott, M. H. Hess, *Transition to phase synchronization of chaos*, Phys. Rev. Lett. **80**, 1642 (1998).

[24] M. Rosenblum, A. S. Pikovsky, J. Kurths, *From phase to lag synchronization in coupled chaotic oscillators*, Phys. Rev. Lett. **78**, 4193 (1997).

[25] P. Perlikowski, A. Stefanski, T. Kapitaniak, *Mode locking and generalized synchronization in mechanical oscillators*, Journal of Sound and Vibration **318**, 329 (2008).

[26] A. Stefanski, *Determining thresholds of complete synchronization, and application*, World Scientific Series on Nonlinear Science A **67** (2009).

[27] T. Kapitaniak, M. Sekieta, M. Ogorzalek, *Monotone synchronization of chaos*, Int. Journal of Bifurcation and Chaos **6**, 211 (1996).

[28] M. Sekieta, T. Kapitaniak, *Practical synchronization of chaos via a nonlinear feedback scheme*, Int. Journal of Bifurcation and Chaos **6**, 1901 (1996).

[29] N. F. Rulkov, M. M. Sushchik, L. S. Tsimring, H. D. I. Abarbanel, *Generalized synchronization of chaos in directionally coupled chaotic systems*, Phys. Rev. E **51**, 980 (1995).

[30] L. Kocarev, U. Parlitz, *Generalized Synchronization, Predictability, and Equivalence of Unidirectionally Coupled Dynamical Systems*, Phys. Rev. Lett. **76**, 1816 (1996).

[31] V. Afraimovich, A. Cordonet, N. F. Rulkov, *Generalized synchronization of chaos in noninvertible maps*, Phys. Rev. E **66**, 016208 (2002).

[32] R. Femat, L. Kocarev, L. van Gerven, M. E. Monsivais - Perez, *Towards generalized synchronization of strictly different chaotic systems*, Phys. Lett. A **342**, 247 (2005).

[33] K. Pyragas, *Properties of generalized synchronization of chaos*, Nonlinear Analysis: Modelling and Control, Vilnius, IMI, 3 (1998).

[34] L. O. Chua, *Chua's circuit an overview ten years later*, J. Circuit Syst. Comp. **4**, 117 (1994).

[35] H. D. I. Abarbanel, N. F. Rulkov, M. M. Sushchik, *Generalized synchronization of chaos*, The auxiliary system approach, Phys. Rev. E **53**, 4528 (1996).

[36] S. Boccaletti, D. L. Valladares, *Characterization of intermittent lag synchronization*, Phys. Rev. E **62**, 7497 (2000).

[37] M. A. Zaks, E. - H. Park, M. G. Rosenblum, J. Kurths, *Alternating Locking Ratios in Imperfect Phase Synchronization*, Phys. Rev. Lett. **82**, 4228 (1999).

[38] D. J. Gauthier, J. C. Bienfang, *Intermittent loss of synchronization in coupled chaotic oscillators: Toward a new criterion for high-quality synchronization*, Phys. Rev. Lett. **77**(9), 1751 (1996).

[39] K. Pyragas, *Weak and strong synchronization of chaos*, Phys. Rev. E **54**, 4508 (1996).

[40] S. H. Strogatz, S. E. Mirollo, P. C. Matthews, *Coupled nonlinear oscillators below the synchronization threshold: Relaxation by generalized Landau damping*, Phys. Rev. Lett. **68**, 2730 (1992).

[41] J.F. Heagy, L.M. Pecora, T.L. Carroll, *Short Wavelength Bifurcations and Size Instabilities in Coupled Oscillator Systems*, Phys. Rev. Lett. **74**, 4185 (1995).

[42] K. Kaneko, *Clustering, coding, swiching, hierarhical ordering, and control in network of chaotic elements*, Physica D **41**, 137 (1990).

[43] V. N. Belykh, I. V. Belykh, M. Hasler, *Hierarchy and Stability of partially synchronous oscillations of diffusively coupled dynamical systems*, Phys. Rev. E **62**(2), 6332 (2000).

[44] V. N. Belykh, I. V. Belykh, E. Mosekilde, *Claster synchronization modes in an ensemble of coupled chaotic oscillators*, Phys. Rev. E **63**(3), 036216 (2001).

[45] S. Yanchuk, Y. Maisterenko, E. Mosekilde, *Partial synchronization and clustering in a system of diffusively coupled chaotic oscillators*, Math. Comp. Simul. **54**, 491 (2000).

[46] S. Yanchuk, A. Stefanski, T. Kapitaniak, J. Wojewoda, *Dynamics of an array of mutually coupled semiconductor lasers*, Phys. Rev. E **73**(1), 016209 (2006).

[47] K. Czolczynski, P. Perlikowski, A. Stefanski, T. Kapitaniak, *Clustering of Huygens' Clocks*, Prog. Theor. Phys. **122**(4), (2009).

[48] K. Czolczynski, A. Stefanski, P. Perlikowski, and T. Kapitaniak, *Clustering and synchronization of n Huygens' clocks*, Physica A **388**(24), 5013 (2009).

[49] P. Perlikowski, A. Stefanski, T. Kapitaniak, *Ragged Synchronizability and Clustering in a Network of Coupled Oscillators*, Recent Advances in Nonlinear Dynamics and Synchronization **254**, 49 (2009).

[50] K. Czolczynski, A. Stefanski, P. Perlikowski, T. Kapitaniak, *Multistability and chaotic beating of Duffing oscillators suspended on an elastic structure*, Journal of Sound and Vibration **322** (3), 513 (2009).

[51] D. G. Fertis, *Advanced Mechanics of Structures*, CRC Press, Akron (1996).

[52] Xiao-Song Yang, *A framework for synchronization theory*, Chaos, Solitons & Fractals **11**, 1365 (2000).

[53] J. N. Blakely, D. J. Gauthier, G. Johnson, T. L. Carroll, L. M. Pecora, *Experimental investigation of high-quality synchronization of coupled oscillators*, Chaos **10**, 738 (2000).

[54] J. Cai, M. Lin, Z. Yuan, *Secure communication using practical synchronization between two different chaotic systems with uncertainties*, Mathematical and Computational Applications **15** (2), 166 (2010).

[55] H. D. I. Abarbanel, N. F. Rulkov, M. M. Sushchik, *Generalized synchronization of chaos*, The auxiliary system approch, Phys. Rev. E **53**, 4528 (1996).

[56] J. Kaplan, J. Yorke, *Chaotic behavior of multidimentional difference equations*, In Functional Differential Equations and Approximation of Fixed Points, Peitgen, H. O. Walther eds., Springer-Verlag: New York, 228 (1979).

[57] C. Huygens, *Horoloquim Oscilatorium*, Paris (1673).

[58] U. Parlitz, W. Lauterborn, *Period-doubling cascades and devil's staircases of the driven Van der Pol oscillator*, Phys. Rev. A **36** (3), 1428 (1987).

[59] L. M. Pecora, T. S. Carroll, *Driving systems with chaotic signals*, Phys. Rev. A **44**, 2374 (1991).

[60] R. Albert, H. Jeong, A. - L. Barabasi, *The diameter of the world-wide web*, Nature (London) **401**, 130 (1999).

[61] L. Kocarev, U. Parlitz, *General Approach for Chaotic Synchronization with Applications to Communication*, Phys. Rev. Lett. **74**, 5028 (1995).

[62] D. J. Watts, S. H. Strogatz, *Collective dynamics of "small-world" networks*, Nature (London) **393**, 440 (1998).

[63] E. - H. Park, Z. Feng, D. M. Durand, *Diffusive coupling and network periodicity: a computational study*, Biophys J. **95** (3), 1125 (2008).

[64] J. Hale, *Diffusive Coupling, Dissipation and Synchronization*, J. Dyn. Diff. Eq. **9** (1), 1 (1997).

[65] S. Barnett, C. Stanley, *Matrix Methods in Stability Theory*, Thomas Nelson and Sons Ltd., Suffolk, 148 (1970).

[66] R. E. Ricklefs, G. L. Miller, *Ecology §6.1 Homeostasis depends upon negative feedback*, Macmillan, 92 (2000).

[67] B. Roos, D. Hamilton, *Formative and Summative Assessment: A cybernetic viewpoint*, Assessment in Education Principles Policy and Practice **12**, 7 (2005).

[68] G. E. Davis, M. A. McGowan, *Formative feedback and the mindful teaching of mathematics*, Australian Senior Mathematics Journal **21** (1), 19 (2007).

[69] A. Ramaprasad, *On The Definition of Feedback*, Behavioral Science **28** (1), (1983).

[70] K. Bar-Eli, *On the stability of coupled chemical oscillators*,Physica D **14**, 242 (1985).

[71] E. - H. Park, Z. Feng, D. M. Durand, *Diffusive coupling and network periodicity: a computational study*, Biophys J. **95** (3), 1126 (2008).

[72] L. M. Pecora, T. S. Carroll, *Master Stability Functions for synchronized coupled systems*, Phys. Rev. Lett. **80** (10), 2109 (1998).

[73] K. Fink, G. Johnson, T. L. Carroll, D. Mar, L. M. Pecora, *Three coupled oscillators as an universal probe of synchronization stability in coupled oscillator array*, Phys. Rev. E **61**, 5080 (2000).

[74] J. Hale, *Diffusive Coupling, Dissipative, and Synchronization*, J. Dyn. Diff. Eq. **9**(1), 1 (1997).

[75] L. Kocarev, U. Parlitz, *General approach for chaotic synchronization with applications to communication*,Phys. Rev. Lett. **74**, 5028 (1995).

[76] S.D. Poisson, *Memoire sur les inegalites seculaires des moyens mouvements des planets*, Journal de l'Ecole Polytechnique XV(1), 1 (1808).

[77] G. D. Birkhoff, *Dynamical Systems*, AMS Colloquium Publications, Providence, 305 (1927).

[78] A. M. Lyapunov, *Probleme General de la Stabilite du Mouvement*, Annals of Mathematics Studies **17**, 203 (1947).

[79] A. Tylikowski, *Liapunov functionals application to dynamic stability analysis of continuous systems*, Nonlinear Analysis-Theory Methods & Applications **63** (5-7), 169 (2005).

[80] S. P. Kuznietsov, *Dynamical Chaos*, Fizmatlit, Moscow, 296 (2001).

[81] V. Oseledec, *A multiplicative ergodic theorem: Lyapunov characteristic numbers for dynamical systems*, Trans. Moscow Math. Soc. **19**, 197 (1968).

[82] T. Kapitaniak, *Chaos for Engineers: Theory, Applications, and Control*, Springer Verlag, 1998.

[83] G. Benettin, L. Galgani, J. M. Strelcyn, *Kolmogorov entropy and numerical experiment*, Phys. Rev. A **14**, 2338 (1976).

[84] I. Shimada, T. Nagashima, *A numerical approach to ergodic problem of dissipative dynamical systems*, Prog. Theor. Phys. **61** (6), 1605 (1979).

[85] M. Henon, C. Heiles, *The applicability f the third integral of the motion: Some numerical results*, Astronomic Journal **69**, 73 (1964).

[86] A. Wolf, J. Swift, H. Swinney, J. Vastano, *Determining Lyapunov exponents from a time series*, Physica D **16**, 285 (1985).

[87] A. Wolf, *Quantifying chaos with Lyapunov exponents*, Chaos (V. Holden eds), Manchester University Press, Manchester (1986).

[88] P. C. Müller, *Calculation of Lyapunov exponents for dynamical systems with discontinuities*, Chaos, Solitons & Fractals **5** (9),1671 (1995).

[89] K. Popp, N. Hinrichs, M. Oestreich, *Analysis of a self-excited friction oscillator with external excitation*, Dynamics with Friction: Modeling, Analysis and Experiment, World Scientific Publishing, Singapore (1996).

[90] A. Stefanski, T. Kapitaniak, *Using chaos synchronization to estimate the largest Lyapunov exponent of non-smooth systems*, Discrete Dyn. Nat. Soc. **4**, 207 (2000).

[91] A. Stefanski, *Estimation of the largest Lyapunov exponent in systems with impacts*, Chaos, Solitons & Fractals **11** (15), 2443 (2000).

[92] A. Stefanski, T. Kapitaniak, *Estimation of the largest Lyapunov exponent of non-smooth systems on the basis of maps synchronization*, Chaos, Solitons & Fractals **15**, 233 (2003).

[93] A. Stefanski, A. Dabrowski, T. Kapitaniak, *Evaluation of the largest Lyapunov exponent in dynamical systems with time delay*, Chaos, Solitons & Fractals **23** (5), 1651 (2005).

[94] A. Stefanski, T. Kapitaniak, *Synchronization of mechanical systems driven by chaotic or random excitation*, Journal Sound and Vibration **260**, 565 (2003).

[95] V. C. Anishchenko, *Complex oscillations in simple systems*, Moscow: Nauka Publisher, 312 (1990).

[96] V. Vaziri, A. Najdecka, M. Wiercigroch, *Experimental control for initiating and maintaining rotation of parametric pendulum*, The European Physical Journal, Special Topics **223** (4), 795 (2014).

[97] J. Strzalko, J. Grabski, J. Wojewoda, M. Wiercigroch, T. Kapitaniak, *Synchronous rotation of the set of double pendula: Experimental observations*, Chaos, **22** (4), 047503 (2012).

[98] E. Pavlovskaia, B. W. Horton, M. Wiercigroch, S. Lenci, G. Rega, *Approximate rotating solutions of pendulum under combined vertical and horizontal excitation*, International Journal of Bifurcation and Chaos **22** (5), 1250100 (2012).

[99] A. S. de Paula, M. A. Savi, M. Wiercigroch, E. Pavlovskaia, *Bifurcation control of pendulum dynamics*, International Journal of Bifurcation and Chaos **22** (5), 1250111 (2012).

[100] M. Wiercigroch, G. Rega, *Dynamics, synchronization and control of parametric pendulums*, Springer Netherlands, IUTAM Symposium on Nonlinear Dynamics for Advanced Technologies and Engineering Design **32**, 185 (2013).

[101] A. S. de Paula, M. A. Savi, M. Wiercigroch, E. Pavlovskaia, *Chaos control methods applied to avoid bifurcations in pendulum dynamics*, Springer Netherlands, IUTAM Symposium on Nonlinear Dynamics for Advanced Technologies and Engineering Design **32**, 387 (2013).

[102] J. M. T. Thompson, M. Wiercigroch, J. Sieber, B. W. Horton, *Dynamics of the nearly parametric pendulum*, International Journal of Non-Linear Mechanics **46** (2), 436 (2011).

[103] G. S. Gorelik, A. A. Witt, *Swing of an elastic pendulum as an example of two paramerticall bound linear vibration systems*, Journal of Tech. Physics **3** (2-3), 294 (1933).

[104] X. Xu, E. Pavlovskaia, M. Wiercigroch, F. Romeo, S. Lenci, *Dynamic interactions between parametric pendulum and electro-dynamical shaker*, ZAMM Zeitschrift fur Angewandte Mathematik und Mechanik **87** (2) 172 (2007).

[105] D. Sado, M. Kot, *Dynamika autoparametrycznego układu z nieidentycznym źródłem energii*, XI Warsztaty Naukowe PTSK **243**, Warszawa (2005).

[106] D. Sado, M. Kot, *Nonlinear oscillations of a coupled autoparametrical system with ideal and nonideal sources of power*,Hindawi Publishing Corporation, Mathematical Problem in Engineering **2006** (2006).

[107] D. Sado, M. Kot, *Chaotic vibration of an autoparametrical system with ideal and nonideal sources of power*, Journal of Theoretical and Applied Mechanics **45** (1), 119 (2007).

[108] K. Czolczynski, P. Perlikowski, A. Stefanski, T. Kapitaniak, *Synchronization of slowly rotating pendulums*, Int. J. Bifurcation Chaos **22**, 1250128 (2012).

[109] K. Czolczynski, P. Perlikowski, A. Stefanski, T. Kapitaniak, *Synchronization of pendula rotating in different directions*, Commun. Nonlinear Sci. Numer. Simul. **17**, 3658 (2012).